Evaluating Pavement Response and Performance with Different Simulative Tests

Yucheng Huang

Dissertation submitted to the faculty of
Virginia Polytechnic Institute and State University
in partial fulfillment of the requirements for the degree of
Doctor of Philosophy
in
Civil Engineering

Linbing Wang, Committee Chair
Montasir M. Abbas
Joseph E. Dove
Cris Druta

May 5th, 2017
Blacksburg, Virginia

Keywords: APT, Fatigue, Rutting, Finite Element Analysis, ABAQUS

Evaluating Pavement Response and Performance with Different Simulative Tests

Yucheng Huang

ABSTRACT

Simulative tests refer to the Full-scale accelerated pavement testing (APT) and laboratory wheel tracking testing, which are widely used for evaluation of pavement responses and performance under a controlled and accelerated damage conditions in a compressed limited time. This dissertation focuses on comparative evaluations under ALF, MMLS 3 and APA tests, in terms of rut depth, strain response, seismic stiffness, and contact stress using both experimental and numerical simulation results. Test slabs extracted from the ALF test lanes, are trafficked with the MMLS3 under comparable environmental conditions at laboratory in Virginia Tech. Some specimens were cut from the slabs for APA tests at VTRC. It is found that the monitored parameters yielded by the MMLS 3 test were comparable to the related full-scale ALF test results in terms of intrinsic material characteristics and pavement performance. The wireless sensor network based on Internet of things technology is implemented in laboratory for the MMLS 3 test, which provides a convenient solution for researchers on long-term observation and monitoring without being physically presented.

The numerical simulations of ALF, MMLS 3 and APA in ABAQUS are used to supplement the investigation on the pavement response and performance under repeated moving loading. The viscoelastic-viscoplastic model is adopted to characterize rate and temperature dependent properties of asphalt mixtures. The 3D finite element models are capable of predicting the pavement response at critical locations while underestimates the rut depth because the permanent deformation induced by volumetric change cannot be represented in simulation.

According to the test results, a power law function fits well for the accumulated rut depth versus number of load repetitions before the material reaches tertiary stage in MMLS 3 test. The rut depth development of APA tests exhibits a close-to-liner regression with number of load cycles after the initial 500 load repetitions. A regression model for predicting rut depth after 500 loads has a satisfying agreement with the experimental measurement. The calibrated MEPDG fatigue model can be used to estimate the allowable load repetitions in MMLS 3 trafficking. Besides, the effects of tire configuration, tire pressure, axle load amplitude, wheel load speed and temperature on pavement responses are investigated in this dissertation using the finite element model.

It is concluded that MMLS 3 is an effective, economic and reliable trafficking tool to characterize rutting and fatigue performance of pavement materials with due regard to the relative structures. MMLS 3 test can be employed as the screen testing for establishing

full-scale testing protocols as desired or required, which will significantly enhance economics of APT testing.

Evaluating Pavement Response and Performance with Different Simulative Tests

Yucheng Huang

GENERAL AUDIENCE ABSTRACT

This dissertation introduces the common simulative tests including the Full-scale accelerated pavement testing (APT) and laboratory wheel tracking testing, which are widely used for evaluation of pavement responses and performance under a controlled and accelerated damage conditions in a compressed limited time. Test results are compared in terms of rut depth, strain response, seismic stiffness, and contact stress under Accelerated Loading Facility (ALF), the third-scale Model Mobile Load Simulator (MMLS 3) and Asphalt pavement analyzer (APA) tests, using both experimental and numerical simulation manners. Test slabs extracted from the ALF test lanes and some specimens cut from the slabs are trafficked with the MMLS3 at laboratory in Virginia Tech and with APA at Virginia Transportation Research Center (VTRC) under comparable environmental conditions. It is found that the monitored parameters yielded by the MMLS 3 test were comparable to the related full-scale ALF test results in terms of intrinsic material characteristics and pavement performance. During the test measurements, the wireless sensor network based on Internet of things technology is implemented in laboratory for the MMLS 3 test, which provides a convenient solution for researchers on long-term observation and monitoring.

The numerical simulations of ALF, MMLS 3 and APA in ABAQUS are used to supplement the investigation on the pavement response and performance under repeated moving loading, which adopted the viscoelastic-viscoplastic model to characterize mechanistic and temperature-dependent properties of asphalt mixtures. It is also found that the 3-Dimensional finite element models are capable of predicting the pavement response at critical locations while underestimates the rut depth because the permanent deformation induced by volumetric change cannot be represented in simulation.

According to the tests and simulations results, a power law function fits well for the accumulated rut depth versus number of load repetitions before the material reaches tertiary stage in MMLS 3 test. The rut depth development of APA tests exhibits a close-to-liner regression with number of load cycles after the initial 500 load repetitions. A regression model for predicting rut depth after 500 loads has a satisfying agreement with the experimental measurement. The calibrated MEPDG fatigue model can be used to estimate the allowable load repetitions in MMLS 3 trafficking. Besides, the effects of tire configuration, tire pressure, axle load amplitude, wheel load speed and temperature on pavement responses are investigated in this dissertation using the finite element model.

It is concluded that MMLS 3 is an effective, economic and reliable trafficking tool to characterize rutting and fatigue performance of pavement materials with due regard to the

relative structures. MMLS 3 test can be employed as the screen testing for establishing full-scale testing protocols as desired or required, which will significantly enhance economics of APT testing.

ACKNOWLEDGEMENTS

First and foremost, I would like to express my sincere gratitude to my advisor, Dr. Linbing Wang, for his continuous support, guidance and encouragement during my Ph. D studies. His dedication and sincere attitude for science and engineering always inspires and encourages me. The dissertation would never been possible without his guidance, support and valuable advices.

I wish to express my appreciation to my committees, Dr. Montasir Abbas, Dr. Joseph Dove, and Dr. Cristian Druta, for their very helpful insights, comments, suggestions and valuable advice.

I must express a particular thankful word to Nelson Gibson, Ph.D., PE. Senior Program Officer for Materials and Construction at Transportation Research Board, who gave the permission to get the slab extracted from FHWA and provided the fatigue performance test results after ALF trafficking. Additionally, great thanks to the continuous support and help of Mark Baker from Geomedia Research & Development.

In addition, I would like to say thank you to my former and current colleagues at Virginia Tech, Yue Hou, Ying Li, Yufeng Liu, Wenjuan Sun, Haocheng Xiong, Wenjing Xue and Yinning Zhang for their warm encouragements and valuable discussions during the preparation of this dissertation.

Last but not least, I am very grateful to my wife, Fang Liu, for her love, patience, support, understanding and taking care of me. Besides, I owe deep appreciation to my parents for their endless love, support, encouragement and understanding.

Yucheng Huang

TABLE OF CONTENT

LIST OF FIGURES

LIST OF TABLES

Chapter 1 INTRODUCTION

1.1 Literature Review

The U.S. transportation infrastructure system is confronted with degradation challenges for decades. A considerable portion of the transportation infrastructure still serving in the U.S. is not maintained at optimal level, and thus in substandard or poor conditions, due to the funding limitations. Accordingly, the highway practitioners are required to provide cost effective design, maintenance, and rehabilitation strategy within constrains of limited financial resource and less environmental impacts.

For these reasons, substantial efforts are devoted to better understanding of mixture and structural design, material properties, new types of structure, and innovative materials. It is of great significance to investigate the mechanic properties of asphalt pavement. Asphalt mixture is a prominent and widely used pavement material, and is a complex composite material comprising asphalt binder, mineral aggregates and miner fillers. In order to better characterize mechanistic properties of asphalt mixtures, numerous laboratory and in-field test apparatuses have been developed both in small scale and full scale. However, most laboratory tests are primarily based upon the cylindrical cores or beam specimens due to the specimen size and compact limitations in laboratory, which are normally fabricated using gyratory compactor or vibratory compacted. In addition, because the laboratory test apparatuses are not capable of providing close to field conditions, whether the laboratory test results can represent material in-situ performance is questionable. Accordingly, there is a great need to establish a link between the laboratory results and the realistic long-term in-situ pavement performance. (Metcalf, 1996; Saeed & Hall, 2003; Hugo & Martin, 2004; Steyn, 2012)

The traditional method to address this gap is to construct an experimental section on actual pavement and monitor the material behavior along with pavement performance under the in-service traffic, which might be labor intensive and time consuming, as well as the uncertainty of the traffic volume due to the unanticipated traffic growth (Metcalf, 1996; Steyn, 2012). Meanwhile, the pavement engineers need to evaluate the potential of new material or structure for application in a quick manner, especially for long-term fatigue performance assessment (Hugo & Martin, 2004; Steyn, 2012). Simulative tests commonly serve as a link between laboratory tests and actual field performance, which include the Full-scale accelerated pavement testing (APT) and laboratory wheel tracking devices. The pavement material withstands complex stress conditions as a wheel load passes over. These stress conditions cannot be reflected or replicated in laboratory simple performance tests. In simulative tests, the traffic loads are modeled to apply on the material which is subjected to close-to-field stress conditions.

In NCHRP Synthesis 235, APT is defined as “the controlled application of a prototype wheel loading, at or above the appropriate legal load limit to a prototype or actual, layered, structural pavement system to determine pavement response and performance under a controlled, accelerated, accumulation of damage in a compressed time period”

(Metcalf, 1996). The objective of APT is to quantify the pavement response and performance under equivalent, often increased loads associated with environmental effects during a much shorter time than the case of normal road under realistic traffic applications. For the past decades, APT studies provided pavement researchers and practitioners with knowledge that improved their understanding of pavement materials and structures, and their behavior under typical traffic and environmental loading, which helps form the basis for developing various theories about pavement behavior and support the current pavement design methods (Steyn& Hugo 2016). It is well accepted that APT program should be supplemented with laboratory and LTPP program for the most benefit. The National Cooperative Highway Research Program (NCHRP) develops three APT synthesis documents APT, NCHRP 235(Metcalf 1996), NCHRP 325 (Hugo and Martin 2004) and NCHRP 433 (Steyn 2012). These syntheses summarized knowledge by evaluating developments and advances around APT, and proposed the future research needs for APT. The full scale APT research topics include but not limited to materials characterization, pavement modeling, behavior and performance of pavement material, calibration and development for pavement design method, economic impacts of full-scale APT programs, development of databases of pavement performance that are shared between different pavement research programs, cost savings through implementing full-scale APT and the development of improved instrumentation and analysis methods (Steyn& Hugo 2016).

A great number of studies have been done using ALF to evaluate properties and performance of new material and new pavement structure. Addis (1989) undertook trials in the Pavement Test Facility at the Transportation Road Laboratory (TRL) for evaluation of the pertain performance of dense bitumen macadam (DBM) and heavy duty macadam (HDM). Kadar (1989) examined the performance of slag road bases under APT. The testing results indicated that the blast furnace slag can be used for high-quality in crushed-rock road bases. This demonstrated that the structural behavior of pavements will change as the material characteristics change. Corté (1997) investigated the fatigue performance of pavement structure with hot and cold mixes under LCPC APT experiments. The experiments were conducted on a newly developed emulsion-bound granular material with a modified binder, named a “double-coated” cold mix, conventional hot-mix asphalt, as well as an emulsion-bound material. Kekwick (1999) implemented the SA-HVS program which has been utilized in South Africa to validate the performance of pavements with well-balanced, deep structures, which have a gradually decreased stiffness with depth. The research indicated that poor-balanced, shallow pavements with higher stiffness on the top of the pavement showed load sensitive. Sharp (1999) conducted Accelerated Loading Facility (ALF) tests on a test section with high asphalt content mix with the lower base. The results demonstrated that these layers could be used in thinner asphalt structures and higher asphalt content improves fatigue performance. Hugo (1999) completed Texas Mobile Load Simulator (TxMLS) tests to evaluate the widely used district pavement design utilizing local gravel siliceous from river flex-base as thin asphalt surfacing. Zhou and Scullion (2002) conducted a program named VESYS on the basis of the results originated from APT to predict rutting performance. Epps (2003) conducted APT research using TxMLS and MMLS3 (one-third scale Model Mobile Load simulator) to analyze stress distribution.

Hugo and Epps (2004) stated that APT is preferable because it not only can simulate the real traffic condition but also can achieve long-term in-service pavement performance in a compressed short period under many load applications. Xu and Meng (2004) conducted ALF tests to evaluate the rutting resistance of pavements. They suggested that the rutting resistance of asphalt pavement with flexible base was equivalent to pavements with semi-rigid base. The research investigated the performance behavior for validation in a mechanistic performance design. Meng (2008) recommended to evaluate rut upheaval deformation under ALF tests since there was good consistency between rutting deformation volume and rutting depth. Saevarsdottir (2012) discussed the results obtained from an Accelerated Pavement Test (APT) using a Heavy Vehicle Simulator (HVS) performed at the Swedish Road and Transport Research Institute (VTI) test facility in Linköping, Sweden, between May and September 2005.

APT has been used to calibrate Mechanical-Empirical models over years. Johanneck et al. (2011) evaluated measured data from MnRoad for Asphalt concrete (AC)/ Portland cement concrete (PCC) pavements and the thermal characteristics accounted for Mechanistic-Empirical Pavement Design Guide (MEPDG), and pointed out thermal inputs should be a part of a process of local calibration and adaptation of the MEPDG. Gibson et al. (2012) used ALF to examine the performance of unmodified, polymer modified asphalt binders and quantified the capabilities of MEPDG incorporated models to predict rutting and fatigue cracking of modified asphalts that were not captured in the calibration data from the Long-Term Pavement Performance program. John et al. (2012) utilized APT to calibrate ME analysis models, and the calibrated ME models is used to solve problems with accelerated pavement testing results. Coleri e al. (2012) calibrated Cal Mechanistic Empirical (ME) analysis rutting prediction models using the results of Heavy Vehicle Simulator (HVS) experiments.

To date, more and more concerns are focused on correlation between APT and Long-Term Pavement Performance (LTPP) database. John et al. (2004) proposed the need for a protocol to standardize the methodology used for establishing and monitoring LTPP sections in conjunction with APT sections was identified, and developed such a protocol for the South African Heavy Vehicle Simulator (HVS) APT program. Anochie-Boateng, et al. (2012) evaluated six years of APT and LTPP data from two sections in South Africa, compared the APT data with LTPP data, and calibrated the pavement behavior models obtained from APT to the realistic pavement outcomes. Anochie-Boateng (2016) discussed more than 10 years APT and LTPP data in the Western Cape province of South Africa. In addition, they found that the APT rutting data needed to be shifted by a factor of five in order to obtain similar LTPP (real life) rutting data, while the surface deflection should be increased by 50 % from the APT data to get an equivalent LTPP data for the low volume traffic. It should be noted that all the calibrations between APT, MEPDG and LTPP data are based on the specific material and local climate. Different locations result in different calibrations.

Typical full-scale APT facilities can be classified into two categories: 1) Test Tracks which are the specially designed and constructed pavement sections subjected to actual

trucks driven through, for instance: WesTrack, Mn/Road, NCAT and SMART Road. 2) Accelerated loading systems, which are specially designed to simulate truck loads moving on the existing or specially paved pavement sections, such as Cal/APT HVS, FHWA ALF, Texas MLS i.e. These full scale APT facilities are capable of providing close-to-field loading and ambient conditions that prompt insight of pavement material properties under realistic conditions.

Since there are increasing interests in APT for evaluating potential materials, new design and features, by now, a wide variety of APT facilities are active and operational in the world, and most of them are constructed at a fixed site. Based on the previous studies (Hugo & Martin, 2004; Sharp, 2004; Steyn, 2012), Table 1-1 tabulates the full-scale APT facilities in different countries over the world by 2016, with the updated information for the APT systems implemented recently.

Table 1-1 APT facilities over the world

APT in U.S. and Canada

Facility Name	Load Magnitude	Tire Details	Load frequency	Linear/Nonlinear (circular, elliptical)	Uni-/Bi-directional	Speed Range
California(CAL/APT)	6.7 to 45 kip (30 to 200 kN)	Dual—(11R22.5) Super single—(425/65R22.5) New wide-base tires—(445/50R22.5 and 455/55R22.5)	10,000 passes unidirectional and 20,000 passes bi-directional per 24 hours	Linear	Both	2 to 12.4 mph (3 to 20 km/h)
U.S. Army ERDC–CRREL(HVS)	2.2 to 46 kip (10 to 205 kN)			Linear	Both	Up to 8 mph (12.8 km/h)
Florida(HVS)	Up to 45 kip (200 kN)			Linear	Both	Up to 8 mph (12.8 km/h)
The U.S. Army ERDC–GSL(WES)	2.2 to 99 kip (10 to 440 kN)			Linear	Both	0.6 to 7.5 mph (1 to 12 km/h)
VDOT-VTTI(HVS)	Up to 45 kip (200 kN)			Linear	Both	Up to 8 mph (12.8 km/h)
FHWA ALF	9.9 to 16.6 kip (44 to 74 kN)	Dual—(11R22.5) Super single—(425/65R22.5) New wide-base tires—(445/50R22.5 and 455/55R22.5) Typically between 100 and 120 psi (690 kPa to 827kPa)	35,000 per week	Linear	Uni-direction	10 to 11 mph (16 to 18 km/h)
Louisiana ALF	9 to 13.5 kip (40 to 60 kN)			Linear	Uni-direction	10 to 12 mph (16 to 19 km/h)
Ohio APLF	8-30kip	Standard single, Standard duals, and wide-base single	250/ hour for unidirectional tests, 500/ hour for	Linear	Both	5mph (8 km/h)

			bidirectional tests			
Indiana DOT ,Purdue University, APTF	20 kip (89 kN) for half axle	Dual—(11R22.5) Super single—(425/65R22.5) Typically between 100 and 120 psi (690 kPa to 827 kPa)		Linear	Bi-directional	5 to 10 mph (8 to 16 km/h)
University of Illinois at Urbana Champaign, ATLAS	0 -80 kips	Truck (single, dual axle)		Linear	Both	10 mph
Texas Mobile Load simulator (MLS), Texas Accelerated Pavement Test Center in Austin	42kip	305/70 R22.5	Up to 6000 per hour	Linear (loop)	Uni-direction	12.5mph (20km/h)(8800axle loads per hour)
Kansas State University - CISL	1 to 5 kip (5 to 22 kN) single axle Double for tandem axle	Conventional over the road		Linear	Bi-directional	5 to 6.8 mph (8 to 11 km/h)
FAA(NAPTF)	901 kip (4 008 kN) (75 kip (334 kN) per wheel)	52*21.0R22, up to 250psi		linear	both	15 mph (24 km/h) maximum
Canada						
The Integrated Road Research Facility	Real truck loads	Dual—(11R22.5) Super single—(425/65R22.5)		Test Track	Uni-direction	Up to 50 mph (80 km/h
Waterloo						

Test Track					
AASHO Road Test	Real truck loads	Real traffic 8 axles on 5 trucks (40 axles total) Live traffic	Real truck	Uni-direction	Up to 50 mph (80 km/h)
Westrack					
NCAT					
MnRoad					
Canada(Waterloo)					
Smart road(Virginia)					

APT in Europe

Facility Name	Load Magnitude	Tire Details	Test Frequency (max)	Linear/Non linear (circular, elliptical)	Uni-/Bi-directional	Spped Range
Denmark(DRTM)	40-130 kN	single or dual tires	900/hour	Linear	Both	30 km/h (18.6 mph)
France(LCPC)	40 to 140 kN		2400/hour	Circular	Uni-directional	105 km/h (65 mph)
Germany(BASt)	0-140 kN		8700/hour			simulate traffic at approximately 20 km/h
Germany (MLS10)	60-150 kN	single or dual tires	6000/hour	Linear	Uni-directional	22km/h
The Netherlands (LINTRACK)	30-200 kN	super single, single axle, dual tire	1000/hour	Linear	Both	20 km/h (12.5 mph)
The Technical University of Iassy, Romania (Road Ring Track)				circular	Uni-directional	
Vuis-Cesty in Bratislava, Slovakia (KSD Circular Track)		Truck wheel		circular	Uni-directional	10 and 50 km/h (7 and 31 mph)

Spain(Test track)	110 and 150 kN (24,200 to 33,000 lb)	Dual—(11R22.5) Super single—(425/65R22.5) New wide-base tires—(445/50R22.5 and 455/55R22.5)	400/hour			60 km/h (37 mph)
Switzerland Ecole Polytechnique Federal de Lausanne (EPFL) HVS (HVS)	Up to 45 kip (200 kN)		Up to 500/h	Linear	Both	Up to 8 mph (12.8 km/h)
Switzerland Ecole Polytechnique Federal de Zurich (EPFZ)				Circular		
Switzerland Swiss Federal Laboratories EMPA and Institute of Technology ETH (MMLS10)	80-130 kN	Dual tired 295/60 R22.5 single or dual tire	6000/hour	Linear	Uni-	22km/h
Sweden, VAG-OCH Transportforskningsinstitut (VTI)	60 to 220 kN	Single or dual tire	1100/hour	Linear	Both	12km/h
United Kingdom Transport Research Laboratory (PTF)	40-200 kN	single or dual tire	1000/hour	Linear	Both	20 km/h (12.5 mph)
United Kingdom University of Nottingham (PTF)	0-12 kN	Single or dual tire	800/hour	Linear	Both	12km/h

APT in Oceania

Facility Name	Load Magnitude	Tire Details	Frequency(max)	Linear/Nonlinear (circular, elliptical)	Uni-/Bi-directional	Speed Range
Australasia(ALF)	80 -200 kN (8,800 to 17,600 lb)	370/hour	370/hour	Linear	Uni-directional	20 km/h (12.5 mph)

New Zealand(CAPTIF)	21 to 60 kN (4,600 to 10,150 lb)	single, wide single and dual-tire		Circular	Uni-directional	50 km/h (31 mph)

APT in Asia

Facility Name	Load Magnitude	Tire Details	Frequency(max)	Linear/Nonlinear (circular, elliptical)	Uni-/Bi-directional	Speed Range
China						
Research Institute of Highway at Chongqing(CCRDI_CTT)	100-150 kN	single or dual tires	3600/hour	Circular	Uni-directional	60 km/h (Max)
Nanjing, Southeast University(CRT)	40 to 140 kN	single or dual tires	2500/hour	Circular	Uni-directional	105 km/h (65 mph)
Nanjing, Southeast University (MLS66)	80-150 kN	single or dual tires	6000/hour	Linear	Uni-directional	22 km/h
Shanghai, Tongji University (MLS66)			6000/hour			
Transportation Research Institute of Liaoning Province at Shenyang (MLS66)						
Beijing, Research Institute of Highway (ALF)	80-200 kN	super single, dual tire	400/hour	Linear	Both	25 km/h
Changsha University of Science& Technology	30-70 kN	super single, dual tire		Linear	Both	30 km/h
Shandong Jiaotong University	Up to 400 kN	Two axle, super single, dual tire		Linear	Both	27 km/h
Xi'an Chang'an University(HVS)	30-200 kN	12R22.5 58 to 145 psi	Up to 500/ hour	Linear	Uni-directional	2 to 12.8 km/h)

		(400 to 1 000 kPa),				
University of Science & Technology Beijing (in construction)	Truck single or dual tires			Linear and Circular		
Japan						
PWRI Pavement Text Field	48-157 kN		255/hour			
Nippon Expressway Research Institute Company Limited(ALES)	4-70 kN	single or dual tires	15000/hour	Circular	Uni-directional	100km/h
Materials and Geotechnical Engineering Research Group of PWRI	45-125 kN	single tire, two axles dual tires	120/hour	Linear	Uni-directional	30km/h
Techno Center of Kajima road co,.ltd.	100-140 kN	single or dual tires	190/hour	Linear	Uni-directional	5km/h
Korea						
Hanyang university	70-250 kN	single or dual tires	300/hour	Linear	Uni-directional	12km/h
Central Road Research Institute (ICRRI)	30-100 kN	12R22.5 Truck tire		Linear	Both	9-15km/h

APT in Africa

Facility Name	Load Magnitude	Tire Details	Frequency(max)	Linear/Nonlinear (circular, elliptical)	Uni-/Bi-directional	Speed Range
Gauteng Department of Public Transport(HVS)	30-205 kN	single or dual tires	1000/hour	Linear	Both	13 km/h
MLS Test Systems Pty Ltd, Stellenbosch	80-160 kN	single or dual tires	6000/hour	Linear	Uni-directional	22 km/h

APT in South America

Facility Name	Load Magnitude	Tire Details	Frequency(max)	Linear/Nonlinear (circular, elliptical)	Uni-/Bi-directional	Speed Range
Brazil (ALF)	0-68.6 kN	single or dual tires	900/hour	Linear	Uni-directional	12 km/h
Federal University of Rio Grande do Sul(PTF)	20-130 kN	single or dual tires	250/hour	Linear	Uni-directional	6 km/h

However, both the test tracks and full-scale accelerated loading facilities are commonly associated with the high initial investment and operational costs as Table 1-2. Regarding of this, the small-scale laboratory wheel tracking equipment is applied to test the asphalt mixtures properties on laboratory compacted samples, such as Hamburg wheel track test, Asphalt Pavement Analyzer (APA) originally known as Georgia Wheel Tracking Device (GWTD), and French rutting tester (FRT). Laboratory wheel tracking tests, also referred as simulative tests, adopt a small rolling loaded wheel to run repeatedly across a prepared asphalt mixture specimen, to measure and predict rutting, fatigue, moisture susceptibility and stripping performance. The performance of the test specimen is correlated to the in-field performance of the pavement using the same material. WesTrack Forensic Team study (WesTrack Forensic Team, 1998) indicates that the 7 mm rut depth APA, 14 mm rut depth in Hamburg Weel-Tracking Device, 10 mm rut depth results in French Rutting Tester, 6.35 mm rut depth in PURWheel, result in a field rut depth of 12.5 mm, which is normally regarded as failure criteria in actual pavement (Zhang et al. 2001). The summary information of laboratory wheel tracking devices is presented in Table 1-3, which is updated based on previous studies (Buchanan, 1997; Cooley et al. 2000; Brown et al. 2001; Zhang et al. 2002;Zhang et al. 2005; Howard et al. 2010).

Table 1-2 Cost comparison between Full scale APT and MMLS 3

Items	MMLS	Full scale APT
Equipment &Facilities	$120000	$2-3 Million
Test Cost	$1000	$80,000
Time	2-3 Weeks	1-2 Years

APA, developed from the Georgia Loaded Wheel Tester, is a second generation wheel tracking device. A loaded aluminum wheel is used in APA to track forth and back across a pneumatic rubber hose over an asphalt mixture specimen. This wheel tracking device is commonly set for 8,000 load cycles using a 100 lb (445 N) load and a 100 psi (689 kPa) hose pressure, and used to test performance of laboratory prepared Hot Mixture Asphalt (HMA) under controlled environmental condition. The test specimens can be prepared in form of either beam or cylinder.

Table 1-3 Laboratory wheel tracking device

Tests Method	Sample size	Tire size	Wheel type	Load magnitude	Temperature	Load frequency	Required load cycles(test duration)
Asphalt Pavement Analyzer (APA)	Cylinder 150mm diameter ×75 mm height or beam 300mm ×125mm ×75mm height	inside diameter of 19.0 mm and the outside diameter of hose as 29.5 mm	Aluminum wheel on pressurized rubber hose	Up to 534 N, pressure up to 827 kPa	-9 to 80 ℃	Up to 120 loads/ min	8000 (2 hours 13min@ 60 cycles/min)
Hamburg Wheel-Tracking Device	Beam 320 mm× 260 mm ×80mm height Cylinder 150 mm diameter× 115mm height	204 mm diameter, 47 mm wide	Steel wheel	705 N load	Wet, 50℃	532 loads/min or reach 20 mm deformation	20,000 (6 hours 18 mins)
French Rutting Tester(LCPC)	Beam 500 mm×180 mm× 100mm height	400mm diameter, 90 mm wide	Pneumatic rubber tire	5 kN load applied to a pneumatic tire inflated to 87 psi (600 kPa)	60 ℃	67 cycles/min	30,000(8 hours)
Purdue University Laboratory Wheel Tracking Device (PURWheel)	Beam 310mm× 290mm×38, 51 or 76 mm height	100 mm diameter, 50 mm wide	Pneumatic rubber tire	1.75kN loadd, Up to 860 kPa	Up to 65 ℃	60 cycles/min	20,000(5hours 30 mins) or 20mm deformation
Rotary Loaded Wheel Tester(RLWT)	Cylinder 150mm diameter ×75 mm height	Steel wheel	Contact pressure up to 690 kPa	125 N load	50 ℃	70 cycles/min	16000 (4hours)
Wessex Dry Wheel Tracker Device	Cylinder 150mm diameter ×75 mm height	Rubber tire	Thick rubber	710 N	50 ℃	26 cycles/min	1000 (45 mins) or reach 15 mm deformation

Model Mobile Load Simulator (MMLS 3)	Slab up to 1200mm length, up to 240mm height	300 mm diameter by 80 mm width	Pneumatic rubber tire	Up to 2.8 kN, up to 827 kPa	Up to 65 ℃	Up to 7200 loads/h	Depends on needs
Wheel Rutting Tester	300 mm× 300mm × 50 mm height	200mm diameter× 50 mm width	Pneumatic rubber tire	30 kN up to 700 kPa	60 ℃	42 cycles/min	60 mins

But in terms of previous studies, these laboratory tests are not conducted under a controlled prototype loading at controlled prototype damage cumulative conditions which are similar to the realistic field conditions (Lee 2004; Bhattacharjee et al. 2011). Moreover, the laboratory specimens are normally produced by either gyratory compactor or vibratory compactor, which are still being questioned for their effectiveness in preparing compacted specimens similar to the field compact conditions. Additionally, none of these tests is performed with the presences of base or subgrade material and most of them use bi-direction loading. For these reasons, even if the laboratory simulative test is much cost friendly, the test conditions under these wheel-tracking devices are not compatible to the field conditions.

1.2 Background

Differentiating from small scale laboratory wheel tracking devices, Model Mobile Load Simulator 3(MMLS 3) is a third scale accelerated trafficking system, which can be set up very conveniently either in the field on an actual pavement or in the laboratory on a model pavement structure. It is an effective wheel-tracking device, which can provide close- to- field conditions on layered pavement structure with a unidirectional vehicle-load simulator using continuous loop for trafficking, assembled with pneumatic tires with tire pressure up to 800 kPa, which is approximate to actual truck tire pressure. The variables can be controlled in MMLS 3 test includes but not limited to, lateral wander, wheel load magnitude, load speed, contact stress, ambient environmental conditions.

As compared to the full-scale APT facilities, MMLS 3 is not only capable of providing similar to field conditions, but has high loading frequency, much lower initial and operational costs, as shown in Table 1-2. In general, full scale APT can only apply up to 5000 load cycles per day, while MMLS 3 is capable of running 7200 loads per hour.

As stated above, MMLS 3 somewhat has similar functionality as a full-scale APT does, but in a small scale, resulting in better efficiency and economy. The comparisons between test results of ALF, MMLS 3, APA can validate the small scaled APT as screen solutions before further full-scale APT implementation to benefit APT efficiency and economy. There are approximately 25 MMLS 3 units being used over the world, and previous studies have pointed out MMLS3 has the potential to predict the performance of pavements in terms of fatigue performance and permanent deformation (Martin Epps et al., 2002; Smit et al., 2003; 2004; Walubita et al. ,2002; Lee &Kim 2004; Bhattacharjee et al. 2011).

Eleven composite asphalt pavement lanes consisting of different content percentage of Recycled Asphalt Pavement (RAP) and Reclaimed Asphalt Shingle (RAS) mixtures employing diverse warm mix asphalt technologies and binder grades were constructed at Turner-Fairbank Highway Research Center (T-F). Prior to the construction of asphalt

pavement layer, the previous experiment's granular aggregate base (GAB) was reconditioned by milling the top 8-inches GAB, and subsequently was paved and compacted at the optimum moisture content. The asphalt surface layer was constructed with two lifts of 50 mm height, and for quality control purpose, the compaction was monitored with a nuclear density gauge (Gibson et al. 2016). A Masonite® Separation Platform system was developed to enable the slabs to be extracted from the pavement layers for subsequent MMLS 3 trafficking test. The detailed implementation procedure was presented at the ISAP international seminar in Sun City South Africa (Hugo et al. 2015). To evaluate the material behaviors and pavement performance under different APTs, three slabs (two from Lane 9 and one from Lane 5) with 100 mm height were successfully extracted and transported to Blacksburg for MMLS 3 trafficking. In order to achieve comparable stress conditions, the 100 mm slabs were sliced into thicknesses of nominally 50 mm, as top lift and bottom lift for MMLS3 trafficking. Each slab could then be placed on neoprene layers lying on a concrete slab as test pavements. The neoprene is a substitute for the aggregate base with similar modulus, which facilitates the pavement construction because it is easy to place or replace the base layer before or after the test. The smoothness of the slab was selected to be ± 2 mm / 2 m. A layer of sand was used to achieve this where necessary (Hugo et al. 2015; Huang et al. 2016). The three slabs are hereinafter denoted as Lane 9 A, Lane 9 B and Lane 5, respectively. In addition, four specimens (denoted as Lane5 top, Lane 5 bottom, Lane9B top, Lane9B bottom lift) cut from the slabs were performed for APA tests with chamber temperature of 20 ℃ in asphalt laboratory at Virginia Transportation Research Council (VTRC).

1.3 Motivation of the Research

Accelerated pavement testing (APT) is an effective method to evaluate various types of materials characteristics and pavement performance. APT helps engineers and researchers to obtain the structural response and pavement performance under a controlled and accelerated damage conditions in a compressed limited time. APT can be used to identify and evaluate the new materials and structural designs prior to the practical implementation. With the aim to study the pavement material response and performance under real field condition, numerous APT facilities are developed and applied across the world. Nevertheless, the differential APT facilities are assembled with various loads magnitudes, trafficking speed and frequency, wheel assemble, and tire configurations. Besides, several scaled down wheel tracking devices are widely used in pavement performance evaluation, particularly in rutting resistance. However, full scale APTs are commonly in conjunction with high cost, time and labor consuming, while the scaled down wheel track devices are questionable for whether the test conditions and specimens preparations are close to the field conditions(Anochie-Boateng et al. 2012). Therefore, there is a great need of a systematic analysis and correlations of the different scaled APTs.

1.4 Objective and Scope

1. The objective of this thesis is to investigate the structure response and pavement performance under f-s ALF, MMLS 3 and APA in terms of seismic modulus, strain under dynamic loads, rutting depth between full-scaled ALF and one-third scaled MMLS 3, and APA for the same HMA slabs. The aim is to validate the application of the reduced scale MMLS3 as an effective experimental equipment to test material under small-scale prototype model with test conditions comparable to the full-scale field conditions. To verify MMLS3 is a useful method for doing screen testing before establishing full-scale testing protocols or scenarios as and when desired or required.

2. Investigate the feasibility of MEPDG model in MMLS 3 test, and calibrate the MEPDG model for the MMLS 3 test based on the test results of the six slabs.

3. Implement the IOT based wireless sensor network in the laboratory MMLS3 test, to investigate the feasibility of such a proposed system for potential long-term wheel load information and pavement performance monitoring.

4. Evaluate the effects of load magnitude, load speed, and temperature on pavement response in APT, and help pavement researchers and practitioners have a systemic understanding of APT.

1.5 Reference:

Addis, R.R.,(1989) "Experience of Pavement Instrumentation at TRRL Measurements: State of the Art Pavement Response Monitoring Systems for Roads and Airfields". *Special Report 89-23*, U.S. Army Corps of Engineers, Vicksburg, Miss.

Anochie-Boateng, J. K., Fisher, C., Jones, D., & Truter, L. (2012). "Calibrating full-scale accelerated pavement testing data using long-term pavement performance data." *Advances in Pavement Design through Full-scale Accelerated Pavement Testing*, 445.

Anochie-Boateng, J. K., Steyn, W. J., Fisher, C., & Truter, L. (2016). "A Link of Full-Scale Accelerated Pavement Testing to Long-Term Pavement Performance Study in the Western Cape Province of South Africa." *In The Roles of Accelerated Pavement Testing in Pavement Sustainability (pp. 67-79)*. Springer International Publishing.

Banerjee, A., J.P. Aguiar-Moya, and J.A. Prozzi(2009), "Texas Experience Using LTPP for Calibration of the MEPDG Permanent Deformation Models," Preprint CD, Preparedfor the 88th Annual Meeting of the Transportation Research Board, Washington, D.C., Jan. 11–15.

Bhattacharjee, S., Gould, J. S., Mallick, R. B., & Hugo, F. (2004). "An Evaluation of use of Accelerated Loading Equipment for Determination of Fatigue Performance of Asphalt Pavement in Laboratory". *International Journal of Pavement Engineering*, 5(2), 61-79.

Brown, E. R, Prithvi S. K, and Zhang, J. (2001). "Performance testing for hot mix asphalt." *National Center for Asphalt Technology Report* 01-05.

Buchanan, M. S., (1997). "An Evaluation of Laboratory Wheel-Tracking Devices," Report Prepared for National Asphalt Pavement Association, National Center for Asphalt Technology.

Corté, J.-F., et al., "Study of Rutting of Wearing Course on the LCPC Test Track*," Proceedings of the 8th International Conference on Asphalt Pavements*, Seattle,Wash., Aug. 10–14, 1997.

Cooley, L. A., Kandhal, P. S., Buchanan, M. S., Fee, F., & Epps, A. (2000). "Loaded wheel testers in the United States: State of the practice." *Transportation Research Board, National Research Council*.

Coleri, E., Wu, R. Z., Harvey, J. T., & Signore, J. (2012). "Calibration of incremental-recursive rutting prediction models in CalME using Heavy Vehicle Simulator experiments*." In Advances in Pavement Design Through Full-Scale Accelerated Pavement Testing-Proceedings of the 4th International Conference on Accelerated Pavement Testing* (pp. 471-481).

Epps, A.L., F. Hugo, L.F. Walubita, and N. Bangera,(2003) "Comparing Pavement Response and Rutting Performance for Full-Scale and One-Third Scale Accelerated Pavement Testing," *Journal of Transportation Engineering*, Vol. 129, No. 4, pp. 451–461.

Gibson, N., Qi, X., Shenoy, A., Al-Khateeb, G., Kutay, M.E., Andriescu, A., Stuart, K., Youtcheff, J. and Harman, T. (2012). "Performance testing for Superpave and structural validation (No. FHWA-HRT-11--45)".

Harvey, J. T., Jones, D., Lea, J. D., Wu, R. Z., Ullidtz, P., & Tsai, B. (2012). "Use of mechanistic-empirical performance simulations to adjust and compare results from accelerated pavement testing". *Advances in Pavement Design through Full-scale Accelerated Pavement Testing*, 461.

Howard, I. L., Doyle, J. D., White, T. D., Ivy, J., & Booth, O. (2010). "PURWheel Laboratory Wheel Tracker." Mississippi State University and Innovative Broadcast Services, CMRC M 10-2 Version 1.

Huang,Y., Hugo, F., Steyn, W., Xiong, H, and Wang, L. (2016). "Comparative Evaluation of Performance of Warm Mix RAP Asphalt Under Accelerated Unidirectional Wheelload Trafficking". *Accelerated Pavement Testing International Conference*, San José, Costa Rica.

Hugo, F., K. Fults, D.-H. Chen, A. Smit, and J. Bilyeu, "An Overview of the TxMLS Program and Lessons Learned" (CD-ROM), *Proceedings of the First International Conference on Accelerated Pavement Testing*, Reno, Nev., Oct. 18–20, 1999.

Hugo, F. and A. Epps Martin, (2004) "Synthesis of Highway Practice 325: Significant Findings from Full-Scale Accelerated Pavement Testing," *Transportation Research Board of the National Academies*, Washington, D.C., 201 pp.

Hugo, F., Huang, Y., Xiong, H., Wang, L., Steyn, W. (2015). "Lessoned Learned During the First Application of MSP for Extracting Asphalt Slabs in Comparative Testing of Fatigue Performance of Warm Mix RAP Asphalt MMLS3 Trafficking". *ISAP 2015Seminar*, SunCity, South Africa.

Johanneck, L., Clyne, T., Tompkins, D., & Khazanovich, L. (2011). "Evaluation and Local Calibration of MEPDG EICM Model Using MnRoad Data." *In 90th Annual Meeting of the Transportation Research Board*, Washington, DC.

Jones, D., Paige-Green, P., & Sadzik, E. (2004). "The development of a protocol for the establishment and operation of LTPP sections in conjunction with APT sections." *In International Conference on Accelerated Pavement Testing*, 2nd, 2004, Minneapolis, Minnesota, USA.

Kadar, P. & P.D. Walter (1989), "The Performance of Slag Roadbases Under Accelerated Trafficking: Results and Findingsof the Prospect ALF Trial," *Research Report ARR 170, Australian Road Research Board*, Vermont South,Victoria, 1989.

Kekwick, S.V., H.L. Theyse, and E.G. Kleyn (1999), "Development of a Long-Term Accelerated Pavement Testing Programme and Structural Design Models" (CD-ROM), *Proceedings of the First International Conference on Accelerated Pavement Testing*, Reno, Nev., Oct. 18–20.

Lee, S.J. and Kim, Y.R. "Development of Fatigue Cracking Test Protocol and Life Prediction Methodology Using the Third Scale Model Mobile Load Simulator", *Proceedings Fifth International RILEM Conference*, Limoges, France, May, 2004.

Martin Epps, A., Ahmed, T., Little, D.C., Hugo, F., Poolman, P. and Mikhail, M. (2002) "Performance prediction with the MMLS3 at Wes-Track", *CD-Rom of Proceedings of the Ninth International Conference on Asphalt Pavements Copenhagen*, 17–22 August. 2002

Metcalf, John B. "Application of full-scale accelerated pavement testing" (1996). *Vol. 235. Transportation Research Board*.

Meng,Q. Chen,J., Li,L., (2008). "Research on Hump of Asphalt Mixture Pavement by Accelerating Loading Facility." *Highway Engineering*, 33(4), 15~19. (in Chinese)

Nagabhushana, M. N., Khan, S., Mittal, A., & Tiwari, D. (2016). "Potential Benefits of APTF for Evaluation of Flexible Pavement for Its Permanent Deformation Behaviour." *In The Roles of Accelerated Pavement Testing in Pavement Sustainability (pp. 227-239).* Springer International Publishing.

Saeed, A., & Hall, J. W. (2003). "Accelerated pavement testing: data guidelines." *NCHRP Report*, No. 512. Transportation Research Board, 57p.

Saevarsdottir, T., & Erlingsson, S. (2012). "Evaluation of flexible pavement structure in an accelerated pavement test." *Advances in pavement design through full-scale accelerated pavement testing*, 237-248.

Sharp, K.G., J.R. Johnson-Clarke, and D.W. Fossey, (1999) "A Review of the Australian ALF Program" (CD-ROM), *Proceedings of the First International Conference on Accelerated Pavement Testing,* Reno, Nev., Oct. 18–20.

Sharp, K. G. (2004). "Full scale accelerated pavement testing: a southern hemisphere and Asian perspective". *In International Conference on Accelerated Pavement Testing*, 2nd, 2004, Minneapolis, Minnesota, USA.

Sivasubramaniam, S., & Haddock, J. E. (2006). Validation of Superpave mixture design and analysis procedures using the NCAT test track. Joint Transportation Research Program, 252.

Smit, A. de F., Hugo, F.R. and Dale Powell, B. (2003) "Model mobile load simulator testing at National Centre for asphalt technology test track", Journal of the Transportation Research Board, Transportation Research Record 1832, Washington, DC, USA.

Smit, A. de F., Hugo, F., Poolman, P., Powell, R.B. and Bacchi, C., "Distress of hot mix asphalt on theNCAT test track due to accelerated wet trafficking", Paper accepted for presentation and publication at the Second International APT Conference, Seattle, USA 2004.

Steyn, W. J. (2012). "Significant findings from full-scale accelerated pavement testing (Vol. 433)." *Transportation Research Board.*

Steyn, W. J., & Hugo, F. (2016). "Perspectives on Trends in International APT Research". *In The Roles of Accelerated Pavement Testing in Pavement Sustainability* (pp. 211-225). Springer International Publishing.

Walubita, L.F., Hugo, F. and Epps Martin, A.L. (2002) "Indirect tensile fatigue performance of asphalt after MMLS trafficking under different environmental conditions", *Journal of the SA Institution of Civil Engineering*, Johannesburg, South Africa 44, November 3.

WesTrack Forensic Team (1998), "Performance of Coarse-Graded Mixes at WesTrack – Premature Rutting," Final Report.

Zhang, J., Cooley Jr, L., & Kandhal, P. (2002). Comparison of fundamental and simulative test methods for evaluating permanent deformation of hot-mix asphalt. Transportation Research Record: Journal of the Transportation Research Board, (1789), 91-100.

Zhang, J., Brown, E. R., Kandhal, P. S., & West, R. (2005). "An overview of fundamental and simulative performance tests for hot mix asphalt." *Journal of ASTM International*, 2(5), 1-15.

Zhou, F., Scullion, T., & Sun, L. (2004). "Verification and modeling of three-stage permanent deformation behavior of asphalt mixes." *Journal of Transportation Engineering,* 130(4), 486-494.

Xu, Q., and Meng, S., 2004. "Study on Accelerated Pavement Testing on Flexible Base Asphalt Pavement." *Proceedings on Symposium about Road Engineering in 2004, 205~210.*

Chapter 2 ALF, MMLS 3, AND APA TEST RESULTS

2.1 ALF, MMLS 3, and APA introduction

The full-scale Accelerated load facility (ALF) studied in this work is located in Turner-Fairbank Highway Research Center, McLean, VA, which can be applied with up to 35,000 simulated axle passes per week, and the wheel load can be varied from 33 kN to 84 kN. ALF is capable of applying a rolling wheel load on a 13.7 m test length of test pavement. An electric motor provides unidirectional loading passes at constant speed up to 19km/h. An infrared heating system is used to provide desired pavement temperature and the thermocouples are employed to monitor the temperature changes. The wheels feature can be set up for lateral wander and the tire configurations can be interchanged, such as standard dual or super single (Pavement Testing Facility).

Laboratory wheel tracking tests commonly refer to experiments performed on laboratory compacted samples using various wheel tracking devices, aimed at stimulating realistic wheel loading in small scale, for instance the Asphalt Pavement Analyzer (APA), Hamburg wheel tracking device, French Rutting Tester, Purdue University Laboratory Wheel Tracking Device (PURWheel), and one- third Model Mobile Load Simulator (MMLS 3 also known as MLS 11 since Jan 2016). It should be noted that the samples of the aforementioned wheel tracking devices (except MMLS 3) are fabricated as either vibratory compacted beams or circular cylinders compacted using Superpave gyratory, which is still under debate whether it can compact the specimen similar to field compacted specimen or over compacted. Besides, few of these simulative tests is performed with the presence of underlying base or subgrade layers and most of them use bi-direction loading instead of uni-direction. For these reasons, even if the laboratory simulative test is much cost friendly, the test conditions under these wheel tracking devices are not compatible to the field conditions. However, MMLS3 is an effective wheel tracking device, which can provide close- to- field conditions on pavement structure and can be conducted both in filed and laboratory. It is a third scale unidirectional vehicle-load simulator using continuous loop for trafficking, assembled with pneumatic tires with tire pressure up to 800 kPa, which is close to actual truck tire pressure. APA is a second generation device derived from the Georgia Load Wheel Tester, with a loaded aluminium wheel forth and back across a pressurized linear hose over a HMA sample, typically used to measure and predict rutting. The APA is used to test performance of laboratory prepared Hot Mixture Asphalt (HMA) under controlled environmental condition, using a 100 lb and a 100 psi hose pressure. The test specimens can be prepared in form of either beam or cylinder (Pavementinterative).

The objective of this paper is to investigate the pavement response and performance under f-s ALF, MMLS 3 and APA, and to determine the correlations of test results from these differential scaled APT facilities. This study is driven by the goal of enhancing the economics of APT testing. For this comparison study, eleven composite asphalt pavement lanes consisting of different content percentage of Recycled Asphalt Pavement (RAP) and Reclaimed Asphalt Shingle (RAS) mixtures employing diverse warm mix

asphalt technologies and binder grades, were constructed at Turner-Fairbank Highway Research Center (T-F). Prior to the construction of asphalt pavement layer, the previous experiment's granular aggregate base (GAB) was reconditioned by milling the top 8-inches GAB, and subsequently was paved and compacted at the optimum moisture content. The asphalt surface layer was constructed with two lifts of 50 mm height, and for quality control purpose, the compaction was monitored with a nuclear density gauge (Gibson et al. 2016). A Masonite® Separation Platform system was developed to enable the slabs to be extracted from the pavement layers for subsequent MMLS 3 trafficking test. The detailed implementation procedure was presented at the ISAP international seminar in Sun City South Africa (Hugo et al. 2015). In this comparative evaluation study, three slabs (two from Lane 9 and one from Lane 5) with 100 mm height were successfully extracted and transported to Blacksburg for MMLS 3 trafficking. The three slabs are hereinafter denoted as Lane 9 A, Lane 9 B and Lane 5, respectively. In addition, four specimens (denoted as Lane5 top, Lane9A top, Lane9B bottom and Lane9B Top lift) were conducted under APA tests with chamber temperature of 20 ℃ in asphalt laboratory at Virginia Transportation Research Council (VTRC). The instrumentations of AFL, laboratory MMLS3 test and APA tests are implemented as Figure 2-1.

Figure 2-1 ALF, MMLS3 and APA test instrumentation

The experimental design of Lane9 and Lane5 asphalt mixture is shown in Table 2-1. As can be seen, these two lanes were constructed using the same virgin asphalt binder (PG 64-22), different RAP content in weight (40 % and 20%) and two mixing process technologies (HMA and WMA). Gibson et al. (2016) conducted a series of laboratory

tests to specify the mixture volumetric and the property of asphalt mixtures for these two lanes, as presented in Table 2-2.

Table 2-1 Experimental design (Gibson et al. 2016)

ALF Test Lane	RAP Content in Weight	Virgin Binder PG	Production Temperature (℃)	WMA Process
5	40%	64-22	149 to 160	-
9	20%	64-22	116 to 132	Water

Table 2-2 Prosperity of Lane 5 and Lane 9 (Gibson et al. 2016)

Lane	**5**	**9**
G_{mm}	2.743	2.736
Air Voids	5.2	3.7
G_{mb}	2.601	2.601
P_b	4.60	4.98
VMA	15.9	15.1
VFA	67.3	75.5
DB Ratio	1.38	1.15
Core AV	7.4	5.2
Specified PG	64-22	64-22
Virgin PG (tank)	66-26	65-24
Recovered PG	86-12	77-18
Avg. Asphalt Thick.(in)	3.9	4.0

The HMA mixtures were Superpave 12.5mm nominal maximum aggregate size designed at 65 gyrations compaction. The loose mixtures were collected during ALF test lane construction for laboratory samples fabrication and mixture testing. Dynamic modulus test was performed on the samples in an Asphalt mixture performance tester (AMPT) at the Federal Highway Administration (FHWA) laboratory (Gibson et al. 2016). Based on the dynamic modulus test results, the master curve of the temperature-dependent asphalt mixture modulus is derived, as presented in Figure 2-2.

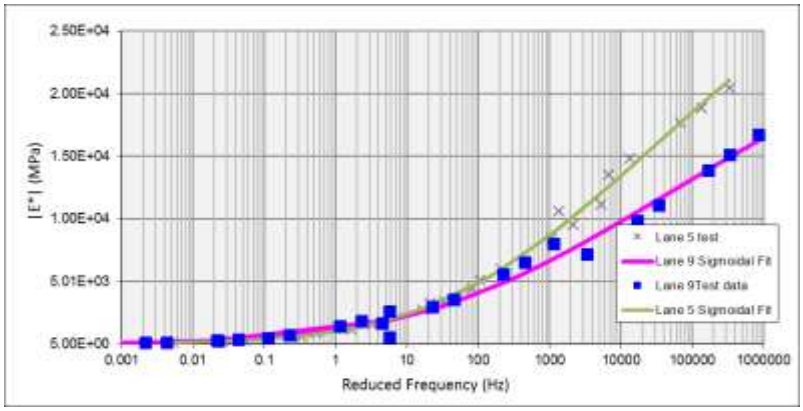

Figure 2-2 Master curve of Lane5 and Lane9 material

The dimensional analysis must be taken into account for the comparisons between differential scales, to determine various scaling factors applied on different parameters comprising geometry and loading. As a result, the stresses and strains within the test samples are compatible to those in the ALF test. The details of the dimensional analysis can be found elsewhere by van de Ven et al. (1998) and Kim et al. (1998). Thus, the three extracted 100 mm slabs were sliced into two thickness of normally 50 mm slabs for MMLS 3 trafficking, as to be performed with comparable stress/strain conditions under f-s ALF. For similarity, the 25 mm neoprene sheets were used as a substitute for the aggregate base, which have similar modulus as base course and make the installation of strain gauges easier. The neoprene sheet has been used in the MMLS 3 test, as alternative of aggregate base, in some previous studies (Bhattacharjee et al. 2011; Lee and Kim, 2004). The tested slabs were placed on top of the two neoprene sheets, which are directly rested on concrete floor in the laboratory. Lane9B top and Lane9B bottom lifts were placed on top of one neoprene sheet. The other four lifts of Lane9A and Lane5 were tested on top of two neoprene sheets, in order to expedite the fatigue damage of the slabs. The interfaces between asphalt slabs and neoprene sheet, as well as between neoprene sheet and concrete floor were bonded with emulsified asphalt, as to be more close to ALF test lane conditions and diminish the small vertical oscillations during MMLS3 trafficking.

2.2 Comparative test results of MMLS3, ALF and APA

Experimental program

This paper evaluated test results of six 50-mm lifts under trafficking with MMLS 3. The KYOWA -70-120-A1-11 L5M3R strain gauges were selected to be attached at the underside of slab to measure the slab response under moving wheel load of MMLS 3, as Figure 2-3. The LORD Microstrain wireless data acquisition system was implemented to monitor the strain history. The seismic stiffness of the slab as measured by the Portable Seismic

Pavement Analyzer (PSPA), was selected as an additional measure of the integrity of the slab during trafficking. The profilometer, with spacing of 2 mm, was used to measure the cross-section profile of the slabs at different positions. On the other hand, vertical tire/surfacing contact stresses were also measured under a MMLS in Pretoria by Steyn (2016).

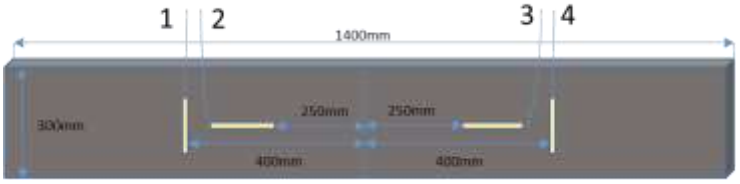

Figure 2-3 Strain gauge instrumentation schematic at underside of test slab

Test Protocol

MMLS 3

For all the tested slabs, trafficking was conducted at the conventional speed of 7200 applications per hour until reaching ca. 300 000. As for the subsequent trafficking, the loading frequency was reduced to 3600/h, in order to increase the strain and fatigue damage. It should be noted that the effective trafficking length of slab under MMLS3 is 1m. Strain gauges were placed in crossed patterns at two positions between the slab and the neoprene at ca. 250 and 750mm along the length of the slab. The data acquisition is processing continuously, and intermittently during the test:

a. Bogie load 2.7kN

b. Tire pressure 689kPa

c. Profiling measurement using profile-meter (measurement point spacing of 2mm.)

d. PSPA seismic stiffness at appropriate positions to capture performance characteristics

e. Temperature was monitored continuously to ensure the test temperature controlled at 20±2ºC. The initial laboratory room temperature is set as 18ºC, because the temperature would increase with accumulation of trafficking.

f. During the trafficking process, the machine was paused at interval of 100,000 wheel passes to measure the cross section profile at four positions along with slab, seismic modulus at three sections.

g. The data acquisition system was programmed to record 10 sec duration data at interval of every 20 minutes.

h. Lateral wander setting was not used in the trial test

i. Cracking occurrence and growth was monitored visually and logged to reflect growth and or special events.

APA

The test specimens are subjected to 5000 load cycles in APA apparatus with ambient temperature of 20 °C. One strain gauge is attached at the underside of the specimen along the wheel load direction.

a. Wheel load = 444.82 N (100 lb)
b. Hose pressure = 100 psi (689 kPa)
c. Load frequency= 60 cycles/ min
d. Strain value is continuously monitored using the data acquisition system.

Comparisons between MMLS3, ALF and APA trafficking

Pavement structure

Figure 2-4 illustrates the layout of pavement structure in ALF test lane, MMLS3 test lift and APA specimen. The pavement structure of ALF test lanes is composed of 10 cm asphalt layer, 56 cm base layer and deep underlying subgrade. Whereas, the down-scaled pavement structure of the MMLS3 consisted of 5 cm asphalt layer, 5 cm neoprene slab and underlying concrete floor. That is, the pavement thickness of ALF test lanes is effectively at least 6.6 times that of the MMLS 3 pavement thickness.

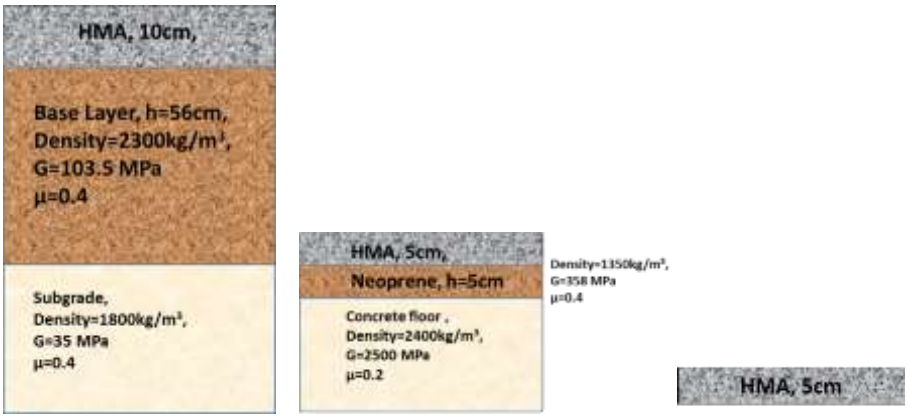

Figure 2-4 Layout of ALF test lane, MMLS3 test lift and APA specimen

Tire configuration

The full-scale ALF is equipped with single axle dual tires (275/80R22.5) or super single tire (425 /65R22.5) depending on the study needs, while the MMLS3 employs the particular 4.00-4 V76 diamond tire with 300 mm diameter by 80 mm width. In APA test, a pneumatized rubber hose across on the sample with up to 800 kPa inflation pressure, with the nominal inside diameter of 19.0 mm (0.75 in.) and the nominal outside diameter of hose as 29.5 mm (1.16 in.). The tire configuration information is specified as the following Table 2-3.

Table 2-3 Summary of ALF, MMLS3 tires and APA wheel

	Tire configuration	Inflation pressure	Axle load	Diameter & width	Load frequency
ALF	425/65R22.5	689 kPa	46.8 kN	1130 mm & 421 mm	Up to 5000/day
MML3	4.00-4 V76	689 kPa	2.7 kN	300 mm & 80 mm	Up to 7200/h
APA	Inflation rubber Hose	689 kpa	533.78N	300 mm & 19mm	Up to 60/min

Tire footprint and contact stress distribution

For simplicity, the tire pavement contact stress is traditionally assumed uniformly distributed over either a circular or rectangular area. However, in light of the realistic in-field measurement, it is found that the distribution of tire-pavement is far from uniformly (Wang, 2006). Figure 2.5 (Gibson et al., 2012) illustrates the tire-pavement contact imprint and the texure of wide-base tire 425 /65R22.5, which is applied in the ALF trafficking. According to previous studies (Elseifi et al. 2005; Wang, 2011), the localized vertical compressive stress at the edge of tread can approach 1000 kPa or more, which is much greater than the average stress with assumption of uniform distribution.

Figure 2-5 425 /65R22.5 Tire and contact imprint (Gibson et al., 2012)

Steyn (2016) measured the MMLS3 tire-pavement contact stress over differential pavement surfaces under 2.7 kN wheel load at static and 3,600 cycles/h condition, using the flexible pressure sensor, as shown in Figure 2-6. The maximum vertical stress was observed more than 1000 kPa, which is approximate to the vertical contact stress of ALF wide-base tire425 /65R22.5. Despite the texture and dimension of MMLS3 tire differentiates from ALF tire, the average and maximum stresses of both tires are

approximate. It can be concluded that the tire-pavement contact stress of MMLS3 and ALF are equivalent, while the contact areas are differing.

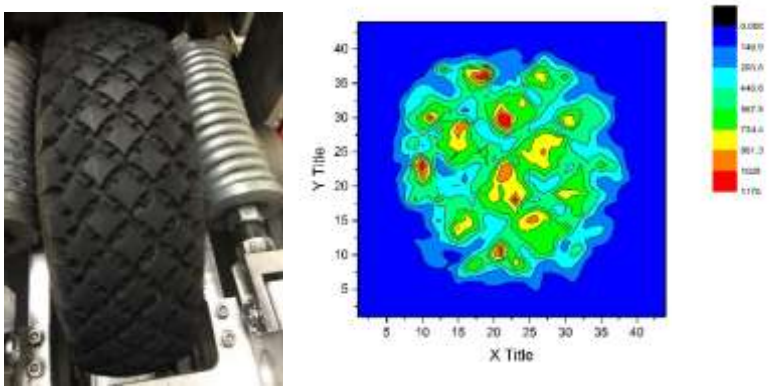

Figure 2-6 Tire and contact stress data map (Steyn et al. 2016)

Figure 2-7 shows the pneumatized rubber hose, which is used to simulate rubber tire in APA tests. The contact pressure in APA test is not measured in previous studies. In this dissertation, the contact pressure in APA is regarded as evenly distributed as 689 kPa.

Figure 2-7 APA pneumatized hose (Asphalt-pavement-analyzer)

Test results

Strain output history

The stain gauges are attached at the underside of Lane5 and Lane9 slabs for monitoring during the MMLS3 trafficking. Figure 2-8 shows typical strain output patterns in both longitudinal and transverse directions. It is noteworthy that the transverse strain gauge shows much higher strain than longitudinal strain gauge. The longitudinal strain consists of a compressive part followed by a tensile part when the loads is approaching and moving over the strain gauge. The strain gauge is also under compressive status when the

load is moving off. However, the transverse strain gauge is entirely in tension status. These findings are in good agreement with previous studies on MMLS 3 tire and actual tire loading (Bhattacharjee et al., 2011, Al-Qadi & Wang 2006). Besides, depending on the patterns of the transverse strain output, it can be seen the strain reduces at a slower rate during the unloading phase as compared with that in loading phase. It can attribute to the viscous property of asphalt mixture.

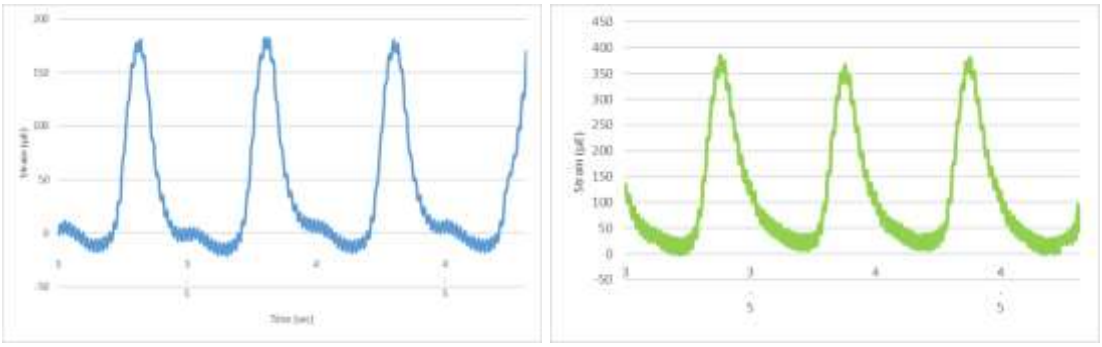

Longitudinal strain output Transverse strain output

Figure 2-8 Strain output history

The strain history at bottom of specimen during APA test is plotted as Figure 2-9. The signal pattern shape is similar to that in MMLS 3 trafficking. It should be pointed out that the measured maximum strain is 1.5 με, which is in much small magnitude compared to that in MMLS 3.

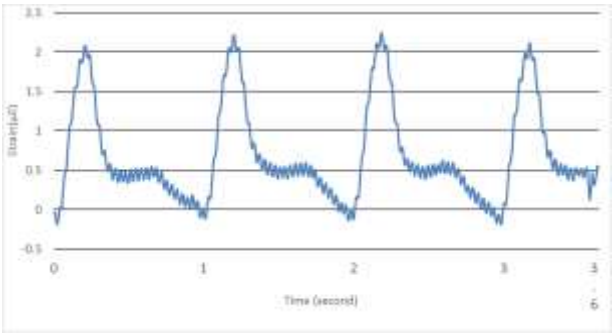

Figure 2-9 APA strain history

PSPA seismic modulus

Portable Seismic Pavement Analyzer (PSPA) is a filed-deployable non-destructive device used to evaluate the seismic stiffness of pavement, base or subgrade material. PSPA is employed in this paper to indicate the integrity change of the slab during the trafficking process. Figure 2-10 shows the seismic modulus measured by PSPA plotted against number of loading cycles for 6 lifts. During the PSPA seismic modulus measurement, the historically assumed incidence of 50% loss of seismic modulus indicates the failure or the initiation of the fatigue failure.

The unexpected early termination of Lane9 top lift which did not reach 50% loss in modulus, is caused by the small vertical oscillations during trafficking. The vertical black dash line in Figure 2-10 illustrates the failure of the slab, while the trafficking of three bottom lifts is continuing because no obvious fatigue cracks are observed on the slabs surfaces. Three points along the centerline of wheelpath and one point at 2cm off the wheelpath edge are marked as measurement points to monitor the stiffness change. The material off the wheelpath is less affected by the repeated moving load and degrades at much lower rate. The three bottom lifts are observed better fatigue resistance than top lifts. Fatigue damage due to the repeated load is relatively concentrated on the wheelpath.

The PSPA measurements of Lane9 during ALF test is shown in Figure 2-10 as well. The seismic modulus reached 50% loss after approximately 500,000 ALF load cycles. It can be noted that the modulus of Lane9 drop to 50% after 500,000 MMLS load applications. Nonetheless, MMLS3 is much more efficient which takes around 4 days to run 500,000 cycles, whereas ALF needs to take 100 days.

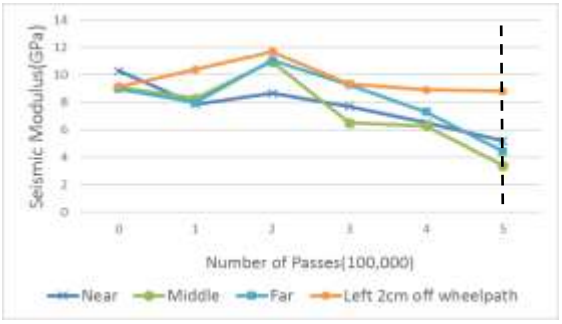

Lane9A top lift

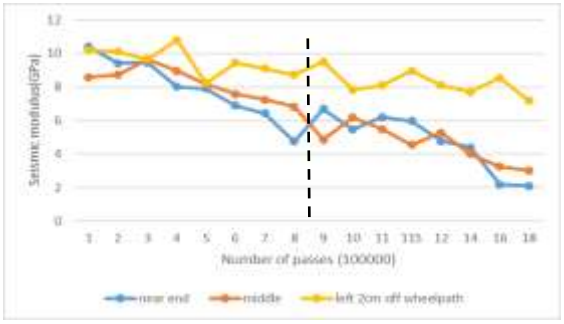

Lane9A bottom lift

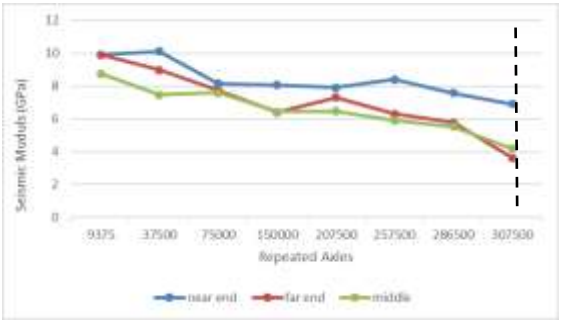

Lane9B top lift

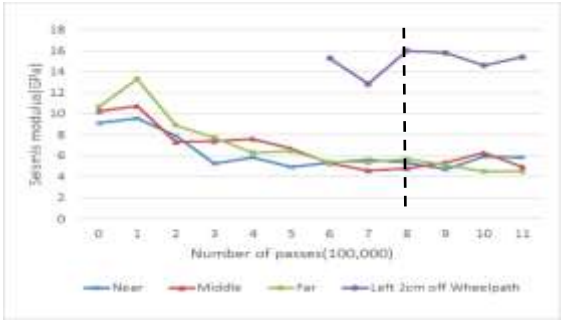

Lane9B bottom lift

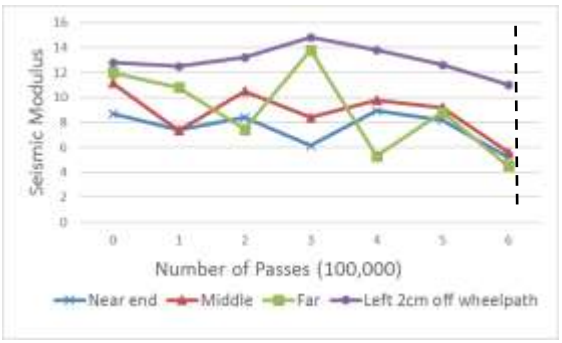

Lane5 top lift

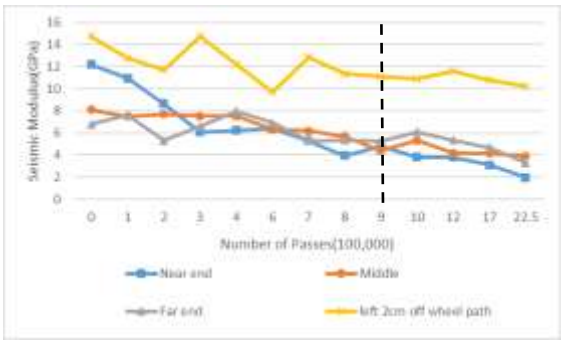

Lane5 bottom lift

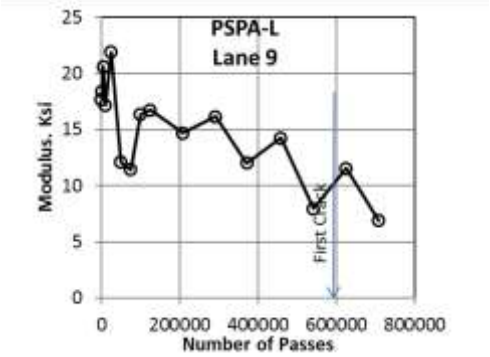

Lane9 ALF (Gibson, 2016)

Figure 2-10 PSPA measurements

Rutting

The profile-meter, with spacing of 2mm, was used to measure the transverse profile of the slab at four different positions. Figure 2-11 illustrates the transverse profiles and rutting at middle position along trafficking direction of all the 6 lifts. Because different lifts are subjected to differential cumulative trafficking before test termination, in this paper, the rutting performances are compared at 500,000 load cycles as Table 2-4.

Table 2-4 Summary of rutting for differential test lifts

	Lane9 A top	Lane9 A bot	Lane9 B top	Lane9 B bot	Lane5 top	Lane5 bot
Rutting depth(mm),after 500,000cycles	3.98	2.68	N/A	3.04	2.59	1.09
Rutting Width(mm)	100	95	100	100	240	200

As shown in Table 2-4 and Figure 2-11, Lane5 40%RAP PG64-22 HMA exhibits better rutting resistance than Lane9 20%RAP PG64-22 foamed WMA in terms of rutting depth. In addition, the rutting width of Lane5 HMA is much greater than Lane9 WMA, which is taken to be as a result of results that Lane5 material is stiffer than Lane9. The bottom lifts are observed lower rutting depth than the top lifts in the same lanes.

According to Figure 4, the pavement thickness of ALF test lanes is effectively at least 6.6 times that of the MMLS 3 pavement thickness. According to a 3D dimensional analysis, this yields a vertical stress ratio of 2.8:1. Earlier studies have supported the hypothesis that the resulting ruts would develop in the same ratio. This was compatible to the actual performance observed. Although the stress is the primary factor affecting the rut performance, other factor need to be taken into account. For instance, the stiffness modulus of the base layer and subgrade is substantially higher than the asphalt layer of the ALF.

On the basis of the above analytical deduction, it was therefore concluded that the rutting performance under MMLS3 trafficking and the f-s ALF, is compatible under the prevailing conditions.

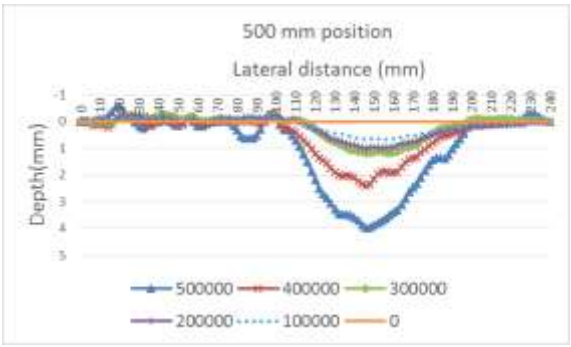

Lane9A top Lift

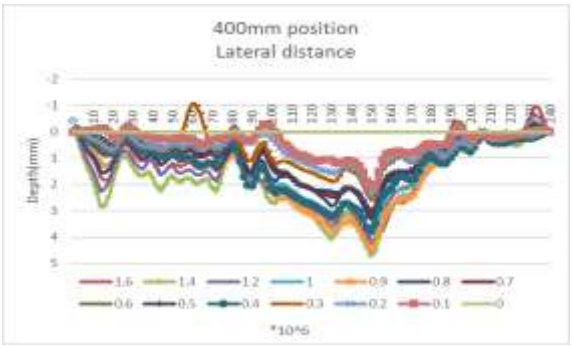

Lane9A bottom lift

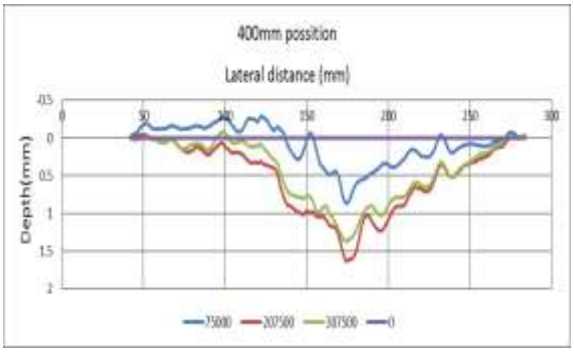

Lane9B top lift

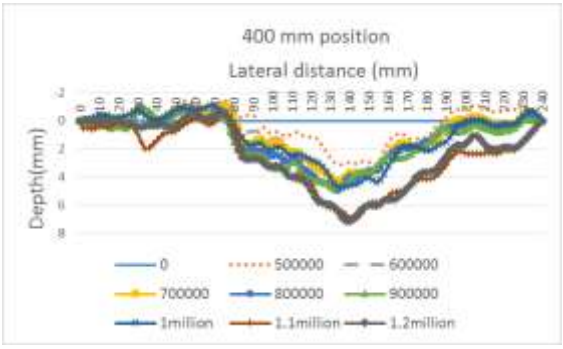

Lane9B bottom lift

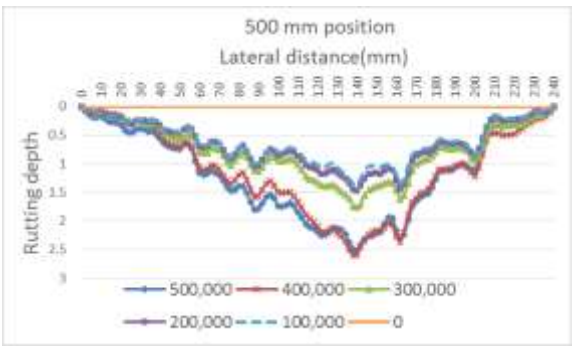

Lane5 top lift

Lane5 bottom lift

Figure 9. Profile at 400mm positions

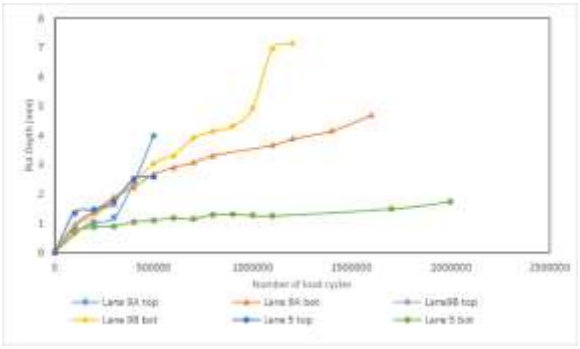

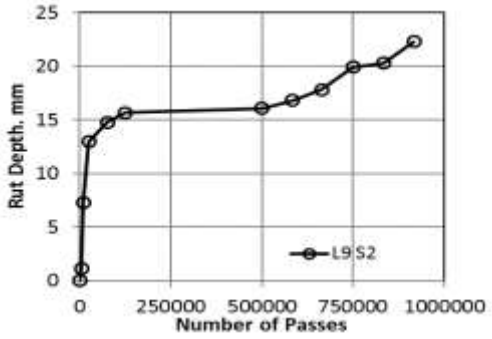

MMLS3

ALF(Gibson, 2016)

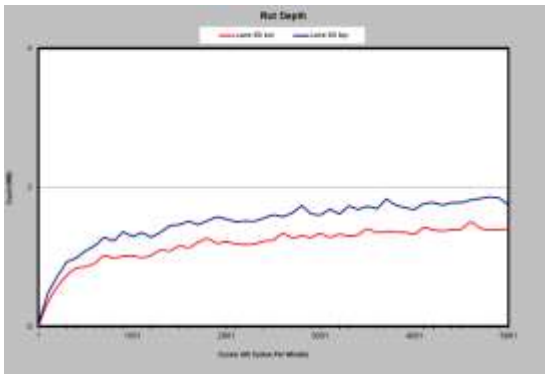

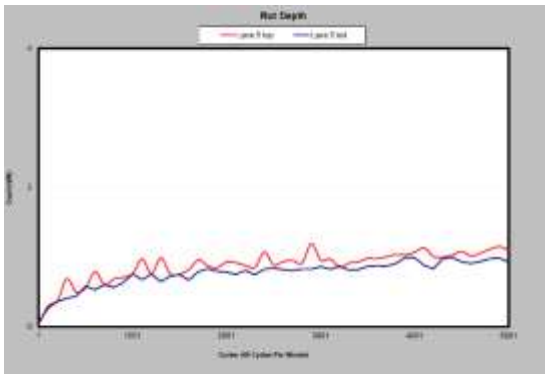

APA tests of Lane9B top and Lane9B bottom lift

APA tests of Lane5 top and Lane5 bot lift

Figure 2-11 Rutting depth versus cumulative number of load cycles

Cracking

The cumulative linear length of cracks was measured by manually tracing new cracks on clear plastic sheets, between the trafficking intervals for distress measurements. Figure 2-

12 and Table 2-5 show the fatigue cracking data of six lifts after MMLS 3 trafficking.

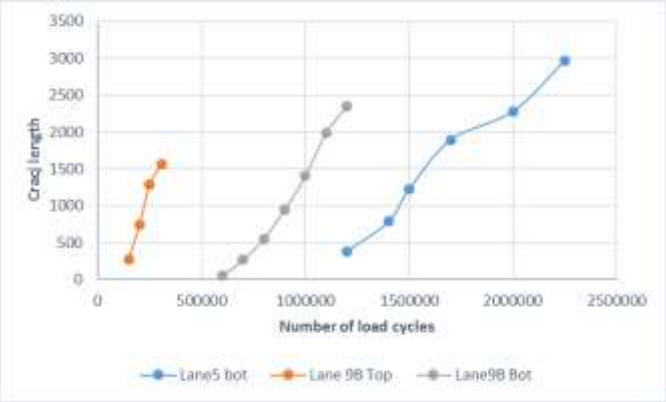

Figure 2-12 Cumulative crack length on Top surface

Table 2-5 Crack length after the termination of test

Slab ID:	load applications	Top surface crack length(mm)	Underside crack length(mm)
Lane9A Top	500,000	1749	1274
Lane9A Bot	1,800,000	618	1341
Lane9B Top	307,500	1566	1097
Lane9B Bot	1,200,000	2352	1752
Lane5 Top	600,000	342	856
Lane5 Bot	2,250,000	2961	1826

In full scale ALF testing, the total linear crack length of Lane9 reached 2,771 mm per meter after 400,000 ALF trafficking cycles, while crack length of Lane5 was measured as 1616mm per meter after 80,000 load applications (Gibson et al., 2016). After the same quantity of load cycles, much less top surface cracks were observed in MMLS3 on both Lane9 and Lane5.

Furthermore, in comparison with the fatigue performance of Lane9, Lane5 test lifts exhibited better fatigue resistance, under MMLS3 trafficking. This is based on the finding that the crack length was less and the later cracks manifested after much more trafficking. However, this comparison result is in contrast to that from ALF. The hypothesis of the authors is that the reason for this is related to the supporting material property under asphalt layer of Lane5 being poorer than that under Lane9. This would not manifest in the case of performance under MML3 trafficking, is due to the shallow nature of the

influence test depth. In contrast, the relative performance of the two asphalt layers is in actual fact more representative of the material properties.

Summary and conclusion

Regarding the discussions and findings in this paper, some conclusions can be drawn as following:

1. The findings from the three MMLS3 comparative tests indicated that the material integrity of the asphalt slabs had not been jeopardized after the extraction from the ALF test lane and transportation to Blacksburg. Based on the correspondence with FHWA, the initial PSPA value of Lane9 is around 16 GPa, which is a slightly larger than the measurements of the un-trafficked slabs in the laboratory. This is ascribed to differences in thickness and supporting structure of the two pavements.

2. After 500,000 trafficked axles, the seismic modulus of Lane9 approaches 50% loss which indicated the onset of fatigue failure. This is comparable to the reported in-situ PSPA stiffness parameters of Lane9 at T-F. However, the MMLS3 is much more efficient in trafficking and takes much less time to reach the failure inertia.

3. Compared with surface crack performance of Lane9 in ALF, much less cumulative crack length is observed in MMLS3 test, despite the contract stresses of these two scale tires are approximate. The possible reason is that the ALF wheel load is much higher which causes deeper damage in the pavement structure. Meanwhile, the difference in structure should be considered. The stiffness modulus of the base layer and subgrade is substantially higher than that in ALF.

4. The initial indicators of performance provided useful comparative indicators related to the slabs tested from Lane5 and Lane9. It was concluded that the parameters that had been monitored served to validate the comparative performance characteristics of the two structural systems and intrinsic material characteristics. This finding is also comparable to earlier studies.

5. The findings from one third scale MMLS3 test and full scale ALF test on pavement fatigue and rutting performance are comparable in terms of of rutting depth, strain response, seismic stiffness and cracking. This validated the MMLS to be an effective, economic and reliable trafficking tool to characterize rutting and fatigue performance of pavement materials with due regard to the relative structures (i.e. surface layer). Accordingly, it can be used to enhance economic pavement designs with unproven composite materials.

6. The Lane5 40%RAP PG64-22 HMA has higher stiffness than the Lane9 20%RAP PG64-22 foamed WMA. It was noteworthy the former material had better resistance to permanent deformation and fatigue cracking than the latter. This is contrary to the ALF findings and was ascribed to factors related to the structural composition of the tested structure.
7. The latter finding is considered to be important for the planning and execution of tests that could be affected in a similar manner.

Acknowledgement

Sincere appreciation is expressed to all the researchers that participated in the respective collaborative projects efforts. The authors are deeply grateful for the sponsors who support the project. Additionally, a particular thankful word to Nelson Gibson, Ph.D., PE. Research Civil Engineer (Highway) of the FHWA, who gave the permission to get the slab extracted from FHWA and provided the fatigue performance test results after ALF trafficking. Besides great thanks to the continuous support and help of Mark Baker from Geomedia Research & Development.

2.3 Reference:

Al-Qadi, I., Loulizi, A., Janajreh, I., & Freeman, T. (2002). "Pavement response to dual tires and new wide-base tires at same tire pressure". *Transportation Research Record: Journal of the Transportation Research Board*, (1806), 38-47.

Al-Qadi, I. L., & Wang, H. (2009). "Full-depth pavement responses under various tire configurations: accelerated pavement testing and finite element modelling". *Journal of the Association of Asphalt Paving Technologists*, 78, 721-760.

"Asphalt-pavement-analyzer" https://asphaltscientist.wordpress.com/asphalt-mixture-performance-tests/asphalt-pavement-analyzer-apa/asphalt-pavement-analyzer/. Sep, 2016.

Bhattacharjee, S., Gould, S.G., Mallick, R. B. and Hugo, F.2011. "An Evaluation of use of Accelerated Loading Equipment for Determination of Fatigue Performance of Asphalt Pavement in Laboratory". *International Journal of Pavement Engineering*, 5:2, PP 61 -79.

Elseifi, M., Al-Qadi, I., Yoo, P., & Janajreh, I. (2005). "Quantification of pavement damage caused by dual and wide-base tires." Transportation Research Record: Journal of the Transportation Research Board, (1940), 125-135.

Gibson, N., Carvalho, R., Li, X., and Andriescu, A. (2016). "Fatigue Cracking of Recycled and Warm Mix Asphalts: Predicted Performance Considering Structural Variability Influences". *Journal of the Association of Asphalt Paving Technologists*. AAPT 2016.

Gibson, N., Qi, X., Shenoy, A., Al-Khateeb, G., Kutay, M.E., Andriescu, A., Stuart, K., Youtcheff, J. and Harman, T. (2012). "Performance testing for Superpave and structural validation (No. FHWA-HRT-11--45)".

Gibson, N., Schwartz, C., Schapery, R., & Witczak, M. (2003). "Viscoelastic, viscoplastic, and damage modeling of asphalt concrete in unconfined compression." *Transportation Research Record: Journal of the Transportation Research Board*, (1860), 3-15.

Huang, Y.H., 2004. *Pavement analysis and design*. 2nd ed. Upper Saddle River, NJ: Prentice Hall.

Hugo, F., Huang, Y., Xiong, H., Wang, L., Steyn, W. (2015). "Lessoned Learned During the First Application of MSP for Extracting Asphalt Slabs in Comparative Testing of Fatigue Performance of Warm Mix RAP Asphalt MMLS3 Trafficking*". ISAP 2015Seminar,* SunCity, South Africa.

Kim, S.M., Hugo, F. and Roeset, J.M. (1998) "Small-scale accelerated pavement testing", *Journal of Transportation Engineering,* ASCE 124(2), 117–122.

Metcalf, J. B. *NCHRP Synthesis of Highway Practice 235: Application of Full-Scale Accelerated Pavement Testing*. TRB, National Research Council, Washington D.C., 1996.

"Pavement Testing Facility". <https://www.fhwa.dot.gov/research/tfhrc/labs/pavement/> (Nov. 12, 2016)

Van de Ven, M., Smit, A. de F., Jenkins, K. and Hugo, F. (1998) "Scaled down APT considerations for viscoelastic materials". *Journal of the Association of Asphalt Paving Technologists* 67, 602–622.

Wang, F., & Machemehl, R. (2006). "Mechanistic-empirical study of effects of truck tire pressure on pavement: Measured tire-pavement contact stress data". *Transportation Research Record: Journal of the Transportation Research Board*, (1947), 136-145.

Wang, G., & Roque, R. (2011). "Impact of wide-based tires on the near-surface pavement stress states based on three-dimensional tire-pavement interaction model". *Road Materials and Pavement Design*, 12(3), 639-662.

Wang, H. (2011) "Analysis of tire-pavement interaction and pavement responses using a decoupled modeling approach." thesis, presented to University of Illinois at Urbana-Champaign, in partial fulfillment of the requirements for the degree of Doctor of Philosophy.

Yoo, P.J. and Al-Qadi, I.L. (2008) "Truth and Myth of Fatigue Cracking Potential in Hot-Mix Asphalt: Numerical Analysis and Validation," *Journal of Association of Asphalt Paving Technologists*, Vol. 77, AAPT, pp. 549-590.

Chapter 3 INSTRUMENTATION FOR SIMULATIVE TEST SYSTEMS

3.1 Traditional instrumentations in actual pavements and APT systems

In the APT system, a wide variety of parameters needs to be monitored for material response and pavement performance analysis. It is of vital significance to specify the appropriate parameters and select corresponding sensors and instruments for monitoring (Steyn et al. 2006). Massive previous studies have been reviewed to ensure the important parameters are not neglected. It is generally accepted that the significant parameters include stress, strains, deformations, moisture and temperature inside pavement layers.

The conventional pavement instrumentations can be classified into instructive and non-instructive measurements. The instructive instrumentations are normally installed at two primary critical locations to observe the pavement responses under vehicular loads. These are at the bottom of the asphalt mixture layer and at the top of the unbound granular base or subbase layers. Consequently, the selections of the instructive sensors depend on these two locations. Some widely and successfully applied gauges and sensors, which are used in previous full scale APTs are introduced as following.

3.1.1 H-bar Strain Gauges

The H-bar strain gauges are routinely installed at the bottom of the asphalt concrete layer to measure the transient dynamic strain subjected to the moving load. The strain gauges should be capable of withstanding high temperature of hot asphalt mixtures, heavy vibratory rolled compaction and having long-term service life under the repeated traffic loads. Figure 3-1 shows one widely used asphalt mixture horizontal and vertical strain gauges from CTLGroup Company (product overview, 2016). There are four active gauges embedded in the horizontal strain gauges, in which two are aligned with longitudinal direction and the other two with transverse direction (Timm et al. 2004). According to the product manual, the maximum range of the strain gauge is $\pm 1500 \varepsilon\mu$, within the estimated strain value at bottom of asphalt mixture layer in realistic pavement.

Figure 3-1 Asphalt mixture Strain gauges (Timm et al. 2004)

3.1.2 Pressure Cell

The pressure cell has been successfully placed on top of base course and top of subgrade, to measure the dynamic vertical stress induced by the traffic loads in previous projects. However, the pressure cells are costly which somewhat impedes the application. The pressure cell manufactured by Geokon Company is shown as Figure 3-2, which has been used in some APT projects. The pressure cell can work in the temperature range of -20 ℃ to 80 ℃ and the maximum pressure range is up to 600 kPa. On the other hand, the Geokon pressure cell is questionable for the large size that may have impact on the pressure measurement, resulting in exploration of smaller pressure cells.

Figure 3-2 Pressure Cell (Pressure cee, 2016)

3.1.3 Time domain reflectometry probe

Time domain reflectometry (TDR) probes are commonly used to measure the moisture contents inside the subgrade. The probes are a wave-guide extension on the end of coaxial cable. The volumetric change of water content surrounding the probe causes the change in probe impendence, which can be observed in the output signal (TDR probes

manual). The TDR manufactured by Campbell Scientific is recommended and applied extensively, as shown in Figure 3.3.

Figure 3-3 TDR probe (Timm, 2004)

3.1.4 Temperature sensors

Most often, the temperature sensors are buried along with the depth of the pavement structures, to observe the temperature gradient within different layers. Either temperature probes or thermistors are routinely positioned outside of the traffic lanes, and the shoulder of highway is the recommended position. Figure 3-4 presents the 107 temperature probe manufactured by Campbell scientific company, with measureable range from -35 ^{o}C to 50^{o}C.

Figure 3-4 Temperature probe (107 temperature sensor, 2016)

3.1.5 Data acquisition system

The data acquisition system is used for data collection, acting as the interface between a computer and sensors, and digitizing incoming analog signals for computer interpretation. The data acquisition hardware can connect to the sensors in full, half or quarter

Wheatstone bridge circuit, depending on the requirement and guideline. The selection of data acquisition system is crucial, because a reliable and intelligent system with functions for automatic measurement and processes can considerably enhance the efficiency and effectiveness of the measurement solution (Saghefar et al. 2013). In reality, the system is placed inside a box for protection, which is relative close to the sensors with the wire connected, then transmitting data to computer either in hardwire or wireless manner.

The aforementioned sensors and data acquisition system are the primary components of an intrusive sensor system, been successfully applied in previous test sections and APT systems. Additionally, some non-intrusive sensors or apparatuses are needed to evaluate the pavement performance along with the accumulation of traffic loading numbers, especially the rutting and fatigue performance, such as the 3D scan laser, non-contact laser based profiling system, Portable Seismic Pavement Analyzer, and light weight deflectometer. In the test sections of actual pavements, the non-intrusive sensors are also used for traffic volume and weight in move system.

3.2 Pavement monitoring system based on wireless sensor network in testing

3.2.1 A Prototype IOT Based Wireless Sensor Network for Traffic Information Monitoring

Abstract:
An Internet of things (IOT) based wireless sensor system, solely using wireless accelerometers, is developed for traffic volume and vehicle classification monitoring in this paper. A series of laboratory test, field test as well as numerical simulation were performed to validate the feasibility and accuracy of the monitoring system. Besides, in order to eliminate the impacts of noises in the output signals, an advanced algorithm is developed to analyze the test data. The findings based on the test results indicate that the system is capable of reliably detecting axles and calculating axle spacing in both laboratory and field tests. In addition, compared with the actual measurements, the numerical simulation further validates the feasibility of the integrated wireless sensor system for traffic information monitoring.

Key words: wireless sensor, accelerometer, traffic volume, vehicle classification

Introduction:

Correctly acquiring traffic information including the traffic volume, traffic density, speed, classification, and axle load, is premise of reliable traffic system design and optimization (Khanafer et al. 2009; Sharma et al. 2011; Kafi et al. 2013; Xue et al. 2015).

With increasing advancement in sensor or transducer technologies, numerous traffic information collection systems were developed in recent decades. The in-situ pavement sensing technology can date back to 1960s (Potter et al. 1969) for monitoring pavement sections conditions. Sebaaly et al. (1991) used pressure cell, strain gauge, thermocouple, and moisture sensor for field evaluation under actual truck loading. After that, the National Center for Asphalt Technology (NCAT) test track, MnROAD owned by Minnesota Department of Transportation, and Virginia smart road, are instrumented with a wide range of test cells to measure the pavement responses and performance (Timm & Priest 2004; Timm et al. 2004; Al-Qadi et al. 2004). Bajwa et al. (2011) and Xue et al. (2015) proposed an In-Situ Wireless Sensing Network for vehicle speed, weight and configuration monitoring.

It can be found that the aforementioned conventional sensing technologies for traffic counts, speed measurement and vehicle classification employ some sensors or strain gauges mounted under pavement in certain depth for measurements (Zhang et al. 2005; Bajwa & Varaiya 2009; Xue et al. 2015), which are prone to damage after subjected to repeated heavy traffic wheels, resulting in the subsequently costly repair or replacement expenses. Besides, these methods are commonly associated with high maintenance costs, complicated installation process, labor intensive, time consuming, and traffic control or lane closure (Coleri et al. 2004; Bargagli et al. 2010; Yousef et al. 2010; Jianming et al. 2012).

In this paper, an Internet of things (IOT) based wireless sensor system is developed for traffic volume and vehicle classification only using wireless accelerometers (as shown in Figure 3-5). The system consisting of wireless sensors, wireless gateways with access to cellular network, cloud computing and storage, enables researchers or industry practitioners to monitor real-time traffic information and access to data information remotely. This wireless system can be installed on roadway shoulder without interfering the ongoing traffic, having the benefits in lower maintenance cost and less time and labor consuming.

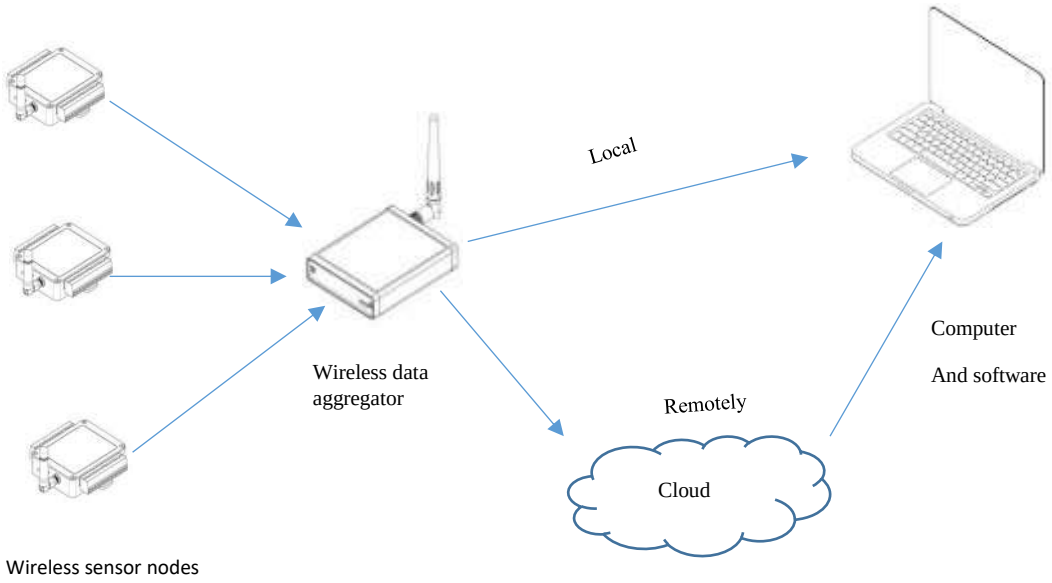

Figure 3-5 IOT system instrumentation

The Microstrain WSDA-1500-LXRS wireless sensor data aggregator and the G-link-LXRS wireless accelerometer node are used to monitor the pavement vibration for analyzing quantity of vehicle axles, axle spacing and vehicle speed under both laboratory tests and actual condition. In this paper, the wireless sensor node measures X,Y and Z accelerations of longitudinal direction along with tire moving, transverse direction perpendicular to the moving and the vertical direction, respectively.

Experiment Setup and Test Procedures

Before the implementation of the proposed system on the realistic pavement, a series of laboratory tests were carried out to verify the feasibility and accuracy of the accelerometer monitoring on the wheel-pavement interaction. The one-third scale model mobile load simulator (MMLS3) is used for the laboratory investigation. The tire load of MMLS 3 is set to be 2.7 kN and the tire pressure is pumped to 689 kPa. The test is conducted at 20 ℃ room temperature. The test slab is cored from Test Lane9 of Turner-Fairbank Highway Research Center (T-F), with size of 140cm by length *30cm by width*5cm by height. The slab is constructed using the PG 64-22 virgin asphalt and 20% recycled asphalt pavement by weight, warm mixed asphalt (WMA) mixing process technology. The detailed with regard to the MMLS 3 test set-up and asphalt mixtures and underlying layers material properties can be found in Chapter 3. In this experiment, the accelerometer sensor was attached to the asphalt concrete slab at 10cm off the wheel path.

To simulate real traffic situation and verify sensor sensitivity under different conditions, four different speeds of MMLS 3 trafficking were applied to monitor the varying asphalt concrete slab responses. Output data was collected by wireless node, transmitted to

Microstrain cloud system through the wireless data aggregator. In the laboratory set-up, only one wireless node was adopted for the data acquisition.

Experiment Results Analysis

Axle Detection Algorithm

Each moving wheel load can be modeled as a moving impulsive force on the pavement. Therefore, the impulse can induce the vibration of pavement together with sensor and the peak impulse in digital signal output can be monitored by the accelerometer accordingly. However, the actual roadway situation is complicated which is associated with environmental noises and traffic sounds, resulting in the difficulty to effectively recognize the peak value on the raw data. For this reason, a signal smoothing methodology is required to detect important patterns and trends while leaving out the unimportant things. A MATLAB program is developed to smooth the output signals and extract the useful information.

Figure 3-6 Signal process flowchart

The signal process flowchart is shown as Figure 3-6. The first step is to divide the raw signal r(n) by 3 times of the noise which is provided by the sensor manufacturer, aiming to amplifier the useful signal. Then the digital signal a(n) are squared to further attenuate the noise and distinguish the impulse induced by the moving wheel load. At the final step, the signal p(n) is to pass through a moving average filter to facilitate to locate the impulse peaks. Figure 3-7 pictures the signal output before and after the smoothing process. One should note that after the signal process, the vertical axle represent the digital numbers without any physical meaning.

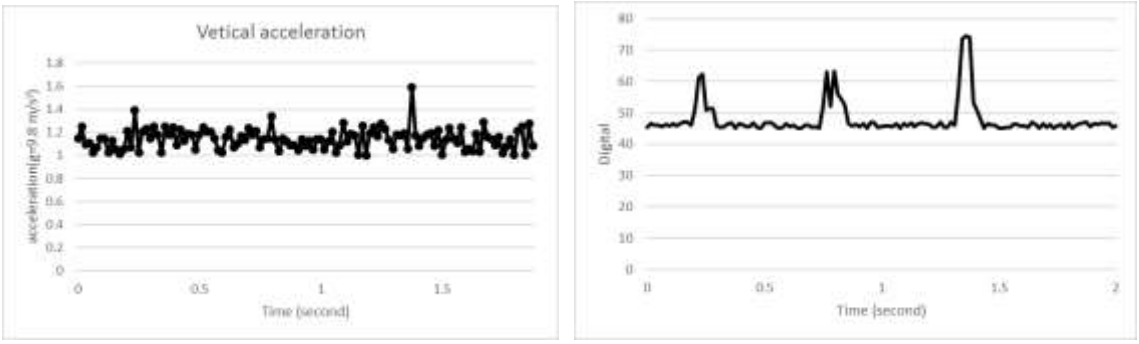

(a) (b)

Figure 3-7 Output Signal before (a) and after (b) process

According to the Figure 3-7 (b), it can be seen that some impulse exhibits twin peaks after the process, and thus it is necessary to filter peaks in the smoothed signal with a minimum peak time separation, denoted as γ(v), which ensures the local variations near peaks are not considered as another individual axle. The distance between MMLS bogies approximates to 1.05 m. The axle spacing of typical vehicles is at least 1.83 m, while the tandem axle has 3.65 to 4.57 m apart. The peak time separation of twin impulse peaks in Figure 3-7 is less than the minimum peak time separation of MMLS 3, therefore only one of the twin peaks is accounted for wheel load.

Axle Spacing and Speed Estimation

The sample frequency of the accelerometer is a 64 Hz, so each spot in the figure 3-7 counts as 0.015s. From output signal, t_n refers to the time of impulse peak induced by axle n passing the sensor. In laboratory tests, as calculated before, the speed of MMLS is known and the axle spacing d_n between axles n and n+1 can be determined as

$$d_n = v(\, t_{n+1} - \, t_n \,) \qquad (3\text{-}1)$$

On the other hand, the wheel spacing of MMLS is also known as d, the speed can be calculated as

$$v = d/\,(t_{n+1} - \, t_n) \qquad (3\text{-}2)$$

Since the speed and the wheel bogies distance are both known in the laboratory tests, any one of them given can help to determine the other one. The primary goal of these tests is to detect the axle which reflects as a peak impulse in signal output for the purpose of vehicle classification by axle quantity.

Sensor Performance

Table 3-1 Noise Root Mean Square (RMS) and Signal Amplitude

	Noise RMS(g=9.8 m/s^2)	*Signal Amplitude (g=9.8 m/s^2)*
X-Axle	*0.000131*	*>0.05*
Y-Axle	*5.477E-5*	*>0.1*
Z-Axle	*0.504*	*>1*

To evaluate the environmental noises of the sensor, the sensor is tested when there is no wheel passing. Table 3-1 compares the noise RMS and signal amplitude of three directions. X and Y-axle have profound lower RMS than the Z-axle due to the gravity acceleration in vertical direction.

Axle Spacing and Speed Verification

Since the accelerometer is the only sensor used in laboratory tests, one of the two variables, speed or axle spacing, can be determined after the other is known. To verify the axle spacing calculated from the impulse peak detection, with a fixed speed (v) and time between each peak (t) which is the distance between two red lines in figure 3-8, the space (s) could be calculate as: s=v*t.

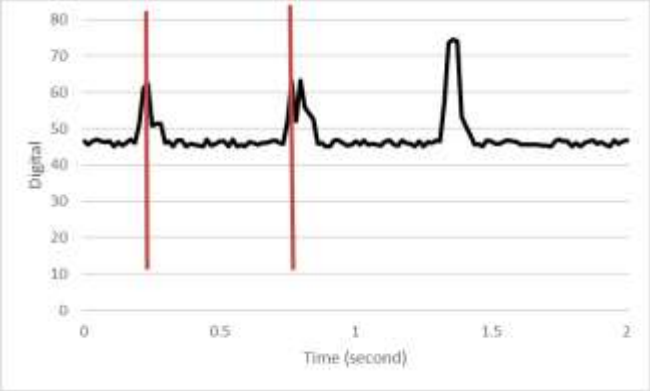

Figure 3-8 Axle Spacing

Because MMLS 3 can be set up trafficking at different speeds, average axle spacing was calculated and compared with the actual wheel bogies distance. Table 3-2 summarizes axle spacing based on the accelerometer detection at different speeds.

Table 3-2 Axle Spacing Summary

MMLS3 trafficking speed(m/sec)	Calculated Average Axle Spacing (m)	Wheel Center Line Distance (inch)	Error Percent (%)

0.65	1.08	1.05	2.85%
1.3	1.12	1.05	6. 7%
1.95	1.13	1.05	7.62%
2.6	1.24	1.05	18.1%

From the comparison results, when the speed is slower the sensor is more susceptible to the axle and the axle spacing calculation is more accurate with an error about 2.85%. While as speed increased, the accuracy of the sensor became lower and the highest error percentage locates on the speed of 2.6 m/s, which approximates 18%. As a result, it can be concluded that the sensor and calibration algorithm are capable of collecting and analyzing the data, determining axle spacing within the accepted range, and are useful for vehicle classification. The reason for that is the lower the speed, the greater strain/ stress is exerted on the pavement, which leads to the larger deformation and stronger acceleration for sensor detection.

Table 3-3 lists the actual speed and speed calculated based on sensor output data. The calculated speeds are within the acceptable error percentage, which indicates that the accelerometer is capable of detecting wheel axle speed.

Table 3-3 Speed Verification Summary

MMLS3 trafficking speed(m/s)	Speed Calculated According to Sensor Signal (m/sec)	Error Percentage(%)
0.65	0.68	4.6%
1.3	1.37	5.38%
1.95	2.23	14.35%
2.6	2.9	11.54%

Finite Element Simulation

The asphalt mixture is modeled as visco-eleastic material in finite element simulation software ABAQUS, while the other underneath layers are assumed as elastic. On the other hand, the dynamic modulus test was carried out on the samples in an Asphalt mixture performance tester (AMPT) at the Federal Highway Administration (FHWA) laboratory [21]. Based on the dynamic modulus test results, the master curve of the temperature-dependent asphalt mixture modulus is derived, as presented in Figure 3-9.

The input parameters are derived by fitting into the Prony series as a generalized Maxwell model.

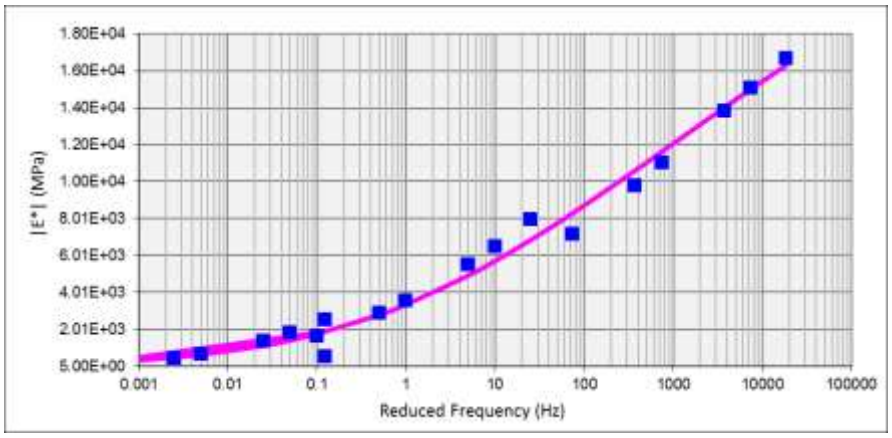

Figure 3-9 Master Curve of test material

The moving load is simulated as the footprint area gradually shifts over the loading area at each step until it cross the section, which means a single wheel pass is completed. The load pressure exerted on the shift footprint area is assumed to be uniformly as 689 kpa. In the simulation analysis, the vertical acceleration was regarded as the primary factor compared with laboratory tests results. Figure 3-10 is the numerical simulation model of MMLS 3 test, which consists of 15288 nodes and 12662 elements. The acceleration of the element at 10cm offset of the wheel path is recorded.

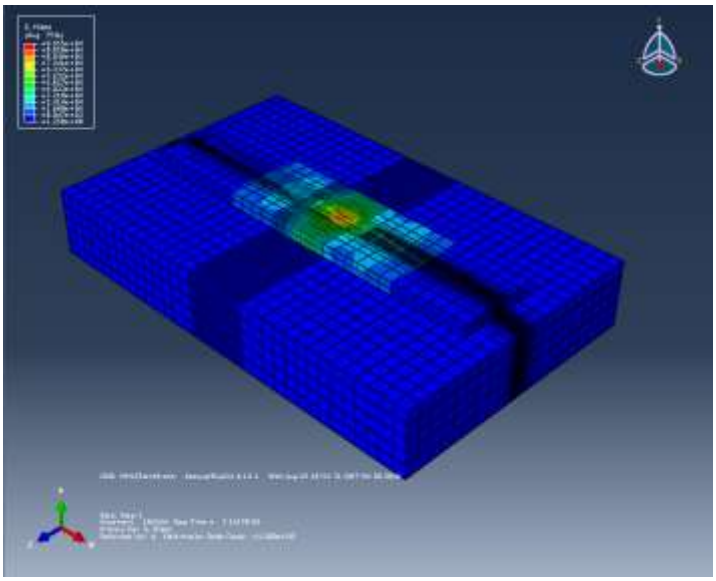

Figure 3-10 Vertical Acceleration

Simulation Results

As can be seen in Figure 3-11, the moving wheel load passing over the measured element is the only vibration excitation during the MMLS3 trafficking. The impulse peak induced

by the moving vehicle can be obviously, because the ambient noises are not considered in the numerical simulation.

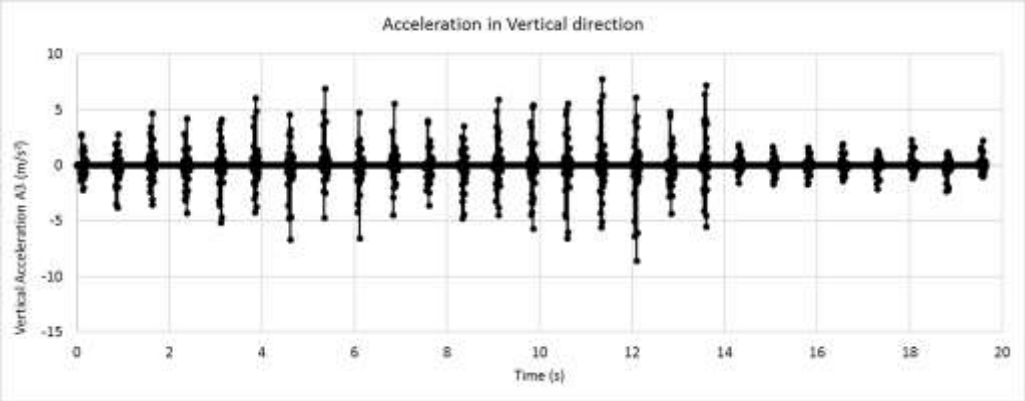

Figure 3-11 Simulation Results of Acceleration

One wheel-induced impulse in simulation result is compared with the test measurement as shown in Figure 3-12. It can be found that the peak impulse in both the simulation and the acquisition outputs from sensor data represents a wheel passing. The actual sensor collected more noise than the simulation, which is reasonable due to the influence of the environmental noise and MMLS 3 machine noise. However, when the moving tire is approaching the measurement spot, the vibration is observed in simulation, while the realistic sensor is not prone to detect the vibration. The probably reason is the gravity is ignored in the simulation, while the gravity sensor somehow impedes the vertical vibration of the sensor.

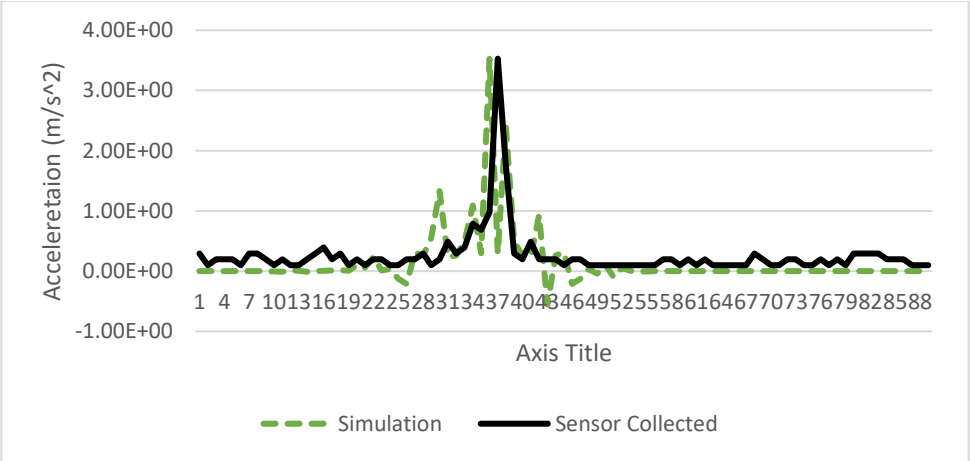

Figure 3-12 Single Wheel-Passing Comparison between Sensor and Simulation

Deployment on Plantation Road

To further verify the accuracy of the developed wireless sensor network for application on actual pavement to monitor the pavement-vehicle interaction, a field test was

performed on Plantation Road, Blacksburg, VA. The GMC Sierra 2500HD truck goes over the test section at speed 35 mph, the speed is also measured by a handheld speedometer to ensure the speed accuracy.

The G-link wireless accelerometer node was installed at the edge of the pavement, with one-meter distance to the wheel path. The wireless sensor data aggregator is placed within a range of 2km from the accelerometer node. All the monitoring data is transmitted to cloud system via the cellular network, which allows the managers and engineers to access the data as long as with Internet availability.

Test Results and Analysis

After comparisons of three accelerometers at different directions, the Z-axle (Vertical) acceleration is more susceptible to vehicle-pavement interaction, as expected. It is likely due to the largest deformation in vertical direction when the truck is passing. Meanwhile, the noises are observed during field measurement as Figure 3-13. The same signal process algorithm is adopted to smooth the testing data acquired from the accelerometer. Figure 3-14 presents the digital signal after process, in which the two axles of the tuck can be easily observed. According to the sample frequency of 64 Hz and the truck speed of 35 mph, equals to 15.64m/s, the time interval between the two peak impulses is 0.0156 second and axle spacing is calculated to be 3.05m, which approximates to the 3.4m axle spacing specified by GMC manufacture.

Due to the limitation of field conditions, only one type of truck was tested and solely speed of 35 mph was adopted. Higher speed cannot be tested because of the speed limitation in the test lane. In the future, more types of vehicles, different speeds and wheel loads combinations will be implemented in field-testing to further validate the proposed wireless sensor monitor system.

Figure 3-13 Sensor Location on Pavement (Zhang 2014)

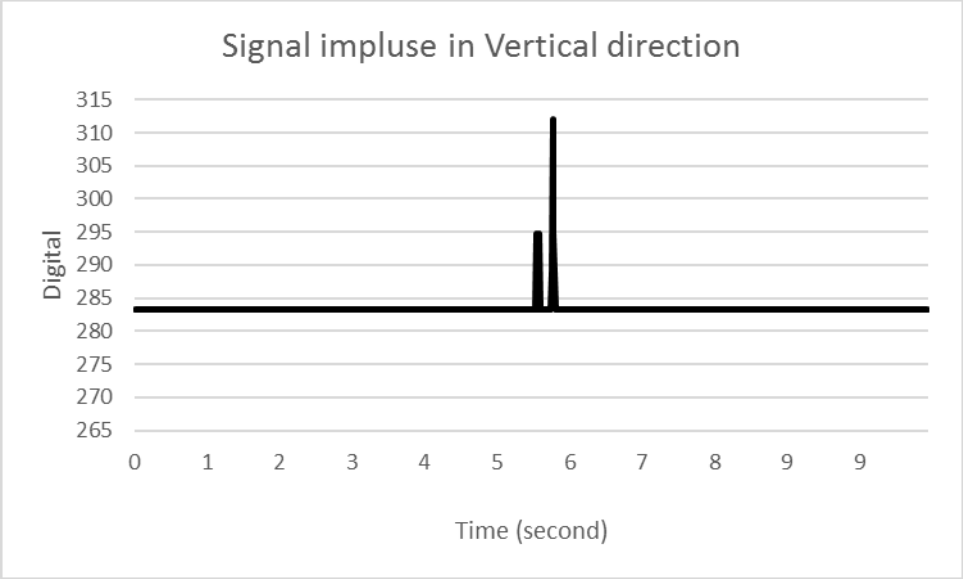

Figure 3-14 Z-axis Acceleration from field Test after processing

Summary and conclusions

The validation of an innovative and convenient traffic volume and vehicle classification monitoring system based on wireless sensor network and Internet of Things(IOT) technology, is performed in laboratory test, field test as well as the numerical simulation method. Since severe signal noises are observed during the accelerometer monitoring process which substantially interferes the recognition of useful signals, an advanced algorithm is developed to process the test data for valuable information extraction. The algorithm consists of a moving average smoothing filter and peak detector that could fruitfully locate each passing axle and report the time interval between two axles. The lowest error rate of this algorithm could be 2.85% for spacing estimation and 4.6 % for speed calculation. The simulation results of MMLS 3 have a good agreement with measurement for vertical acceleration. The in-field implementation for truck axle detection demonstrates the validation of the system. Based on all the test results sated above, it can be concluded that the IOT based wireless accelerometer system is feasible and sufficient accurate for traffic volume monitoring and vehicle classification.

However, due to the limitations of the test equipment and field conditions, more scenarios and improvements to the current testing method, including multi-embedded sensor system and multi-lanes conditions, still need to be evaluated for further validation of the system.

3.2.2 Strain gauges for wheel load information and asphalt mixture slab health monitoring

The strain gauges are actively connected to the data logger throughout the process of the MMLS3 trafficking, until the failure and damage of the gauges. Different speeds are applied to observe the relevant strain response. In the MMLS3 trafficking, the strain gauges are attached at the underside of the slab as shown in Figure 2.3, two in longitudinal direction and the other two in transverse direction.

The typical strain output pattern is presented in Figure 3-15. When the moving tire is passing over the strain gauge, the digital signal arrives the peak value in both longitudinal and transverse direction. As a result, through the counts of peak impulse, the number of passing load cycles can be extrapolated, which can be used for gaining wheel load information. As shown in Figure 3-15, the time interval between the two signal peaks as two black dash line can be obtained based upon the sensor sample frequency. The space between the bogie wheel in MMLS 3 is already known, then the velocity of the wheel can be calculated.

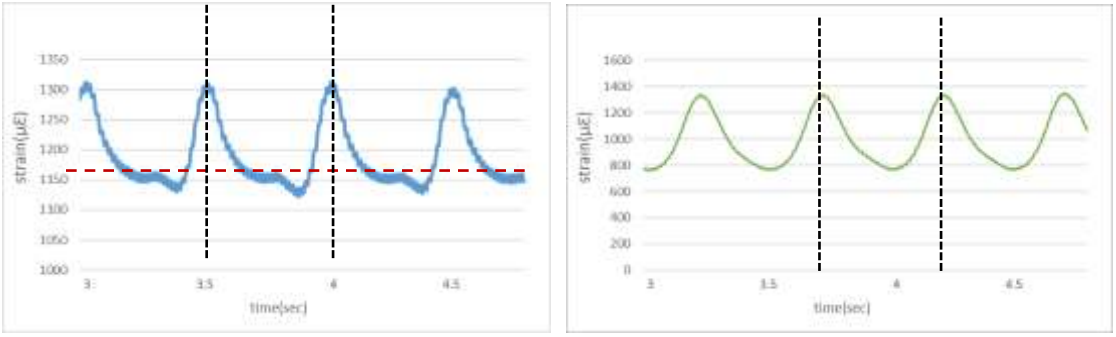

Longitudinal strain output Transverse strain output

Figure 3-15 Strain output history

The strain gauges are set up to record 10 sec duration data at interval of every 20 minutes continuously. Figure 3-16 demonstrates the strain history along with the accumulation of traffic load cycles in Lane 9B bottom and Lane 5 bottom lift tests. It can be noted that at the initial loading cycles, the strain value decreases immediately, which is due to the densification of the material resulting the stiffness increase. After that, the strain increases with the number of passes as expected due to the decrease of the stiffness, which is induced by damage of the repeated loads. However, after 40,000 to 50,000 load applications, counterintuitively, the tensile strain values decrease. The interpretation of this response is that asphalt mixtures become damaged and strain gauges loses strength and the ability to remain anchored or adhesive to the material and reflect smaller strain than the actual values. This phenomenon is also found in the ALF test (Gibson et al .2012), in which the strain decreases a short time of loading. In the full-scale ALF test, the strain gauges as Figure 3-1 is embedded in the pavement to measure the strains. Both the adhesive and embedded strain gauges are found not capable to record the strain changes in APT for long term monitoring. It is necessary to develop or find the strain gauges with high adhesive and anchored ability with asphalt mixtures.

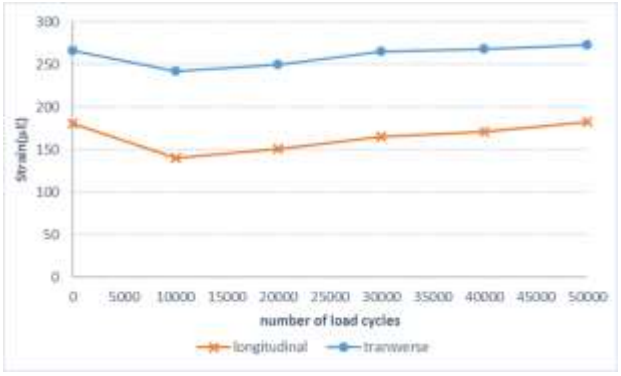

Lane 9B bottom lift

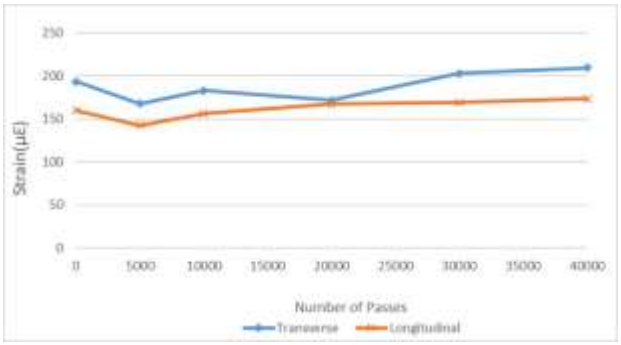

Lane 5 bottom lift

Figure 3-16 Strain history of Lane 9B bottom and Lane 5 bottom lift

The stiffness obtained from PSPA tests before approaching number of loads where the strain decreases, is plotted in Figure 3-17. The numerical simulation is implemented to calculate the tensile strain value at bottom of slab, which is pictured in Figure 3-17 as well. The trend of the calculated strain is in good agreement with the actual measurement indicating that the strain gauges somehow can be used to reflect stiffness decrease of the pavement, at least at the initial load period.

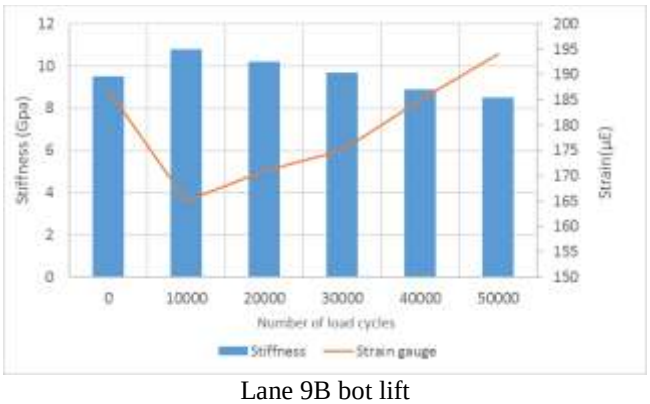

Lane 9B bot lift

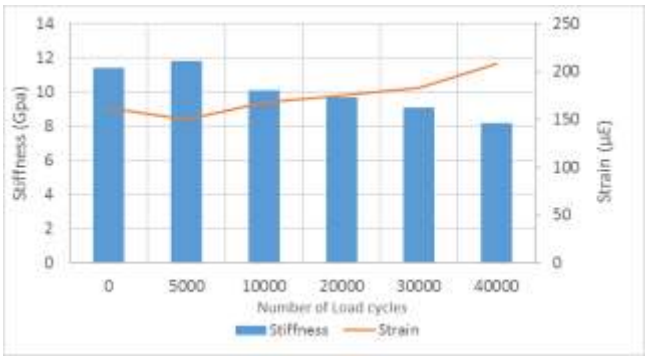

Lane 5 bot lift

Figure 3-17 Predicted strain based on stiffness

To acquire the speed effect on the pavement strain response, MMLS3 is set for trafficking at four different frequencies, 7200, 3600,2400, 1800 cycles/h, which correspond to speed of 2.6, 1.3,0.867, 0.65 m/s, respectively. It can be seen that, faster speed results in lower strain value of the same material, as depicted in Figure 3-18. These findings are consistent with the results of full scale APT (Sarkar, 2016). Both the longitudinal and transverse tensile strain has a good polynomial correlation with load frequency.

$$\varepsilon_{trans} = 0.0000023 \times f^2 - 0.04186f + 338.705$$
$$\varepsilon_{longi} = 0.0000035 \times f^2 - 0.04665f + 255.958$$

Where,

$\varepsilon_{trans} = Transverse\ tensile\ strain\ at\ bottom\ of\ asphalt\ layer$

$\varepsilon_{longi} = Longitudinal\ tensile\ strain\ at\ bottom\ of\ asphalt\ layer$

$f = load\ frequency$

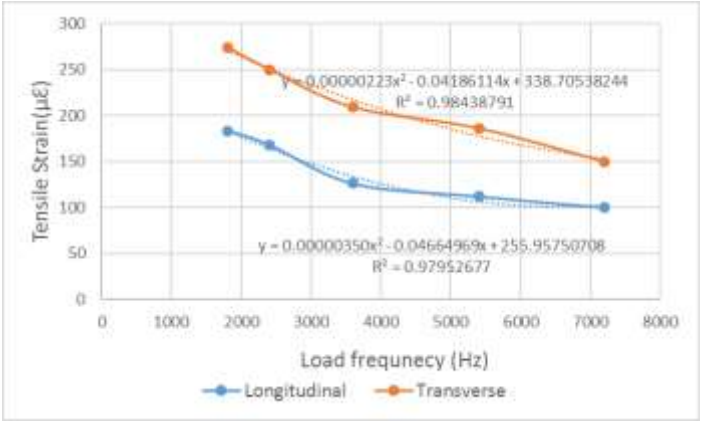

Figure 3-18 Strain values against loading frequency

In the lane 9B bottom lift test, the wheel load in MMLS 3 is adjusted to 1.8 kN, 2.1kN, 2.4 kN and 2.7 kN to measure the corresponding tensile strain responses at bottom of slab, as shown in Figure 3-19. The increase of wheel load leads to the greater boost of tensile strain. The strain gauge can also be used to identify different wheel load

magnitudes in MMLS 3 test. It is found that the longitudinal and transverse tensile strain has a good polynomial correlation with wheel load.

$$\varepsilon_{trans} = 36.222 \times L^2 - 62.167L + 181.25$$
$$\varepsilon_{longi} = 52.778 \times L^2 - 191.83L + 315.25$$

Where,

$\varepsilon_{trans} = Transverse\ tensile\ strain\ at\ bottom\ of\ asphalt\ layer$
$\varepsilon_{longi} = Longitudinal\ tensile\ strain\ at\ bottom\ of\ asphalt\ layer$
$L = Wheel\ Load$

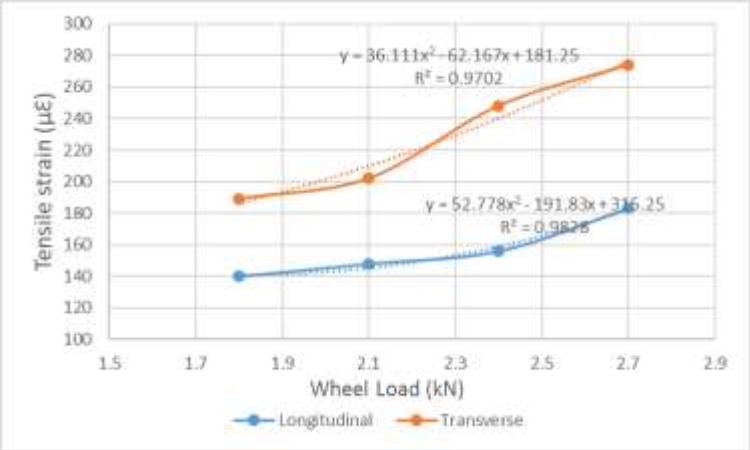

Figure 3-19 Tensile strain at bottom versus wheel load

Above all, both the accelerometer and strain gauges can be used to observe the wheel load speed. Besides, the strain gauges are capable of monitoring the modulus change of material, load frequency and wheel load magnitude.

3.3 Reference:

Al-Qadi, I. L., A. Loulizi, M. Elseifi and S. Lahouar (2004). "The Virginia Smart Road: the impact of pavement instrumentation on understanding pavement performance." *The Journal of APPT* 73: 427-465.

Bajwa, R., Rajagopal, R., Varaiya, P., & Kavaler, R. (2011). "In-pavement wireless sensor network for vehicle classification". *In Information Processing in Sensor Networks* (IPSN), 2011 10th International Conference on (pp. 85-96). IEEE.

Bajwa, R., & Varaiya, P. (2009). "Weigh-in-motion system using a mems accelerometer". *Technical report, EECS Department*, University of California, Berkeley.

Barbagli, B., Magrini, I., Manes, G., Manes, A., Langer, G., & Bacchi, M. (2010, July). "A distributed sensor network for real-time acoustic traffic monitoring andearly queue detection." *In Sensor Technologies and Applications (SENSORCOMM), 2010 Fourth International Conference* on (pp. 173-178). IEEE.

Coleri, S., Cheung, S. Y., & Varaiya, P. (2004, September). “Sensor networks for monitoring traffic”. *In Allerton conference on communication, control and computing* (pp. 32-40).

Jianming, H., Qiang, M., Qi, W., Jiajie, Z., & Yi, Z. (2012). “Traffic congestion identification based on image processing”. IET Intelligent Transport Systems,6(2), 153-160.

Gibson, N., Carvalho, R., Li, X., and Andriescu, A. (2016). “Fatigue Cracking of Recycled and Warm Mix Asphalts: Predicted Performance Considering Structural Variability Influences”. *Journal of the Association of Asphalt Paving Technologists*. AAPT 2016.

Gibson, N., Qi, X., Shenoy, A., Al-Khateeb, G., Kutay, M.E., Andriescu, A., Stuart, K., Youtcheff, J. and Harman, T. (2012). “Performance testing for Superpave and structural validation (No. FHWA-HRT-11--45)”.

Kafi, M. A., Challal, Y., Djenouri, D., Doudou, M., Bouabdallah, A., & Badache, N. (2013). “A study of wireless sensor networks for urban traffic monitoring: applications and architectures”. *Procedia computer science*, 19, 617-626.

Khanafer, M., Guennoun, M., & Mouftah, H. T. (2009). “WSN architectures for intelligent transportation systems”. In *New Technologies, Mobility and Security (NTMS), 2009 3rd International Conference on* (pp. 1-8). IEEE.

Lukanen, E. O. (2005). “Load testing of instrumented pavement sections.” Minnesota Department of Transportation, Research Services Section

“107 temperature sensor” < http://www.campbellsci.com/107> (Sep 30. 2016)

Potter, J. F., H. C. Mayhew and A. P. Mayo (1969). “Instrumentation of the full scale experiment on A1 trunk road at Conington, Huntingdonshire”. *Report LR296*, Road Research Lab /UK/: 41.

“Product overview” <http://www.ctlgroup.com/uploadedfiles/file_assets/pdfs/other/a10a2278-a248-46b1-a0cc-5ce4ec91199b.pdf>. (Sep 29. 2016)

“Pressure Cell”< http://www.geokon.com/4815>. (Sep 29. 2016)

Saghefar, M., Frink, E., Bortz, B. S., & Hossain, M. (2013). Instrumentation Experience at the Kansas Accelerated Pavement Testing Facility. In Airfield and Highway Pavement 2013: Sustainable and Efficient Pavements (pp. 1409-1423). ASCE.

Sharma, A., Chaki, R., & Bhattacharya, U. (2011). “Applications of wireless sensor network in Intelligent Traffic System: A review”. In *Electronics Computer Technology (ICECT), 2011 3rd International Conference on* (Vol. 5, pp. 53-57). IEEE.

Steyn, W., Du Plessis, L., Denneman, E. (2006). “Technical memorandum: instrumentation for APT and LTPP”. CSIR. Jan-2006. http://hdl.handle.net/10204/2957.

Timm, D. H., & Priest, A. L. (2004). “Dynamic Pavement Response Data Collection and Processing at The NCAT Test Track.” NCAT Report, 04-03.

Timm, D. H., Priest, A. L., & McEwen, T. V. (2004). “Design and instrumentation of the structural pavement experiment at the NCAT test track.” National Center for Asphalt Technology, Auburn University.

“TDR probes manuals” < https://s.campbellsci.com/documents/sp/manuals/tdr-probes.pdf> (Sep 30.2016)

Xue, W., Wang, D., & Wang, L. (2015). “Monitoring the Speed, Configurations, and Weight of Vehicles Using an In-Situ Wireless Sensing Network”. *IEEE Transactions on Intelligent Transportation Systems*, 16(4), 1667-1675.

Xue, W., Wang, L., & Wang, D. (2015). “A prototype integrated monitoring system for pavement and traffic based on an embedded sensing network”. *IEEE Transactions on Intelligent Transportation Systems*, 16(3), 1380-1390.

Yousef, K. M., Al-Karaki, M. N., & Shatnawi, A. M. (2010). “Intelligent traffic light flow control system using wireless sensors networks”. *Journal of Information Science and Engineering*, 26(3), 753-768.

Zhang, M., Song, J., & Zhang, Y. (2005). “Three-tiered sensor networks architecture for traffic information monitoring and processing.” In *Intelligent Robots and Systems, 2005.(IROS 2005). 2005 IEEE/RSJ International Conference on* (pp. 2291-2296). IEEE.

Zhang,W.(2014). “Vehicle Axle Detection and Spacing Calibration Using MEMS Accelerometer” thesis, presented to Virginia Polytechnic Institute and State University, in partial fulfillment of the requirements for the degree of Master of Science.

Chapter 4 NUMERICAL MODELS OF DIFFERENT SIMULATIVE TESTS

The numerical simulation in pavement engineering is an effective and efficient method to investigate the pavement response and performance under the moving vehicular loads. In this study, the commercial finite element software ABAQUS was adopted to simulate the pavement structure, in which the constitutive models of the material and the parameters directly affects the accuracy and precision of the simulation results. Some complicated constitutive models for asphalt mixtures are reviewed in this chapter. For simplicity, the base course and subgrade course is assumed as elastic material. Moreover, due to the material limitations, no plasticity relevant tests such as flow number and flow time are performed to attain the corresponding parameters for model calibration. Here, the viscoplasticity parameters for model are derived using the inverse methodology, according to the APA test results.

4.1 Literature review of constitutive model for asphalt mixture

Asphalt mixture is a sophisticated and complicated composite material consisting of asphalt mastic, miner aggregate and air voids. In addition, due to the different composition and source of asphalt as well as gradation, shape and angularity of aggregates, and diverse air void contents, asphalt mixtures exhibit varying mechanical properties and diverse damage modes at different conditions. Moreover, the properties and behaviors of asphalt mixtures are much relevant to temperature, loading time and rate, stress or stain level and stress state (Huang, 2008). The response of asphalt mixtures under the applied stress contains viscoelastic (recoverable) and viscoplastic (unrecoverable) strain components, which are time dependent and can occur simultaneously. Asphalt mixture exhibits linear or nonlinear prosperity depending on the combination of stress or strain level, temperature, and loading rate (Huang, 2008). Considerable efforts were devoted to develop constitutive models for predicting the performance of asphalt mixtures. Numerous models were proposed to characterize the complicated mechanical responses of asphalt mixtures. However, the most constitutive models focused on predicting a specific pavement distress that is associated with certain ranges of temperature and loading rates, including the linear and nonlinear viscoelastic models, viscoplatic and viscoelastoplastic models (Huang, 2008).

4.1.1 Viscoelastic models

Linear viscoelastic models

The behavior of asphalt mixture is typically described using linear viscoelastic models at low-strain conditions. The typical linear viscoelastic models include Maxwell model, Kelvin model, Burgers model and generalized Maxwell model.

Linear Equations (Schapery,1969)

The ratio of strain response is shown as follows, when a constant stress is applied at t=0,

$$\frac{\varepsilon}{\sigma} = D(t) \tag{4-1}$$

Where, $D(t)$ is named creep compliance. The stress-strain relation for the compliance can transformed to:

$$\varepsilon = D_0\sigma + \Delta D(t)\sigma \tag{4-2}$$

Where,

$D_0 \equiv D(0)$ = initical value of compliance

$\Delta D(t) \equiv \mathrm{D}(t) - D_0$ = transient component of compliance

Similarly, application of a constant strain at t=0 provides the stress relaxation modulus E(t)

$$\frac{\sigma}{\varepsilon} = \mathrm{E}(t) \tag{4-3}$$

$$\sigma = E_e\varepsilon + \Delta E(t)\varepsilon \tag{4-4}$$

Where,

$\mathrm{E}_e \equiv E(\infty)$ = initial value of modulus

$\Delta E(t) \equiv \mathrm{E}(t) - E_e$ = transient component of modulus

When D(t) is known, the strain response to an arbitrary stress is calculated by means of the Boltzmann superposition integral,

$$\varepsilon = D_0\sigma + \int_{0^-}^{t} \Delta D(t-\tau)\frac{d\sigma}{d\tau}d\tau \tag{4-5}$$

Similarly, the relaxation data can be used to calculate stress response to an arbitrary strain input:

$$\sigma = \mathrm{E}_e \varepsilon + \int_{0^-}^{t} \Delta E(t-\tau) \frac{d\varepsilon}{d\tau} d\tau \tag{4-6}$$

The equation can completely define linear stress-strain viscoelastic behavior of a given material.

Maxwell model

Maxwell model is represented as the spring in series with the dashpot, as shown in Figure 4-1. James Clerk Maxwell first proposed the model in 1867, to characterize viscoelastic material having the properties both of elasticity and viscosity (Roylance, 2001).

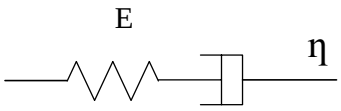

Figure 4-1 Illustration of Maxwell model

Governing equation:

$$\varepsilon = \varepsilon_1 + \varepsilon_2 \tag{4-7}$$

$$\dot{\varepsilon} = \dot{\varepsilon_1} + \dot{\varepsilon_2} \tag{4-8}$$

$$\dot{\varepsilon_1} = \frac{\dot{\sigma}}{E} \quad , \quad \dot{\varepsilon_2} = \frac{\sigma}{\eta} \tag{4-9}$$

$$\dot{\varepsilon} = \frac{\dot{\sigma}}{E} + \frac{\sigma}{\eta} \tag{4-10}$$

This equation can be applied either to the shear strength or to uniform tension with small deformation.

Kelvin Model

Kelvin model is represented by a spring and dashpot connected in parallel, as presented in Figure 4-2.

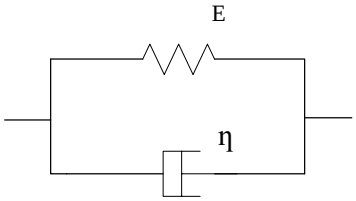

Figure 4-2 Illustration of Kelvin model

Governing equation:

$$\sigma = \sigma_1 + \sigma_2 \tag{4-11}$$

$$\dot{\sigma_1} = E\varepsilon \quad , \ \dot{\sigma_2} = \eta\dot{\varepsilon} \tag{4-12}$$

$$\eta\dot{\varepsilon} + R\mathcal{E} = \sigma \tag{4-13}$$

The Maxwell and Kelvin models are two fundamental components to characterize the viscoelasticity of material, but these two models are not capable to characterize the complicated mechanical properties of asphalt material independently. (Minnesota DOT, 2016). The Maxwell Kelvin model can characterize the stress relaxation behavior, but cannot exhibit the delayed elastic deformation. The Kelvin model is only able to describe the creep behavior but not able to represent stress relaxation process of material. The appropriate combinations of Maxwell and Kelvin models can improve the accuracy to characterize the viscoelastic response of material.

Burgers Model

The Burgers model consists of a Maxwell model and Kevin model in series. (See Figure 4-3)

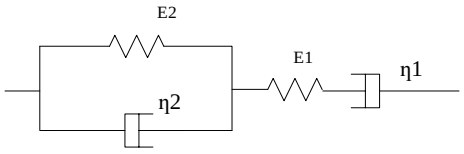

Figure 4-3 Illustration of Burgers Model

Governing equation:

$$\sigma = p_1\dot{\sigma} + p_2\ddot{\sigma} = q_1\dot{\varepsilon} + q_2\ddot{\varepsilon} \tag{4-14}$$

$$p_1 = \frac{\eta_1}{E_1} + \frac{\eta_1}{E_2} + \frac{\eta_2}{E_2}, \ p_2 = \frac{\eta_1\eta_2}{E_1E_2}, q_1 = \eta_1, q_2 = \frac{\eta_1\eta_2}{E_2} \tag{4-15}$$

$$\sigma + \left(\frac{\eta_1}{E_1} + \frac{\eta_1}{E_2} + \frac{\eta_2}{E_2}\right)\dot{\sigma} + \frac{\eta_1\eta_2}{E_1E_2}\ddot{\sigma} = \eta_1\dot{\varepsilon} + \frac{\eta_1\eta_2}{E_2}\ddot{\varepsilon} \tag{4-16}$$

The Laplace transform and inverse transform of above equations yield:

$$\varepsilon(t) = \sigma_0\left[\frac{E_1+E_2}{E_1E_2} + \frac{t}{\eta_1} + \frac{1}{E_2}e^{-\lambda t}\right] \tag{4-17}$$

$$\sigma(t) = \frac{\varepsilon_0}{\sqrt{p_1^2 - 4p_2}}[(-q_1 + \alpha q_2)e^{-\alpha t} + (q_1 - \beta q_2)e^{-\beta t}] \quad (4\text{-}18)$$

Where:

$$\lambda = \frac{E_2}{\eta_2} \quad (4\text{-}19)$$

$$\alpha = \frac{1}{2p_2}(p_1 + \sqrt{p_1^2 - 4p_2}) \quad (4\text{-}20)$$

$$\beta = \frac{1}{2p_2}(p_1 - \sqrt{p_1^2 - 4p_2}) \quad (4\text{-}21)$$

Burgers model describes the permanent deformation of asphalt mixtures as time dependent in linear function, while not able to reflect the consolidation effect for asphalt mixtures permanent deformation.

Generalized Maxwell Model

Generalized Maxwell model is represented by several Maxell elements assembled in parallel, pictured in Figure 4-4.

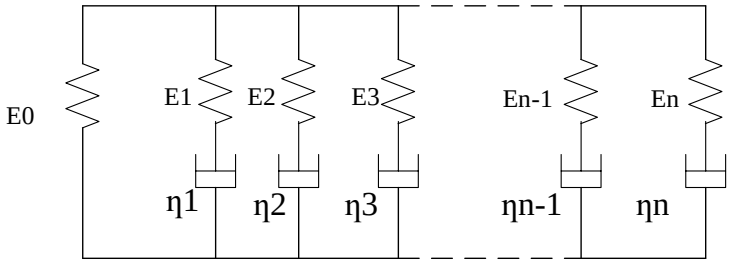

Figure 4-4 Illustration of Generalized Maxwell Model

Governing equation:

$$\sigma = \sum_{i=0}^{n} \sigma_i \quad (4\text{-}22)$$

When $i = 1,2, \dots, n$, the governing equation is as below,

$$\sigma_i + \frac{\eta_i}{E_i}\dot{\sigma_\iota} = \eta_i \dot{\varepsilon} \quad (4\text{-}23)$$

Through Laplace transform and inverse Laplace transform, the following equations can be derived,

$$\sum_{k=0}^{n} p_k \frac{d^k \sigma}{dt^k} = \sum_{k=1}^{n} q_k \frac{d^k \varepsilon}{dt^k} \quad (4\text{-}24)$$

Where,

$$(\frac{d}{dt})^0 = 1 \quad (4\text{-}25)$$

The generalized Maxwell model can characterize the complicated stress relaxation behavior. When the strain ε_0 is constant, the relaxed stress as follows,

$$\sigma(t) = \varepsilon_0 \sum_{k=1}^{n} E_k e^{-\frac{E_k}{\eta_k}t} \quad (4\text{-}26)$$

To date, the linear viscoelastic model is widely applied in numerical simulation method such as finite element technique, to predict the time-dependent response of flexible pavement. Moreover, the liner viscoelastic relationship can be easily and directly implemented in commercial finite element software ABAQUS, resulting in the popular application. For simplicity, nonlinear response was not taken into consideration in many studies, even though the experimental observations exhibited non-linear behavior of asphalt mixtures when subjected to higher level of stress or strain.

Non-Linear viscoelastic models

Asphalt mixtures behave as nonlinear viscoelastic once the stress/ strain exceeds a certain threshold value. Since the Boltzmann superposition is not valid for nonlinear material and the multiple integral is too complex, a modified superposition principle is used by incorporating nonlinearity into a single integral with a nonlinear integrand. The Schapery's single-integral constitutive model is the most widely used model and has been applied to characterize the nonlinear behavior of engineering materials. (Schapery 1969, Huang, 2008). The constitutive relation can be expressed as following equation,

$$\varepsilon(t) = g_0 \mathrm{D}_0 \sigma^t + g_1 \int_0^t \Delta D[\psi^t - \psi^\tau] \frac{d(g_2 \sigma^t)}{d\tau} d\tau \quad (4\text{-}27)$$

Where D_0 is the instantaneous elastic compliance, ΔD is the transient compliance, and ψ^t is the reduced time,

Where,

$$\psi^\tau = \int_0^t \frac{d\zeta}{\alpha_T \alpha_s} \quad (4\text{-}28)$$

Where,

g_0, g_1, and g_2 are the nonlinear parameters relevant to stress or , α_T is the temperature shift factor, and α_s is the stain or stress shift factor. g_0 is related to nonlinear instantaneous compliance, g_1 is associated with the nonlinear transient compliance, and g_2 is related to the loading rate effect on nonlinear response (Huang, 2008).

4.1.2 Viscoplastic models

Overwhelming experiments show that the Young's modulus, the initial yield stress, the hardening parameters, the peak strength, and the residual strength are not only a function of the strain and plastic strain, but also a function of the strain rate (Wang,2012). It is found that asphalt mixture exhibits viscoplastic behavior at high temperatures and high deformations. Even though considerable viscoplasticity theories were proposed, most of them were based on and derived from Perzyna model.

Perzyna model (1966)

In Perzyna model, the visco-plastic strain rate $\dot{\varepsilon}^{vp}$ tensor is defined as following:

$$\dot{\varepsilon}^{vp} = \gamma \langle \frac{F}{\sigma_Y} \rangle^N \frac{\partial Q}{\partial \sigma} \tag{4-29}$$

Where, γ= the material fluidity, the yield function F is rendered non-dimensional by the uniaxial yield stress value σ_Y. The $\langle X \rangle$ is defined as:

$$\langle X \rangle = \begin{cases} 0 & when \;\; X \leq 0 \\ X & when \;\; X > 0 \end{cases} \tag{4-30}$$

The yield function is directly equivalent to the plastic potential in the Perzyna model:

$$\mathrm{F} \equiv \mathrm{Q} \tag{4-31}$$

Therefore, the visco-plastic strain rate can be simplified as:

$$\dot{\varepsilon}^{vp} = \gamma \langle \frac{F}{\sigma_Y} \rangle^N \frac{\partial F}{\partial \sigma} \tag{4-32}$$

As above stated Perzyna model coupled the plasticity of material and loading times.

4.1.3 Two stage models

Elasto-viscoplastic models

Asphalt mixture behaves as elastic and liner viscoelastic at low temperatures or small deformation, as nonlinear viscoelastic and viscoplastic at high temperature and large deformation. Previously, some elasto-viscoplastic models were developed to represent asphalt mixture behavior, but these models did not take into account the nonlinear viscoelastic behavior of recoverable component. (Seibi et al., 2001; Oeser and Moller, 2004; Dessouky, 2005)

Viscoelastoplasitc model

Lu and Wright (1998; 2000), Lu et al. (2002) proposed a power-law visco-elastoplastic constitutive model based on Perzyna viscoplastic theory. Chehab et al. (2003) proposed a viscoelastoplastic continuum model to characterize asphalt mixtures subjected to uniaxial loading. Gibson (2006) proposed a purely empirical viscoelastoplastic model for the compressive behavior of asphalt mixture. A series of studies have been conducted by researchers from Texas A&M University to investigate viscoelasoplastic constitutive models of asphalt mixtures. However, these models are not capable to characterize the recovery behavior during creep-recover tests and repeated loading-unloading process.

Viscoelastic-Viscoplastic models

Consequently, it is necessary to model the viscoelastic and viscoplastic component separately, in order to develop a constitutive law describing the behavior of corresponding components. Huang (2008) incorporated the Schapery nonlinear viscoelastic model and Perzyna's viscoplastic model to represent the recoverable component and irrecoverable component, respectively. Levenberg et al. (2004) developed a tri-axial cross-anisotropic viscoelastic-viscoplastic constitutive model for asphalt mixture for small-strain domain. Saadeh et al. (2007) proposed an anisotropic nonlinear viscoelastic-viscoplastic model to capture asphalt mixture response and behavior under a wide range of temperatures, loading rates and stress states. However, these models do not consider the radial strain and are not capable of describing the stiffness degradation due to micro-cracks.

On the other hand, several models considering damage modes are developed and are capable to describe or predict the damage mechanism of asphalt mixture. Abu Al-Rub et al. (2010) put forth a micro-damage healing model that improves the ability of an integrated nonlinear viscoelastic, viscoplastic, and viscodamage constitutive model based on continuum damage mechanics for predicting the fatigue life of asphalt mixtures. Konartakheh (2011) proposed a thermos-viscoelastic-viscoplastic-viscodamage healing constitutive model based on the assumption of Helmohelotz free energy function and a form for the rate of entropy production. Sun et al. (2012) developed a two-stage viscoelastic-viscoplastic damage constitutive model for characterize different mechanical deformation response of asphalt mixture under various loading conditions. This model decomposes strain response into viscoelastic and viscplastic components and takes into account damage.

4.2 Numerical simulation using Finite element method

To compare the different scaled simulative tests in a more sophisticated manner, the numerical models of APA, MMLS3 and full scale ALF were developed using commercial finite element software ABAQUS. Although the natures of HMA and base layers were anisotropic, they are approximately modelled as homogeneous isotropic materials in this dissertation, for the purpose of simplicity and time saving of computation. Despite a great amount of efforts have been devoted on anisotropic simulation of asphalt mixture with three phases, all these simulations are performed on

the cylinder specimens only. For the case of large-scale pavement modeling, it is impractical to carry out the simulation work in ABAQUS for the current computer systems, because it is extremely time consuming for computation. On the other hand, Masad et al. (2006) reported that such an approximation has shown only marginal impact on pavement fatigue lives. Accordingly, the asphalt mixture was modelled as a homogeneous viscoelastic-viscoplastic material. In order to model the realistic mechanical properties of asphalt mixture, the relaxation modulus and plastic parameters must be taken into account. It is known that the base layer and subgrade course are not elastic which results in permanent deformation, while most of the deformation are recoverable and can be regarded as elastic (Huang 2004). Thus, material behavior of underlying layers is regarded as liner elastic, which are commonly used in previous studies.

4.2.1 Tire-pavement contact area and stress in simulation

For more closely simulation of actual pavement response under vehicular loads, the tire-pavement contact area and contact stress should be determined accurately. Many previous studies have been conducted to determine the exact tire-pavement contact area and the distribution of stress inside pavement structure (Al-Qadi et al, 2002; 2005; 2007). Regarding the measurement of actual tire-pavement contact stress, it is found the distribution of the contact stress is not evenly. The maximum stress is observed at edge of tread, which could be more than 1,000 kPa (Al-Qadi et al, 2007). In this study, the tire-pavement contact area and distribution of stress were simulated as Figure 4-5, when investigating pavement responses. For the evaluation of rut susceptibility, the tire contact area is assumed square and the pressure is assumed evenly distributed.

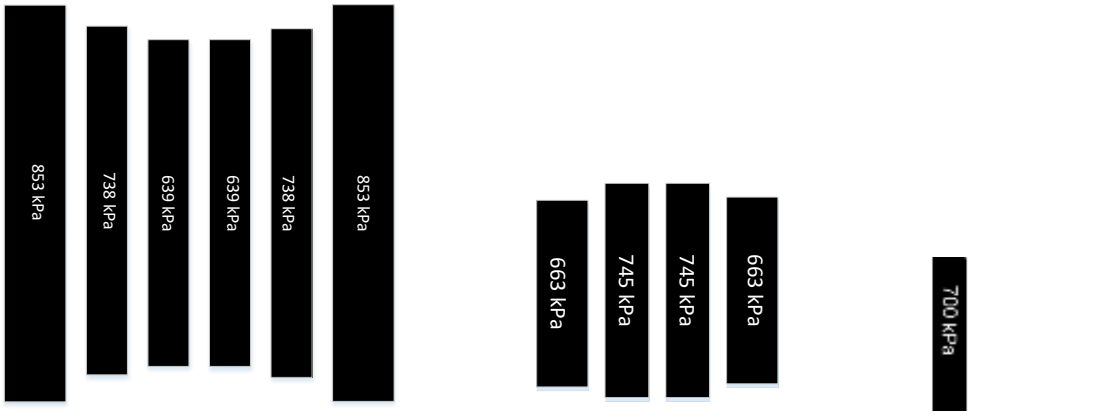

Super Single tire (Elseifi et al. 2005) MMLS3 tire APA pressure hose

Figure 4-5 Tire footprint simulation of ALF, MMLS3 and APA

4.2.2 Dynamic loading method

To simulate the moving vehicular loading at a certain speed, in the FEM simulation, a user defined load function is applied to represent the moving load. The concept of modeling the actual rolling tire as an independent part is tried at first, but the significantly low computational efficiency and the discontinuities that violated the boundary conditions introducing incompatibilities in the stress equilibrium leads to the abandon of the concept for realistic tire simulation. Consequently, for the purpose of simplification and computational time saving, the moving load is simulated as the footprint area gradually shifts over the loading area at each step until a single wheel pass is completed. A linear loading amplitude is adopted to more accurately simulate the entrance and exit parts of the tire as in Figure 4-6. The load sequence for multiple loads axles is specified in Figure 4-7, T= one load cycle time, T_0 = time of entrance and exit part of the tire imprint are, T_1= time of load passing over the tire imprint area.

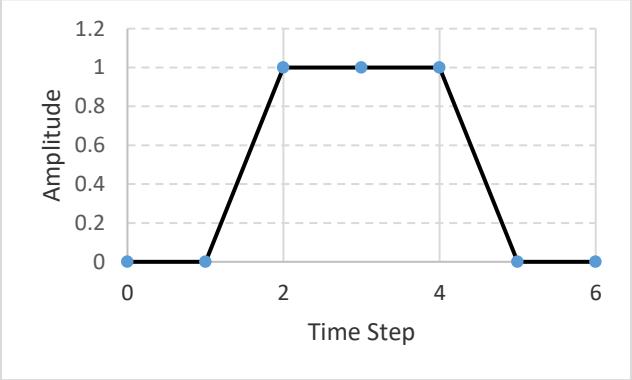

Figure 4-6 Schematic of the trapezoidal loading amplitude

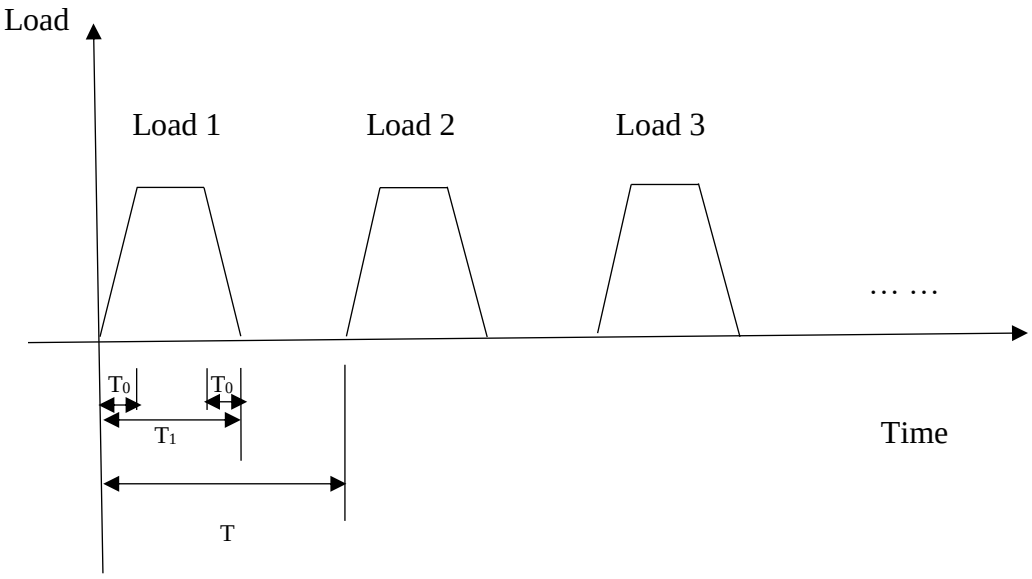

Figure 4-7 Sequence of the cyclic loading

Besides, the concept of continuously moving load (Yoo et al., 2008) is applied in this paper, as presented in Figure 4-8, which can more accurately represent the moving wheel load. At initial step the load is exerted on 1 to 4 element, then removing the load on element 1 and imposing on the element 5, until the imprint passes the loading area as one load cycle. On the other hand, in the ABAQUS modelling work of this dissertation, the shear contact stresses (longitudinal and transverse) are applied on the tire imprint area as well. The maximum longitudinal shear stress is assumed 12% of the tire-induced vertical stress, while the maximum transverse shear stress is assumed to be 48% of vertical stress. The shear contact stresses are assembled into the equivalent concentrated forces on the element nodes in tire imprint area. The More detailed information with respect to the moving load simulation can be found elsewhere (Yoo et al. 2008).

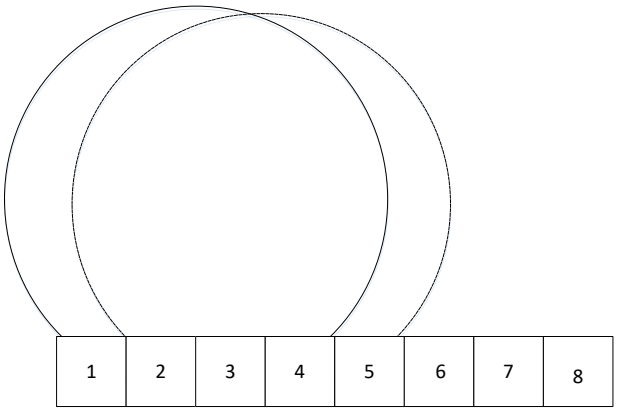

Figure 4-8 Loading step at the surface of specimens

One can note that the typical simplification is to use cyclic plate loads to represent the repeated moving wheel loads. The cyclic load time is equivalent to load duration at certain speed. However, in accordance with previous study (Brown & Chan 1996, Carvalho 2012), the cyclic plate loads produce much lower permanent deformations than moving loads do with similar load magnitude and number of cycles due to the shear stress reversal. Because the direction principal stresses rotate, resulting shear stress reversals (tension to compression or vice –versa). Thus, compared to cyclic plate loads approach, despite of more computational effort, the moving load simulation is more close to the realistic wheel load mechanism.

The dynamic transient analysis is used in this dissertation considering the inertia effect induced by the moving load, damping effect, and frequency-dependence of material properties. Previous studies points out that the dynamic effects of moving loads on pavement strain responses are significant and should not be neglected, and the dynamic transient analysis produces greater strain and residual stress in flexible pavement at low or intermediate temperatures (Zafir, 1994; Yoo & Al-Qadi, 2007). The implicit analysis mode in ABAQUS is incorporated in the simulation, because the transient mechanic response of asphalt mixture is more effectively simulated using the implicit integration method as dynamic equilibrium equation solution.

4.2.3 Simulation Parameters determination

The HMA mixtures were Superpave 12.5mm nominal maximum aggregate size designed at 65 gyrations compaction. The loose mixtures were collected during ALF test lane construction for laboratory samples fabrication and mixture testing. Dynamic modulus test was performed on the samples in an AMPT at FHWA laboratory (Gibson et al. 2016), and the dynamic modulus data is tabulated as following Table 4-1.

Table 4-1 Dynamic Modulus Data for the two lane material

Temperature (°C)	Frequency(Hz)	Dynamic Modulus(Pa)	
		Lane 9	Lane 5
4.4	25	16698000	20437000
	10	15138000	18862000
	5	13867000	17656000
	1	11089000	14806000
	0.5	9825000	13522000
	0.1	7184000	10620000
21.1	25	7990000	11145000
	10	6554000	9529000
	5	5556000	8419000
	1	3585000	5994000
	0.5	2945000	5099000
	0.1	1683000	3293000
37.8	25	2590000	4433000
	10	1850000	3414000
	5	1412000	2754000
	1	700000	1553000
	0.5	501000	1180000

	0.1	238000	608000
54.4	25	565000	1238000
	10	384000	880000
	5	286000	660000
	1	136000	320000
	0.5	100000	231000
	0.1	62000	121000

Master curve

According to Mechanistic-Empirical Pavement Design Guide (MEPDG), the dynamic values at different temperatures and frequencies are used to develop the master curve, which is constructed using the principle of time-temperature superposition. The data at varying temperatures is shifted with respect to time until merging into a smooth curve, based upon a reference temperature. In light of the master curve, the stiffness of the HMA at all levels temperatures and load rate can be determined. The master curve of dynamic modulus built in this manner describes the time dependency feature of the material. The amount of shifting at each temperature represents the temperature susceptibility of the mixture.

In the MEPDG, the master curve of dynamic modulus can be represented by a sigmoidal function as Equation 4-33,

$$\log(E^*) = \delta + \frac{\alpha}{1+e^{\beta+\gamma(\log t_r)}} \quad (4\text{-}33)$$

Where,

t_r = reduced time of loading at reference temperature

δ= minimum value of E^*

$\delta + \alpha$= maximum value of E^*

β, γ = parameters describing the shape of the sigmoidal function

The shift factor can be shown as follows,

$$a(T) = t/t_r \quad (4\text{-}34)$$

Where,

$a(T)$ = Shift factor

t= time of loading

t_r = Reduced time of loading at reference temperature

T= target time

For the purpose of precision, the relationship between the shift factor and temperature can be expressed as:

$$\text{Log } a(T_i) = aT_i^2 + bT_i + c \quad (4\text{-}35)$$

Where,

$a(T_i)$ = Shift factor

T_i = Temperature of interest

a, b and c = Coefficients of the function

The Excel Solver function is used to obtain the nonlinear optimization result for Equation 4-33 to 4-35. Based upon the above calculations, the master curve of the temperature-dependent Lane 5 and Lane 9 asphalt mixture modulus is derived, as presented in Figure 4-9. The shift factor is approximated by the Willams-Landell-Ferry (WLF) function. C_1 , C_2, T_r and modulus at long term are input to determine the dynamic modulus curve.

$$\text{Log } a(T) = -\frac{C_1(T-T_r)}{C_2+(T-T_r)} \quad (4\text{-}36)$$

Where,

T= temperature of interest

T_r = reference temperature

C_1, C_2= empirical constants

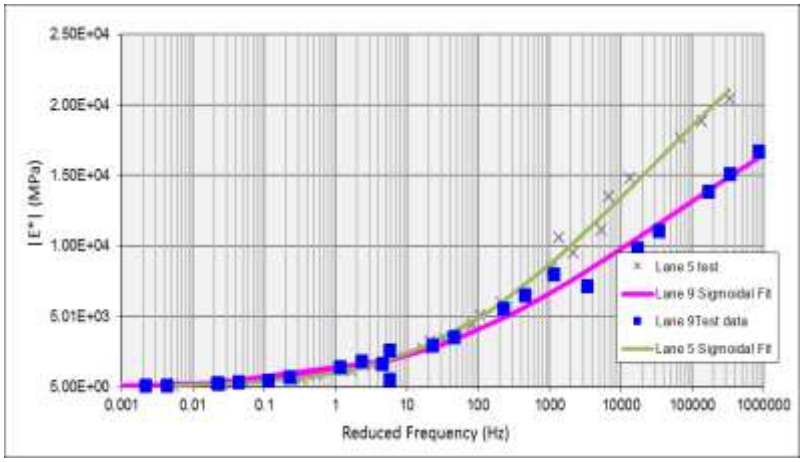

Figure 4-9 Master curve of Lane9 and Lane5 material

The relaxation modulus and creep compliance

The dynamic modulus E^* is a commonly measured property of asphalt concrete, which is the ration between the peak dynamic stress and peak dynamic strain. The storage modulus E' and loss modulus E'' are the real and imaginary components of dynamic complex modulus (Findley et al. 1989 and Gibson et al. 2003).

$$\mathrm{E}'(\omega) = |\mathrm{E}^*(\omega)|\, cos\emptyset(\omega) \tag{4-37}$$

$$\mathrm{E}''(\omega) = |\mathrm{E}^*(\omega)| sin\emptyset(\omega) \tag{4-38}$$

$$E^* = \mathrm{E}'(\omega) + \mathrm{iE}''(\omega) \tag{4-39}$$

Where,

ω =Frequency

$\emptyset$ = Phase angle

The storage and loss moduli corresponding to a Generalized Maxwell model can also be represented in terms of Prony series,

$$\mathrm{E}'(\omega) = E_0 \sum_{i=1}^{N} \frac{\rho_i^2 \omega^3 E_i}{1+\omega^2 \rho_i^2} \tag{4-40}$$

$$\mathrm{E}''(\omega) = \sum_{i=1}^{N} \frac{\overline{g_i}^P \tau_i \omega}{1+\omega^2 \tau_i^2} \tag{4-41}$$

Where,

E_i = elastic stiffness in the generalized Maxwell model

ρ_i = viscous relaxation times in the generalized Maxwell model

In order to characterize the viscoelasticity of asphalt mixture, a Prony series to represent the relaxation modulus and creep compliance can be used for Generalized Maxwell model.

$$E(t) = E_0 + \sum_{i=1}^{m} E_i e^{-\frac{t}{\rho_i}} \tag{4.42}$$

$$D(t) = D_0 + \sum_{j=1}^{n} D_j (1 - e^{-\frac{t}{\tau_j}}) \tag{4.43}$$

Where,

E_0 = long time equilibrium modulus;

E_i = elastic stiffness of each Maxwell spring;

ρ_i = relaxation times of each Maxwell dashpot;

D_0 = initial or glassy compliance; D_j = compliance; τ_j = relaxation times.

Given the master curve of dynamic modulus, and phase angle in master curve over a range or reduced frequency, the relaxation modulus can be determined (Gibson et al. 2003). After the interconverting the Equation 4-40 to 4-43 and the corresponding parameters, the storage and loss moduli can be expressed as below (ABAQUS Analysis User's Manual),

$$\mathrm{E}'(\omega) = E_0[1 - \textstyle\sum_{i=1}^{N} \overline{g_i}^P] + E_0 \textstyle\sum_{i=1}^{N} \frac{\overline{g_i}^P \tau_i^2 \omega^2}{1+\omega^2\tau_i^2} \tag{4-44}$$

$$\mathrm{E}''(\omega) = E_0 \textstyle\sum_{i=1}^{N} \frac{\overline{g_i}^P \tau_i \omega}{1+\omega^2\tau_i^2} \tag{4-45}$$

Where,

ω =angular frequency

N = the number of terms in Prony series

$\overline{g_i}^P, \tau_i$= material constants

In ABAQUS simulation, $\overline{g_i}^P$ *and* τ_i are specified as Prnoy series parameters to characterize the viscoelastic properties of asphalt mixtures.

For simplicity, the granular aggregate base (GAB) and subgrade are assumed as isotropic linear elastic and time-independent material. The neoprene sheets used in MMLS 3 are assumed isotropic elastic material in the ABAQUS modelling as well. The assumption for GAB and subgrade as linear elastic material also excludes the consideration of rutting for underlying courses. The specific material parameters in each layer and the layout of

the test pavement structure of ALF, MMLS3, and APA are shown in Figure 2-4. It can be seen that the total thickness of pavement structure for ALF, MMLS 3 and APA trafficking is 96 cm, 40cm, and 5cm respectively.

4.2.4 Parameters for Plasticity

It is well known that asphalt mixture behaves both viscoelasticity and viscoplasticity, thus in order to better characterize the mechanical properties of asphalt mixture, the numerical simulation in this study must accounts for the viscoplasticity, which is primary mechanism inducing permanent deformation of asphalt concrete. The parameters for viscoelastic component can be derived as state above. However, as a result of the limitations for the test conditions and amount of the mixtures and the complexity of the collaborative project, no tests for characterizing the plasticity of asphalt mixtures were conducted to attain the corresponding parameters which can be adopted in the numerical simulation.

In this work, the inverse method is used to obtain the parameters, which is based on a trial and error method (Wang, Y., 2005). The objective function is defined as following,

$$\text{Obj(u)} = \sum_1^N (D_i^E - D_i^S)^2 \quad (4\text{-}46)$$

Where,

i= the number of loading cycles,

D_i^E, D_i^S= permanent deformation from experimental measurement and model simulation after ith load cycles.

Obj= the objective function which is expected to approximate 0, or as small as possible.

u = the target model parameter.

Wang Y. (2007) obtained the parameters using the inverse methods and developed an iterative program to optimize the parameters by comparing the experimental measurements and model simulations. She characterized the asphalt mixture properties using a two-layer Elasto-viscoplasticity Model with 10 parameters (For elastic part, elastic modulus E and Poisson's ratio μ; for the viscous part, four parameters: A, m, n, and f; for the plastic part, four parameters: initial yield-stress Y_0, B, C, and D).

The equation for plasticity in the two-layer Elasto-viscoplasticity model is as follow,

$$\dot{\varepsilon}^{cr} = (A\sigma_{cr}^n((m+1)\varepsilon^{cr})^m)^{\frac{1}{m+1}} \quad (4\text{-}47)$$

Where $\dot{\varepsilon}^{cr}$ = uniaxial creep strain rate, ε^{cr} = creep strain,

$$\varepsilon^{cr} = \frac{1}{m+1} A\sigma_{cr}^n t^{m+1} \quad (4\text{-}48)$$

σ_{cr} = the uniaxial creep stress. t is the total time. A, n, and m are material constants depending on temperature.

In accordance with Wang Y. (2005) findings, the viscous parameter f and initial yield stress Y_0 are the most sensitive parameters for the permanent deformation, and the other parameters are material constants depending on temperatures. Since the dynamic modulus test for the asphalt mixtures was performed at FHWA at Turner-Fairbank

Highway Research Center (T-F), and thus, the parameter inverse method is only explored for parameters with regard to plasticity in this dissertation. The main objective of the parameters inverse method is for the permanent deformation, while the viscoelastic component is the most computational time consuming part and the viscosity in viscoelastic component has little effect on the permanent deformation. Thus in the plasticity parameter inverse approach, the APA test simulation employs the elastic-viscoplastic model instead of viscoelastic-viscoplastic model to compare the permanent deformation with measurement results at 50 load cycles. The elastic properties are determined from the dynamic modulus master curve of the asphalt mixture for the corresponding temperature and loading rate at APA test.

The two-layer elastic-viscoplastic model provided in ABAQUS is adopted to characterize the viscoplastic component of asphalt mixture is this dissertation, which is useful for modelling materials with significant time-dependent and plastic behaviour.
Using the inverse method, the parameters are optimized accordingly and the simulated permanent deformation at 500-550 load cycles based upon optimized parameters are presented in Figure 4-10, in which the APA test rutting measurements are compared with that obtained from simulation. Because it is commonly accepted that the rut depth before the 500 cycles is mainly caused by the post compaction and densification, which cannot be represented in the numerical simulation of this study. Therefore, the parameters optimization is based on the rut depth minus rut depth at 500 cycles for the load repetitions more than 500.

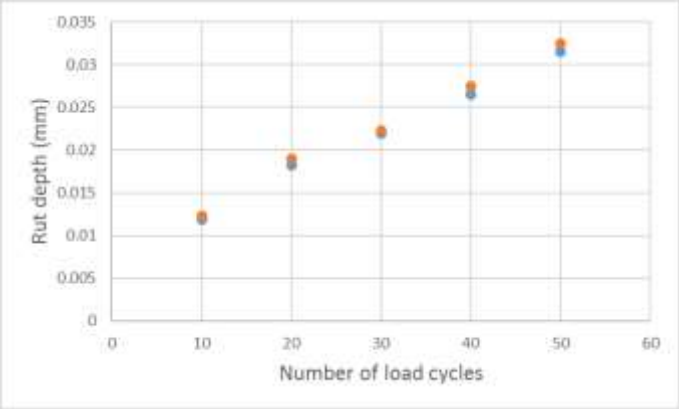

Figure 4-10 Optimized simulation results for 500-550 load cycles

4.2.5 Boundary conditions

In the ALF test, the layered test lanes are constructed as the realistic pavement structure. Thus, in the finite element method (FEM) simulation, the nodes at bottom are considered as encastre (fixed for all degrees), while the perimeter faces of the geometric model is set for symmetry in the perpendicular direction to the face. In the MMLS 3 trafficking, the asphalt mixture slab and neoprene sheets are placed above the concrete floor which is considered as subgrade in the simulation. The nodes on perimeter of two upper layers are free without restriction, and the bottom of concrete floor are considered encastre, while

the perimeter faces of the bottom layer is considered symmetry in direction perpendicular to the faces. The beam specimen for APA test is confined within the metal rigid mold during the wheel loading. Therefore, in the FEM simulation, the nodes at bottom side are encastre, while the perimeter faces are only restricted in horizontal direction. The detailed boundary conditions are pictured as Figure 4-11.

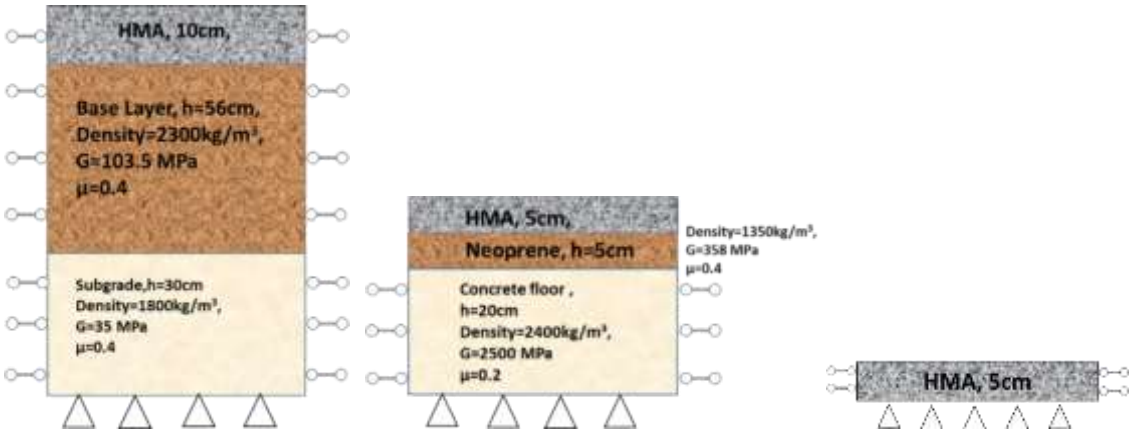

Figure 4-11 Boundary conditions of the ALF, MMLS 3 APA tests

4.2.6 Mesh size effect

In the three different simulations using ABAQUS, the element type is selected as Eight-node brick element with reduced integration (C3D8R). As is well known that, the element mesh size has a critical influence on the computational accuracy, while the fine mesh size results in more computational time. Therefore, the determination of the fine element mesh size should take into account both the computational efficiency and accuracy. For this reason, a series of fine element analysis is performed with decreasing element size to determine the optimal size. In addition, to insure the accuracy of the numerical calculation, the area close to wheel path is meshed in finer sizes. As for APA geometry model, three kinds of meshes with a total of 2500, 4800 and 7500 elements are compared to check the convergence of the solution. The total deformation of top surface at wheel path after 50 load cycles are presented in Figure 4-12. It can be seen, that the increasing of element numbers from 4800 to 7500, does not leads to evident difference in total deformation, but it saves a large amount of computational time. Consequently, the APA model is determined to be meshed with 4800 elements as the optimal balance between the mesh size and computational time. Similarly, the number of elements in MMLS 3 and AFL models are determined as 12665 elements and 28704 elements, respectively.

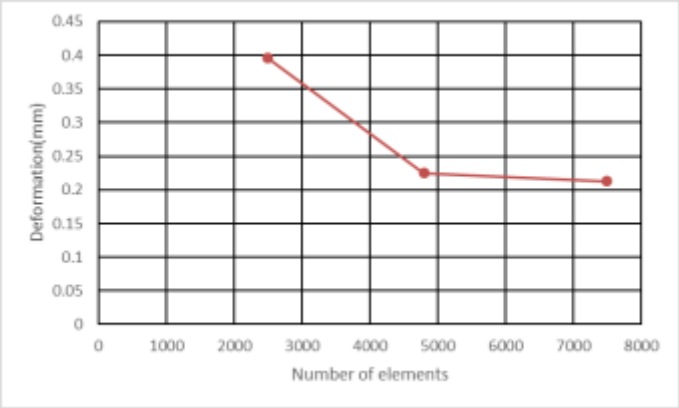

Figure 4-12 Deformation vs. number of elements

4.2.7 Results and Discussion

The 3-dimensional models of ALF, MMLS 3 and APA tests are presented as below. To promote the calculation accuracy, the mesh size is much finer at the moving load area, as can be seen in Figure 4-13. In the MMLS 3 and APA experiments, the strain at the bottom side of surface layer is monitored during the trafficking, which records the transient response of surface material under the moving load. The verification of the simulation is conducted by comparison between tensile strain of simulation result and experimental tensile strain measurement.

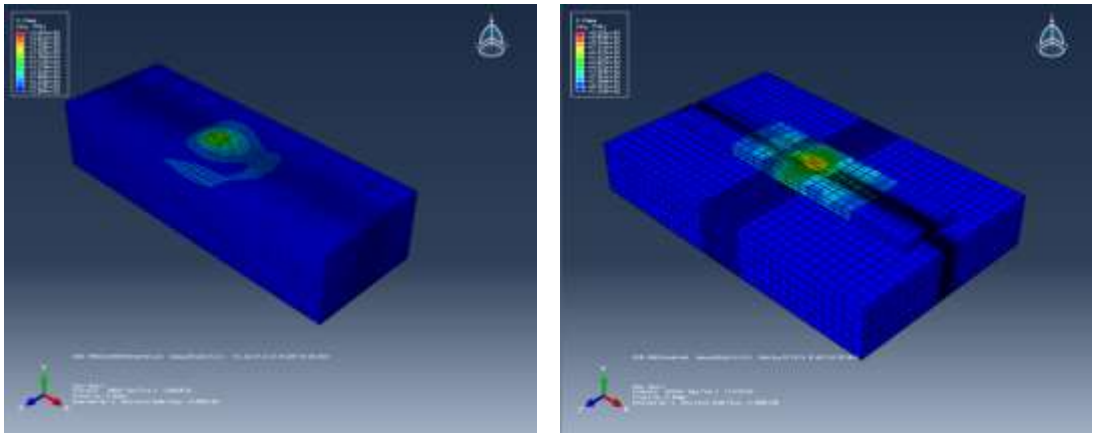

APA MMLS 3

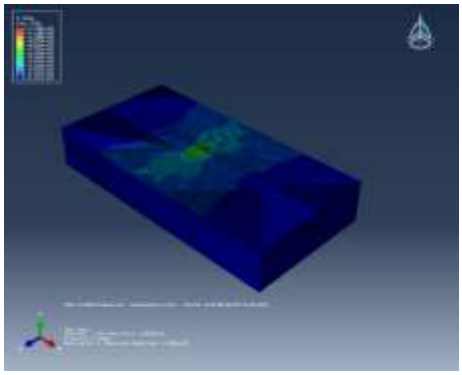

ALF

Figure 4-13 Simulations in finite element analysis software ABAQUS

Tensile Strain at bottom of surface layer

The tensile strain history at the bottom side of MMLS 3 testing is shown in Figure 2-8, while the strain output obtained from simulation versus time history is depicted as Figure 4-14. It is noteworthy that the simulated tensile strain history exhibits the similar pattern as that from actual measurement (as Figure 2-8), which likewise shows a compressive part followed by a tensile part when the loads is approaching and moving over the strain gauge. When the load is moving off, the strain gauge is also under compressive status, while the transverse tensile strain gauge is entirely in tension status during the approaching and leaving status of the tire. In addition, compared with the measured strain output history of MMLS 3, the simulated maximum longitudinal tensile strain is about 194 με, which is close to the experimental measurement as 180 με, while the measured maximum transverse strain is more than 350 με, which is much greater than that of simulation result. The likely reason is that the maximum tire-pavement localized contact stress at the edge of tread is more than 1000 kPa when the tire pressure is 689 kPa, according to the actual measurement as shown in Figure 2-5. Nevertheless, in the model simulation as shown in Figure 4.5, the maximum contact pressure in the middle tread is solely 745kPa, which is evidently lower than the measured contact stress.

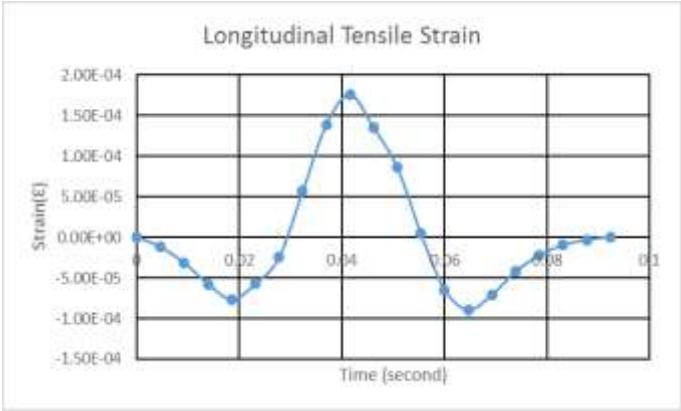

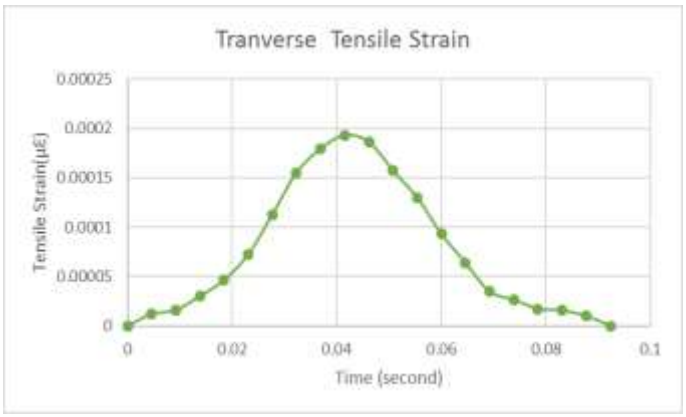

Figure 4-14 Simulated tensile strain history in MMLS3

Shear stress

The shear stress reversal of a wheel path element in MMLS 3 simulation can be observed in Figure 4-15, indicating the simulation is capable of representing the shear stress responses of asphalt mixture under moving load, of which the pattern approximates to the actual measurement and the previous finite element simulation under moving wheel load (Brown & Chan 1996, Carvalho 2012).

Figure 4-15 Shear stress reversal vs. time

There is a good agreement between the predictions using simulations and the actual measurements, indicating the viscoelastic-viscoplasitic model is feasible and accurate to represent the responses of asphalt mixtures under MMLS 3 trafficking, and the parameters obtained from inverse method can accurately predict the permanent deformation in APA test.

Pavement responses comparisons between Lane 5 and Lane 9 material

The maximum strain at bottom of asphalt layer and the compressive stress at top of subgrade for Lane 5 and Lane 9 under ALF, MMLS 3 and APA obtained from

simulations are compared in Table 4-2. Lane 5 is composed of 40 % of RAP and Lane 9 material contains 20% of RAP by weight, implying that Lane 5 material is stiffer than Lane 9. According to the numerical simulation results, the maximum strain value at bottom of asphalt layer and the compressive stress at top of subgrade of Lane 5 tests are slightly less than Lane 9 materials, which is consistent with the greater stiffness of Lane 5 material.

Table 4-2 Comparisons of pavement response of Lane 5 and Lane 9

	APA		MMLS 3		ALF	
	Strain at bottom of AC layer(με)	Compressive stress at top of subgrade(Pa)	Strain at bottom AC layer(με)	Compressive stress at top of subgrade(Pa)	Strain at bottom AC layer(με)	Compressive stress at top of subgrade(Pa)
Lane 9	1.92	N/A	194	117012	403	32100
Lane 5	1.56	N/A	167	103918	365	30390

4.3 Reference:

ABAQUS, I. (2012). ABAQUS User Manual.

Al-Qadi, I.L., Loulizi, A., Janajreh, I., and Freeman, T.E. (2002) "Pavement Response to Dual Tires and New Wide-Base Tires at Same Tire Pressure," *Transportation Research Record*, No. 1806, TRB, Washington, D.C., pp. 38-47.

Al-Qadi, I.L., Elseifi, M.A. and Yoo, P.J. (2005) "Characterization of Pavement Damage Due to Different Tire Configurations," *Journal of the Association of Asphalt Paving Technologists*, Vol. 84, AAPT, pp. 921-962.

Al-Qadi, I.L., and Elseifi, M.A. (2007) "State-of-the-Practice of the New Generation of Wide-Base Tire and Its Impact on Trucking Operations," *Transportation Research Record*, No. 2008, TRB, Washington, D.C., pp. 100-109.

Brown, S. F., and F. W. K. Chan. (1996). "Reduced rutting in unbound granular pavement layers through improved grading design." *Proceedings of the Institution of Civil Engineers. Transport*. Vol. 117. No. 1. Institution of Civil Engineers.

Carvalho, R. L. (2012). "Prediction of permanent deformation in asphalt concrete." thesis, presented to University of Maryland, in partial fulfillment of the requirements for the degree of Doctor of Philosophy.

Chehab, G. R., Kim, Y.R., Schapery, R.A., Witczak, M.W., and Bonaquist, R. (2003). "Characterization of asphalt concrete in uniaxial tension using a viscoelastoplastic model." *Journal of the Association of Asphalt Paving Technologists*, 72, 315-355.

Collop, A.C., Scarpas, A. T., Kasbergen, C., and de Bondt, A. (2003). "Development and finite element implementation of stress-dependent elastoviscoplastic constitutive model with damage for asphalt." *Transportation Research Record 1832, Transportation Research Board*, Washington, DC, 96-104.

"Creep from BBR.pdf"<http://www.dot.state.mn.us/mnroad/projects/Low%20Temperature%20Cracking/PDF's%20&%20Images/Task%20Reports/T3.3b%20-%20Creep%20from%

20BBR.pdf> (03, 2016).
Dessouky, S., (2005). “Multiscale approach for modeling hot mix asphalt.” thesis, presented to Texas A&M University, in partial fulfillment of the requirements for the degree of Doctor of Philosophy.
Elseifi, M., Al-Qadi, I., Yoo, P., and Janajreh, I. (2005). “Quantification of Pavement Damage Caused by Dual and Wide-Base Tires.” *Transportation Research Record*, 1940(1), 125–135.
Patrick, J., Kathirgamanathan, P., Cook, S., Herrington, P., and Arampamoorthy, H. (2011). “Small-scale accelerated pavement testing machine.” *Road and Transport Research*, 20(3), 33–40.
Findley, W.N., Lai, J.S., and Onaran, K. (1989). “Creep and Relaxation of Nonlinear Viscoelastic Materials.” Dover, New York.
Gibson, N., Schwartz, C., Schapery, R., & Witczak, M. (2003). “Viscoelastic, viscoplastic, and damage modeling of asphalt concrete in unconfined compression.” *Transportation Research Record: Journal of the Transportation Research Board*, (1860), 3-15.
Gibson, N. H. (2006). “A viscoelastoplastic continuum damage model for the compressive behavior of asphalt concrete.” thesis, presented to Univ. of Maryland, College Park, MD, in partial fulfillment of the requirements for the degree of Doctor of Philosophy.
Graham, M. A. (2009). “Viscoelastic–viscoplastic damage model for asphalt concrete”. thesis, presented to Texas A&M University, TX, in partial fulfillment of the requirements for the degree of Master.
Huang, C. (2008). "Development and numerical implementation of nonlinear viscoelastic-viscoplastic model for asphalt materials." thesis, presented to Texas A&M University, in partial fulfillment of the requirements for the degree of Doctor of Philosophy.
Konartakhteh, M. (2011) "Thermo-viscoelastic-viscoplastic-viscodamage-healing modeling of bituminous materials: Theory and computation." thesis, presented to Texas A&M University, in partial fulfillment of the requirements for the degree of Doctor of Philosophy.
Levenberg, E. and Uzan, J., (2004). “Triaxial small-strain viscoelastic-viscoplastic modeling of asphalt aggregate mixes”. *Mechanics of Time-Dependent Materials*, 8(4), pp.365-384.
Lu, Y., and Wright, P. J. (1998). “Numerical approach of visco-elastoplastic analysis for asphalt mixtures.” *Journal of Computers and Structures*, 69, 139-157.
Lu, Y., Wright, P.J., (2000). “Temperature related visco-elastoplastic properties of asphalt mixtures”. *ASCE J. Transp. Eng*. 126 (1), 58–65.
Masad, E., Tashman, L., Little, D., Zbib, H., (2005). “Viscoplastic modeling of asphalt mixes with the effects of anisotropy, damage and aggregate characteristics”. *Mech. Mater*. 37 (12), 1242–1256.
Masad, E., Dessouky, S., Little, D., (2007). “Development of an elastoviscoplastic microstructual-based continuum model to predict permanent deformation in hot mix asphalt”. *ASCE Int. J. Geomech*. 7 (2), 119–130.
Oeser, M. and Moller, B. (2004). “3D constitutive model for asphalt pavements.” *International Journal of Pavement Engineering*, 5, 153-161.

Park, D., Martin, A.E., Masad, E., (2005). “Effects of nonuniform tire contact stresses on pavement response”. *ASCE J. Transp. Eng*. 131 (11), 873–879.

Park, S.W. and Schapery, R.A. (1999). “Methods of Interconversion Between Linear Viscoelastic Material Functions. Part I – A Numerical Method Based on Prony Series.” *International Journal of Solids and Structures*, Vol. 36, 1999, pp. 1653-1675.

Perzyna, P. (1966). “Fundamental problems in viscoplasticity”. *Advances in applied mechanics*, 9, 243-377.

Roylance, D. (2001). “Engineering viscoelasticity”. Department of Materials Science and Engineering–Massachusetts Institute of Technology, Cambridge MA, 2139, 1-37.

Sun, Lu, Haoran Zhu, and Yaoting Zhu. "Two-stage viscoelastic-viscoplastic damage constitutive model of asphalt mixtures." *Journal of Materials in Civil Engineering* 25, no. 8 (2012): 958-971.

Saadeh, S., Masad, E. and Little, D., (2007). “Characterization of asphalt mix response under repeated loading using anisotropic nonlinear viscoelastic-viscoplastic model”. *Journal of Materials in Civil Engineering*, 19(10), pp.912-924.

Schapery, R. A. (1969). “On the characterization of nonlinear viscoelastic materials”. *Polymer Engineering & Science*, 9(4), 295-310.

Seibi, A. C., Sharma, M. G., Ali, G. A., and Kenis, W. J. (2001). “Constitutive relations for asphalt concrete under high rates of loading.” *Transportation Research Record 1767*, Transportation Research Board, Washington, DC, 111-119.

Wang, L. B. (2012). Mechanics of asphalt: microstructure and micromechanics. *International Journal of Pavement Research and Technology*, 5(1).

Wang, Y. (2007). “Digital Simulative Test of Asphalt Mixtures Using Finite Element Method and X-ray Tomography Images”, thesis, presented to Virginia Polytechnic Institute and State University, in partial fulfillment of the requirements for the degree of Doctor of Philosophy.

Yoo, P.J. and Al-Qadi, I.L. (2007). “Effect of transient dynamic loading on flexible pavements”. *Transportation Research Record*, 1990, 129–140.

Zafir, Z., Siddharthan, R., & Sebaaly, P. E. (1994). “Dynamic pavement-strain histories from moving traffic load.” *Journal of transportation engineering*, 120(5), 821-842.

Chapter 5 COMPARISONS ON PAVEMENT RESPONSE AND RUTTING PERFORMANCE UNDER ALF, MMLS 3 AND APA

5.1 Dimensional analysis

5.1.1 Introduction

In engineering domain, it is necessary to perform the engineering judgement, observation, and study on the prototype or scaled models prior to the large-scale implementation. Regarding this, the dimensional analysis is required to link the different scaled systems in terms of dimensional quantities, which have the same values in the prototype and model.

Buckingham Pi theorem, in engineering, applied mathematics, and physics, is the basis in dimensional analysis, formalized in Rayleigh's method of dimensional analysis (Hanche-Olsen, 2004), which states that if there is a physically meaningful equation involving a certain number n of physical variables, then the original equation can be written in p=n-k dimensionless parameters,π_1, π_2, ... π_p instead of the original variables (Wikipedia, Buckingham π theorem).

The dimensions involving in the most mechanic problems include length (L), mass (M), and time (T). Because asphalt mixture is affected by temperature considerably, temperature is considered as the fourth dimension. The dimensional analysis with regard to traffic loads was conducted in 1940s to 1960s by a wide variety of researchers for evaluation of effects of tires on soils. That study was focused on the modeling of tires instead of the behavior of pavements. It is well accepted that the behavior of pavement material and structure is affected by the variables of different layers including the pavement thickness, elastic properties, contact area, load velocity, mass densities.

Let λ is the scale factor for the geometric dimension, and the material of model and prototype in corresponding each layer is the same. In order to ensure the model and the prototype subjected to the same stress and pressure, the forces must be scaled by λ^2, the time scale should be equal and the velocity scale should be equal to length scale, with the consideration of viscosity and inertia effects. The more details with respect to dimensional analysis can be found elsewhere (Van de Ven et al., 1998; Kim et al., 1998).

Therefore, when the layering material properties are the same and assuming the material is liner elastic, if the scale factors are achieved as below (Kim et al., 1998), the strain and stress will be same in the model and prototype.

1. Length, 1: λ
2. Load, 1: λ^2
3. Time rate of loading, 1: λ
4. Material properties, 1:1

5. Pressure on the surface, 1:1

5.1.2 Dimensional analysis in numerical simulation

In the subsequent context, the finite element software ABAQUS will be used to verify the dimensional analysis using different scaled system. One full-scale 3-layered pavement structure and a completely one-third scale pavement system are simulated in ABAQUS. The stress/strain at the critical positions of two systems will be compared to further investigate the validation of dimensional analysis on pavement engineering, in which the asphalt mixtures are assumed to be linear viscoelastic, base/subbase and subgrade material is elastic. It indicates that the dimensional analysis is conducted under relatively low temperature for pavement, because asphalt mixture is temperature dependent material and behaves liner viscoelasticity under low temperature.

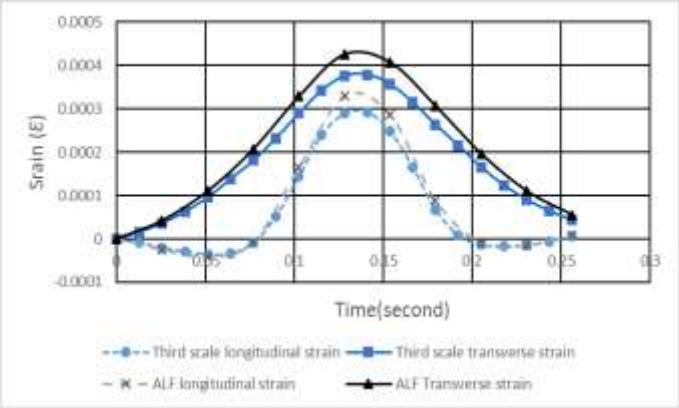

Figure 5-1 Horizontal tensile strain at bottom of asphalt layer

The horizontal tensile strain at bottom of asphalt layer in full scale and third scale system is plotted in Figure 5-1. As can be seen, the pattern shape of strain history is approximate in the two different scales, while the amplitude of the maximum strain value in full scale ALF is greater than the third scale for both longitudinal and transverse strain. The possible reason is that the asphalt mixture is simulated as viscoelastic material instead of the elastic material, which is not consistent with the assumption in above dimensional analysis.

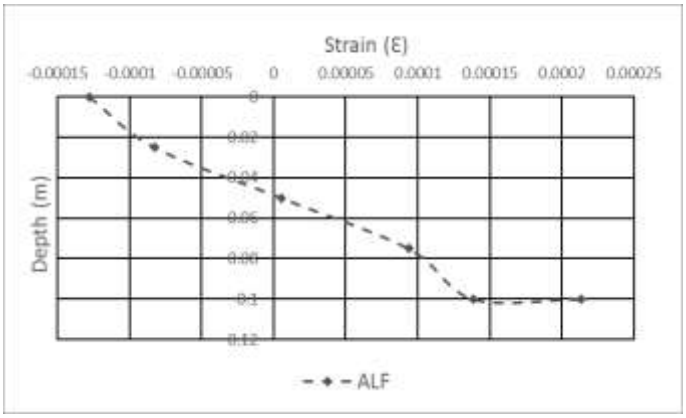

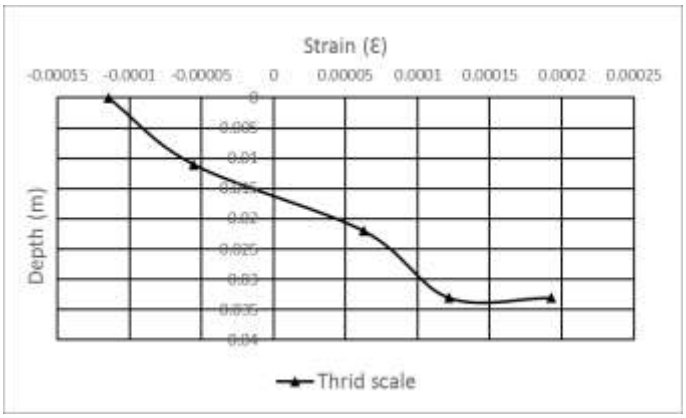

Figure 5-2 Longitudinal strain along the depth of pavement structure

Figure 5-2 compares the longitudinal strain distribution along with pavement depth in ALF and third scale system. Despite the distribution trend is similar in full scale and third scale, the longitudinal strain at the same position in third scale is slightly less than that in full scale.

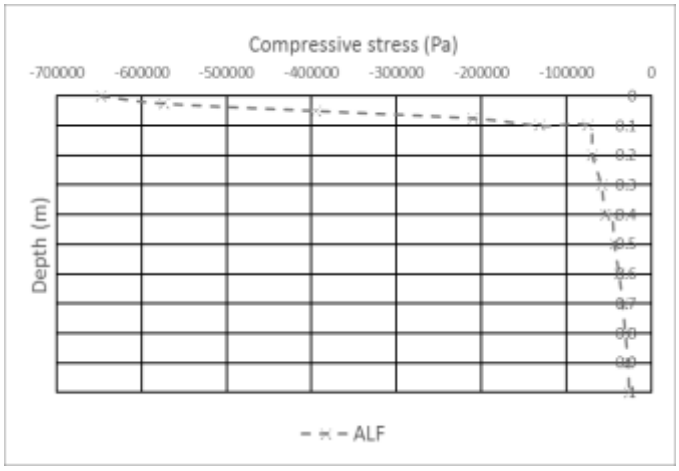

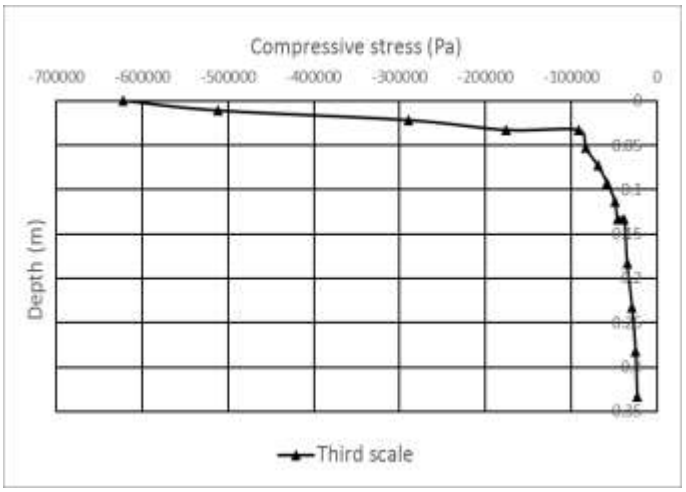

Figure 5-3 Compressive stress along the depth of pavement structure

The comparisons of compressive stress along the depth of pavement is shown in Figure 5-3, demonstrating the similar distribution pattern. As the finding for longitudinal strain, compressive stress in the full scale is greater than that in third scale system.

Based on the results from above numerical simulations, it is found that once the scale factor is achieved, the material response in the model is comparable to that in prototype. Slight difference is observed in the strain and stress due to the non-elastic properties of materials.

5.2 Comparisons in ALF, MMLS 3 and APA

The geometry of the specimens in ALF, MMLS 3 and APA are presented in Figure 2-3. The tire configuration, wheel load, wheel velocity and load frequency are specified in Table 2-3. It also should be pointed out that the maximum contact pressure is more than 1000 kPa in both ALF and MMLS 3 when the tire pressure is 689 kPa, which is normally located at the edge of tire thread. However, for simplicity in this study, the tire contact is assumed as evenly distributed in the tires and rubber hose. Therefore, since the tire pressure is the same in the three scale APTs, the contact area ratio among ALF, MMLS 3 and APA equals to the ratio of wheel load.

$$A_{ALF}: A_{MMLS\,3}: A_{ApA} = Load_{ALF}: Load_{MMLS\,3}: Load_{APA} = 46.8: 2.7: 0.445$$

The thickness of asphalt layer of ALF, MMLS 3 and APA are 10cm, 5cm, 5cm respectively.

In the reality, it is difficult to achieve the complete scale factors in the model and prototype, and thus in this study, it is necessary to compare the pavement response under ALF, MMLS 3 and APA.

5.2.1 Scale factor in ALF, MMLS 3

Because APA test is not performed with a layered pavement system, the scale factor analysis is not considered for APA. The layering material properties are the same in MMLS 3 and ALF, and the corresponding scale factors are listed as following，

1. Length, L=1:11
2. Load, F=2.7:46.8= 1:17.3
3. Time rate of loading, T=1/2.6: $\sqrt{17.3}$/5=1:2.163
4. Depth of the asphalt layer, D=5:10=1:2

According to the numerical simulations, the pavement surface deflection at center of tire of ALF, MMLS 3 and APA is shown in Table 5-1. For comparison purpose, the linear

elastic pavement calculation software BISAR is used to estimate the tensile strain at bottom of asphalt mixture layer. It is found that layered linear elastic theory underestimates the tensile strain, compared with actual measurement and numerical simulations.

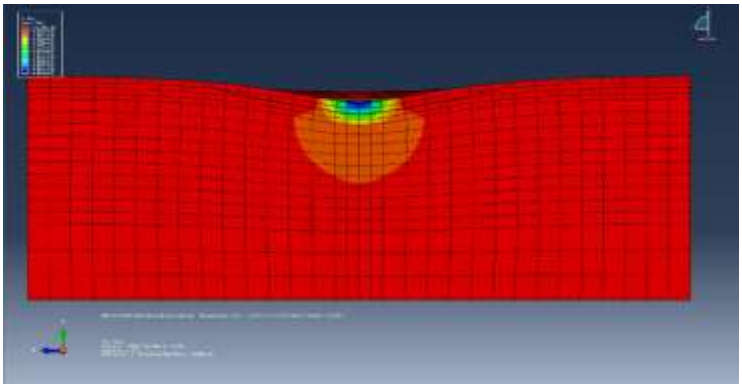

ALF

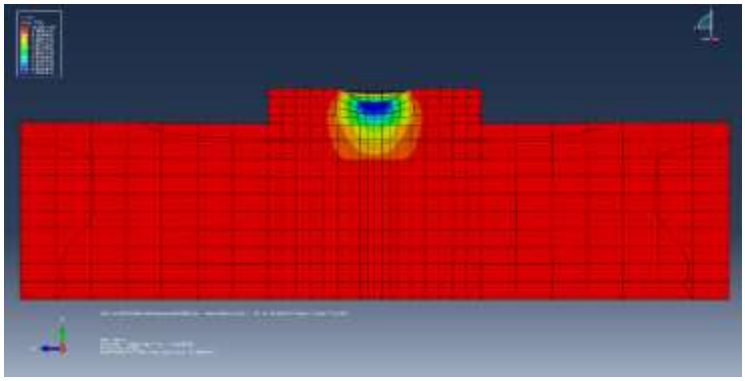

MMLS3

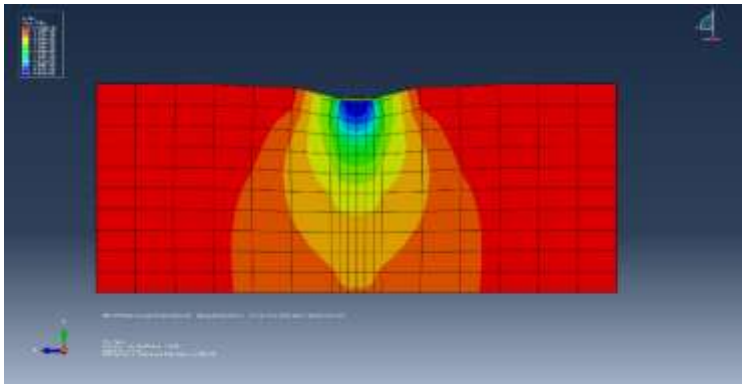

APA

Figure 5-4 Compressive stress distribution in ALF, MMLS 3 and APA

Table 5-1 Summary of comparisons in ALF, MMLS 3 and APA based on simulations

	Load	Deflection at center of Wheel path	Strain at bottom of asphalt layer (με)			
			BISAR		Simulation	
			Lane 9	Lane 5	Lane 9	Lane 5
ALF	46.8 kN	0.379 mm	391	347	408	365
MMLS 3	2.7 kN	0.243 mm	137	124	194	167
APA	445 N	1.12×10^{-3} mm	1.45	1.19	1.71	1.56

5.2.2 MMLS 3 vs ALF on realistic pavement

The above dimensional analysis is on the whole pavement structure and wheel load system. However, it is hard to achieve to the complete scale factor for pavement system in realistic world. The response of actual full-scale pavement under MMLS 3 and ALF is compared in the numerical models using finite element method ABAQUS, as shown in Figure 5-5.

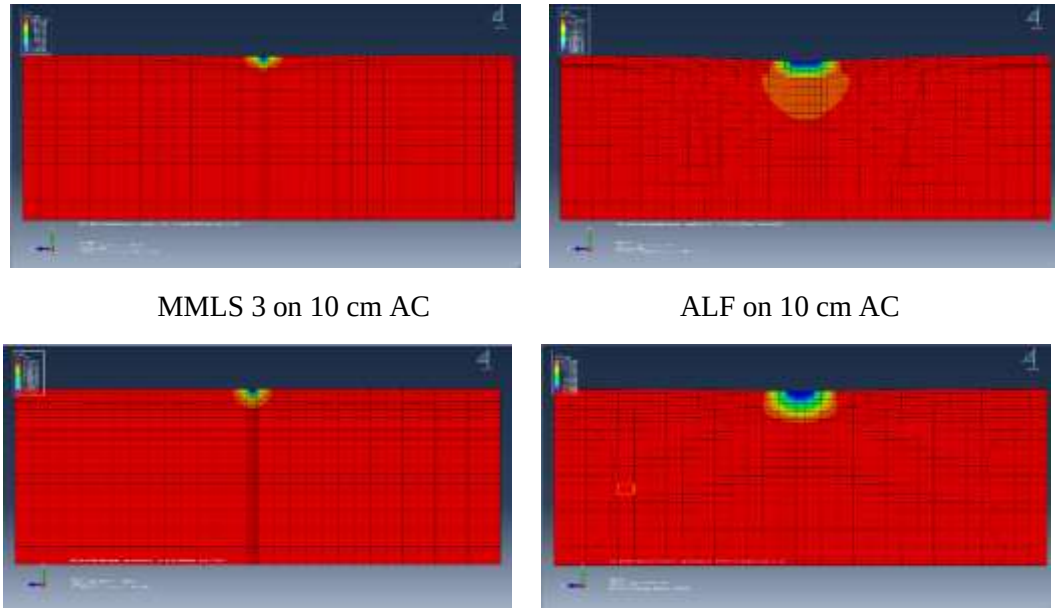

MMLS 3 on 10 cm AC ALF on 10 cm AC

MMLS 3 on 20 cm AC ALF on 20 cm AC

Figure 5-5 Compressive stress on 10cm and 20cm asphalt layer in MMLS3 and ALF

Two thickness of asphalt layers are simulated to further compare the effects of MMLS 3 and ALF tires on vertical stress. In the 10 cm asphalt layer system, MMLS tire has significant compressive stress on top 8.5 cm, while it has evident compressive stress on top 12.5 cm in the 20 cm asphalt layer system. It can be seen that wheel load of ALF has profound effect on the whole asphalt layer in both 10 cm and 20 cm asphalt layer, while the profound effect is also observed in the base layer of the 10 cm asphalt layer, indicating that the thick surface layer distributes more stress and protects the underlying

layers. It also implies that MMLS 3 trafficking only results in effective stress/strain conditions in 10 cm layer of realistic pavement. If the pavement thickness is more than 10cm, it is not suitable to be trafficking under MMLS 3.

5.2.3 Tensile strain

The tensile strain history at the bottom side of ALF, MMLS 3 and APA testing is shown in Figure 5-6. It is noteworthy that all the tensile strain histories from simulations exhibit the similar pattern as that obtained from actual measurement (as Figure 2-8), which consist of a compressive part, following a tensile part then one more compressive part, while the transverse tensile strain gauge is entirely in tension stage. In addition, compared with the measured strain output history of MMLS 3, the simulated maximum longitudinal tensile strain in MMLS 3 are 194 με and 167 με for Lane 9 and Lane 5 material respectively, which are close to the experimental measurement as 183 με and 152 με, while the numerical simulation significantly underestimates the transverse tensile strain at bottom of asphalt layer as compared to the experimental measurement. The likely reason is that the maximum tire-pavement localized contact stress at the edge of tread is more than 1000 kPa when the tire pressure is 689 kPa and the asphalt mixtures are modelled as isotropic homogeneous material, which could not reveal the properties at different directions.

It is noted that the simulated tensile strain at bottom of asphalt layer in ALF is around 400 με, tensile strain in MMLS 3 approximates to 180 με. However, the tensile strain at bottom of APA specimen is significantly less than those of ALF and MMLS 3. It is generally accepted that the fatigue cracking is mainly caused by the repetition of tensile strains at the bottom of HMA. Therefore, APA test is not capable of subjecting the tested samples under the strain/stress condition as MMLS 3 and ALF, which are more close to the field conditions. However, there are some studies have been done to investigate the fatigue performance of asphalt mixtures in APA test but using soft base or placing the sample on the two support points, as freely supported beam, which can subject the specimen to much greater tensile strain.

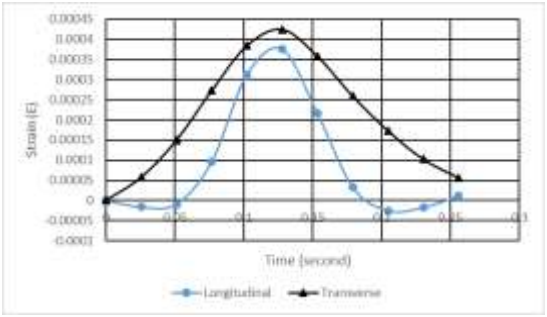

Lane 9

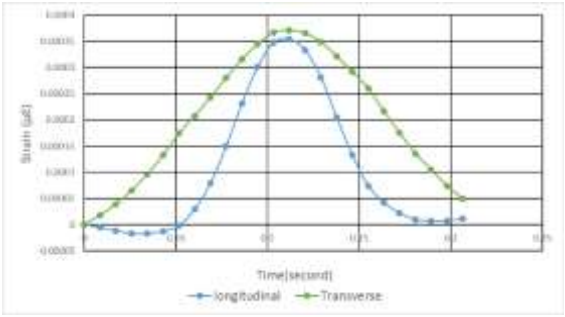

Lane 5

ALF

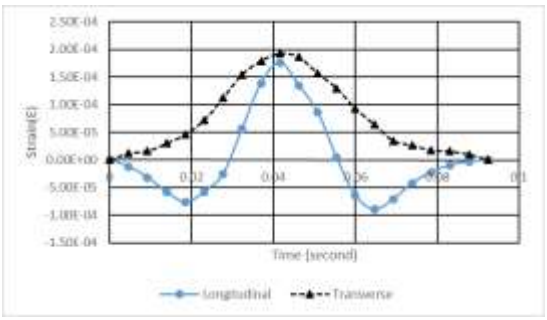

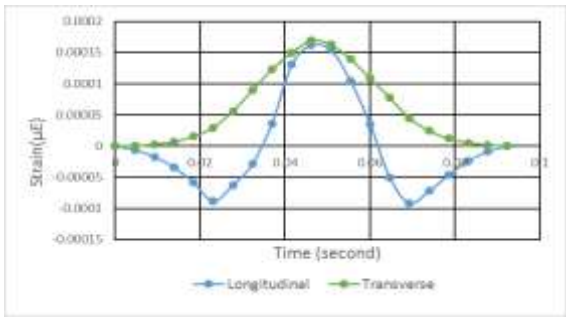

Lane 9 Lane 5

MMLS 3

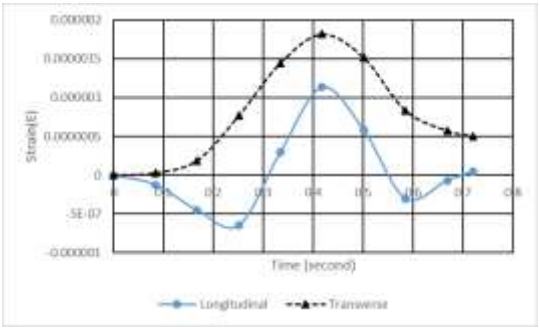

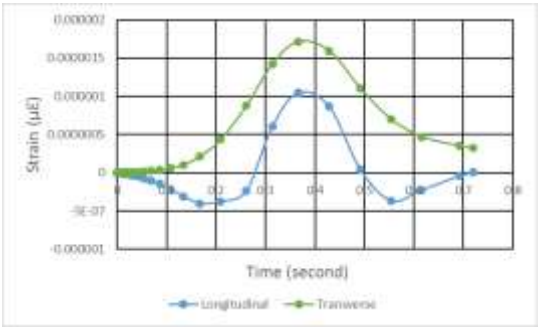

Lane 9 Lane 5

APA

Figure 5-6 Simulated tensile strain history in MMLS3

The tensile strain along with pavement depth in ALF, MMLS 3 and APA test is depicted in Figure 5-7. For both Lane 9 and Lane 5 material, the tensile strain within asphalt mixture layer under MMLS 3 has similar trend along with depth as that under ALF trafficking, while in smaller amplitude. One can note that the tensile strain in APA test is observed much smaller amplitude and different trend with increase of depth. The maximum tensile strain is observed in the middle depth of specimen. It can be concluded that the APA test is subjecting specimen under very different tensile strain condition compared with ALF and MMLS 3.

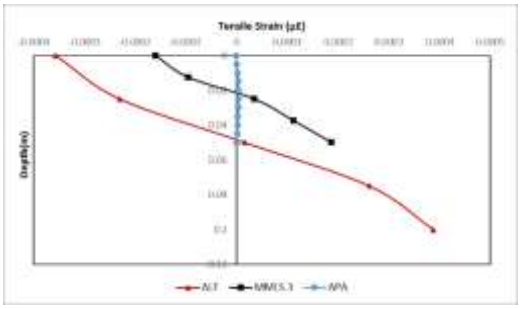

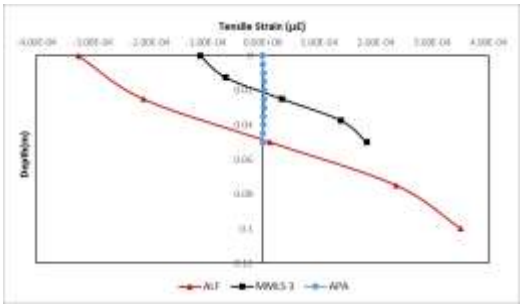

Lane 9 Lane 5

Figure 5-7 Tensile strain along depth

Figure 5-8 plots the seismic modulus history of Lane 9 obtain from PSPA test versus the number of load cycles under the ALF trafficking. As can be seen, the seismic modulus drop to a-half of the initial value after 500,000 load applications. According to findings on Figure 5-7, the Lane 9 top lift is regarded as failure status after 500, 000 load cycles. With consideration of the load frequency, MMLS3 is a much more efficient wheel track device which takes around 4 days to achieve 500,000 cycles, whereas ALF needs to take 100 days.

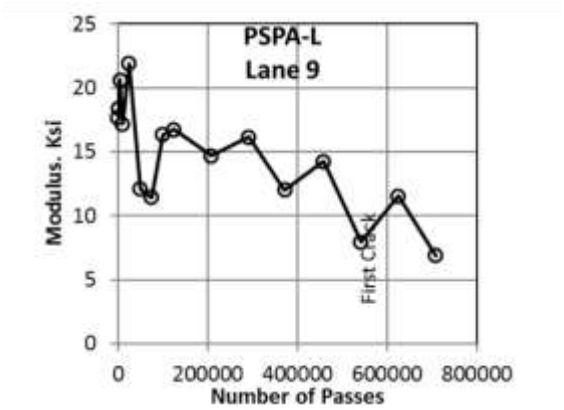

Figure 5-8 Seismic modulus history of Lane 9 during ALF trafficking (Gibson, 2016)

5.2.4 Compressive stress

The compressive stress of ALF, MMLS 3, and APA, along with the pavement structure depth at the wheel path center is presented in Figure 5-9. It can be seen that the vertical compressive stress at the bottom of asphalt layer in ALF and APA approximates to 100,000 kPa, while that of MMLS 3 is much greater, approaching 450, 000 kPa. With the same tire pressures, under the wheelpath centerline, the asphalt layer in MMLS 3 is subjected to the almost equivalent compressive stress as the top lift in ALF, indicating that MMLS 3 is capable of producing similar compress stress condition for the test slabs as full-scale ALF. However, at the same depth, the sample in APA test is undergoing much smaller compressive stress.

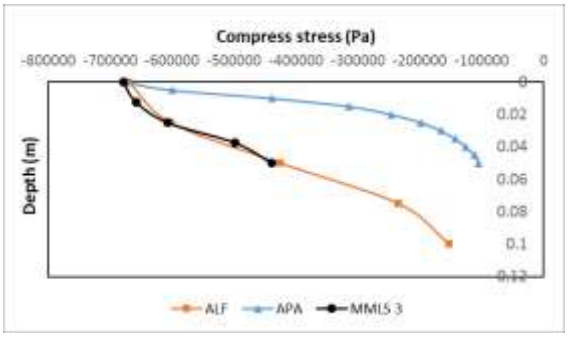

Lane 9 material

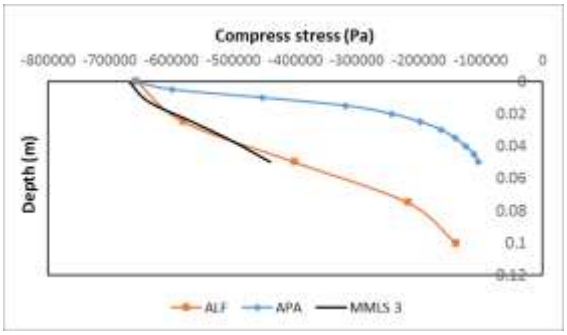

Lane 5 material

Figure 5-9 Compressive stress along the depth of pavement

5.2.5 Rutting depth

Comparisons among experimental results

Rut depth of Lane 9 versus number of ALF and MMLS 3 load cycles is plotted in Figure 5-10. Prior to the 100,000 load cycles, the Lane 9 material is in primary creep stage, being in secondary creep stage between 100, 000 to 500, 000 load applications, and being in tertiary creep stage after 500, 000 loads, indicating the failure starts. It is consistent with the PSPA test measurements that Lane 9 material is observed failure after 500,000 passes.

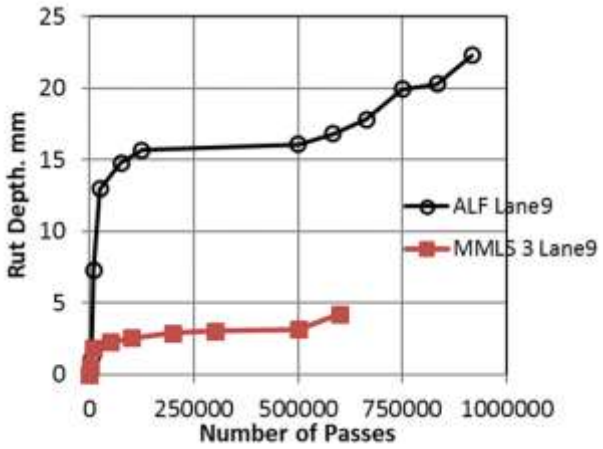

Figure 5-10 Rut depth versus number of passes during ALF and MMLS 3 trafficking (Gibson, 2016)

Based on Figure 2-11, the rut depth of Lane9 lifts in MMLS 3 test is 3.5 mm after 500,000 cycles, while the rut depth is 16.08 mm in ALF test. On the other hand, the rut depth of APA test is presented in Figure 5-11. It is interesting to note that the rut depth in APA after 5000 load cycles is 1.78 mm, while rut depth in ALF is 1.18 mm after 5000 passes. The MMLS 3 rut depth is measured around 1 mm after 100,000 load cycles. It is found that the load in APA test induces a greater permanent deformation than that in ALF and MMLS 3 test in the same ambient condition. It can be concluded that APA test is an efficient and effective method to rank rutting resistance of asphalt mixtures, while it could overestimate the rut depth in the field.

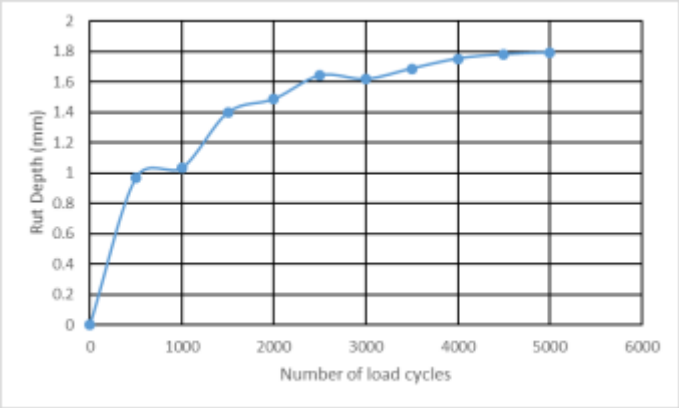

Figure 5-11 Rut depth versus number of load cycles in APA

Rut depth in numerical simulation

The total 500,000 load cycles applied in ALF and MMLS 3 is aiming to be replicated in the finite element simulation. However, it would take 45 minutes to compute one load cross the specimen and thus it is impractical to simulate a large number of cycles for rutting susceptibility investigation due to the tremendous computational time and storage requirement. One alternative method is to design a load equivalency procedure in which more cycles are simulated without adding extra computational time (Carvalho, 2012). Then, the simulation results for a large number of load cycles can be extrapolated.

The typical equivalent load procedure applies a long-term load to represent the time duration for repeated load cycles. The main problem with this approach is that the principal stress rotations and shear stress reversal cannot be represented because the plate load is adopted instead of the more realistic moving load. Besides, the long-term plate load is not capable of representing the increments of residual stresses between the load intervals.

The load equivalent approach employed in this dissertation is to set the load duration progressively increased to represent more cycles and retain the development of the residual stress during the trafficking. As for the 100 load cycles, the first 20 loads is simulated as the actual load pass time. After the first 20 load cycles, the load time of every 20 load is doubled as that of the previous set of 20 loads. For example, the load time for the second set of 20 loads is equivalent to 40 cycles. This process makes 100 load cycles in simulation equal to 500 realistic cycles, as shown in Figure 5-12.

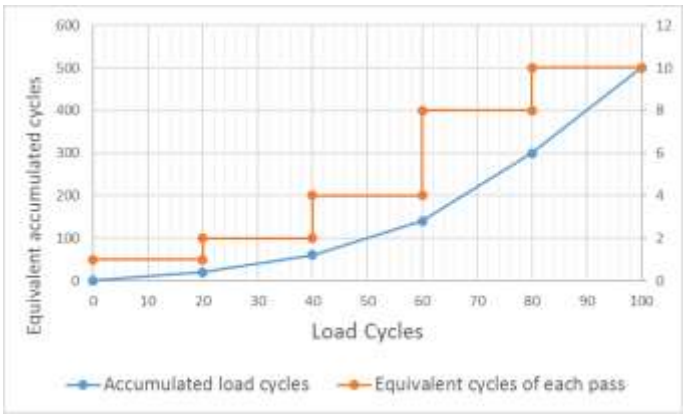

Figure 5-12 Accumulated load cycles-equivalent cycles of each pass versus actual cycles

Figure 5-13 presents the rutting prediction for 500 load cycles using the equivalent load approach, in which the permanent deformation for 100 simulated loads is plotted as well. The simulated results of actual 100 cycles are in good agreement with that using equivalent load procedure, indicating that the equivalent load scheme is feasible and accurate enough as an alternative for simulating a large number of loads (Carvalho, 2012).

The results in Figure 5-13 is used to extrapolate the permanent deformation after 500,000 loads. Power law functions is employed to fit the finite element simulation result as Equation 5-1, and the linear regression is used in the logarithm of predicted rutting and number of load cycles as equation 5-2 (Carvalho, 2012). The fit power function in Figure 5-14 is $RD = 0.086N^{0.4301}$, R^2=0.9835.

$$RD = aN^{b} \tag{5-1}$$

$$\log(RD) = \log(a) + b\log(N) \tag{5-2}$$

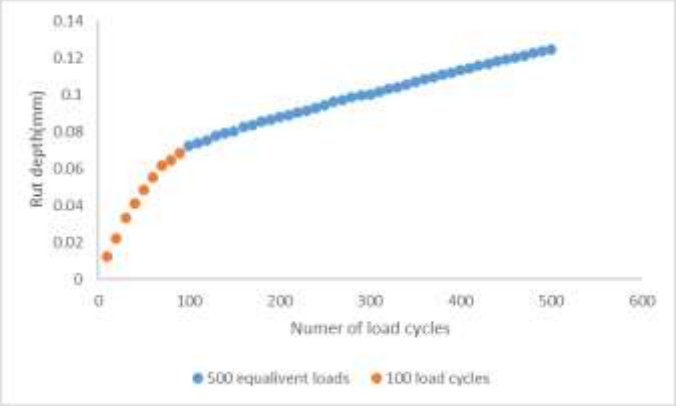

Figure 5-13 Rut depth in numerical simulation for 500 loads

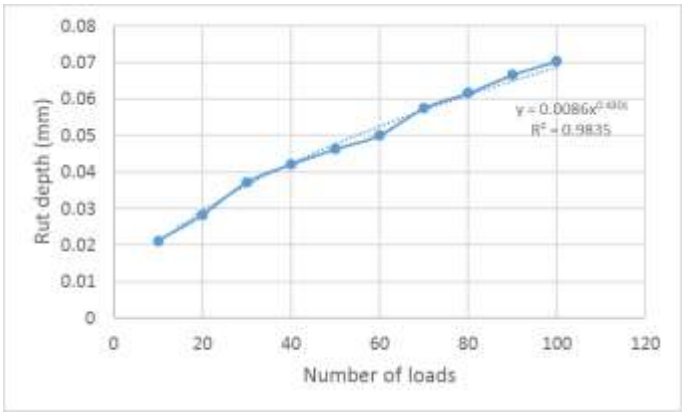

Figure 5-14 Fitted power function for 100 load cycles

The multiplier of the power model varies at different load cycles. Thus, an adjustment parameter AF was developed to correct the value based on the model fitted for 100 cycles as reference,

$$\mathrm{AF} = \frac{a_N}{a_{100}} = f(N) \tag{5-3}$$

The correlation between a_N *and* a_{100} is also fitted using a power function dependent on the number of cycles, N, as shown in Figure 5-15.

$$\mathrm{AF} = \frac{a_N}{a_{100}} = 0.3395N^{0.2383} \tag{5-4}$$

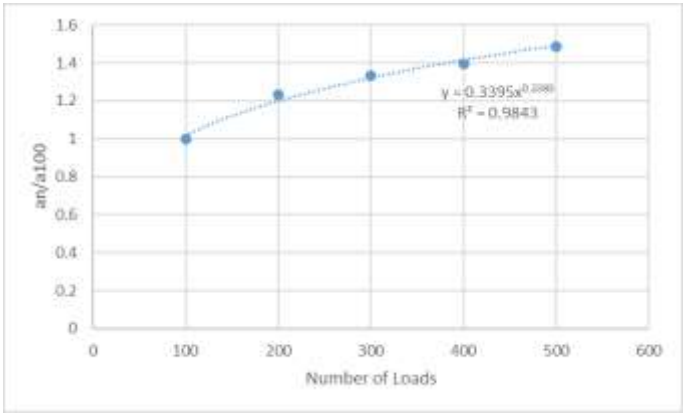

Figure 5-15 aN/a100 versus number of load cycles

The adjusted model for extrapolation on different number of load cycles is described as follows,

$$\mathrm{RD} = (\mathrm{AF} \times \mathrm{a}_{100})N^{b_{100}} \tag{5-5}$$

$$\mathrm{RD} = 0.00292 \times \mathrm{N}^{0.6684}$$

Where,

RD=rutting depth (mm),

N= number of load cycles.

The measured APA experiment result is compared with the extrapolation based on the Equation 5-5. In the APA test for Lane 9 samples, the rut depth is 1.78 mm after 5000 load cycles. The predicted rut depth is 0.866 mm at 5000 load cycles. But if adds the rut depth caused by densification which is considered as 40%×1.78mm=0.71mm, the predicted rut depth is 0.866+0.71=1.576 mm for 5000 load cycles, which is approximate to the actual measurement. In order to compare the rut depth in ALF, MMLS 3 and APA, the rut depth at 500,000 load cycles is extrapolated to be 25.916 mm, which is greater than measurement in ALF test.

Following the above procedures, the rut depth prediction for Lane 5 material in APA test is $RD = 0.00245 \times N^{0.5912}$. It is calculated as 0.376mm after 5000 load cycles in simulation. The assumed 40% rut depth induced by densification is 0.44 mm. Then the APA predicted rut depth at 5000 loads is 0.816 mm, which is slightly smaller than the measurement.

Using the above stated procedures, the rut depth development with the number of load cycles of ALF and MMLS 3 test is extrapolated based on the simulation for 100 load repetitions. The extrapolation equations for rut depth computation of Lane 9 and Lane 5 material in ALF and MMLS 3 test are presented in Table 5-2.

Table 5-2 Extrapolated equation for rut depth

	Lane 9	Lane 5
ALF	$RD= 4.5961\times N^{0.0853}$	$RD=3.417\times N^{0.075}$
MMLS 3	$RD= 0.0682\times N^{0.2526}$	$RD=0.0014\times N^{0.4753}$

Based on the above equations, the accumulated rut depth development with the number of load cycles are pictured in Figure 5-16 as dash curves. It can be seen that the predicted rut depth is smaller than the actual measurements. The possible reason is that the finite element models adopted in this study cannot represent the rut depth caused by densification. According to previous studies (Carvalho, 2012; Gibson et al. 2012), in ALF test, the densification leads to 1.5% air void reduction under the wheel-path. Therefore, in this study, the rut depth induced by deification is considered as 1.5% of pavement thickness in both ALF and MMLS 3 test. The predicted rut depths adding the 1.5% of pavement thickness are also shown in Figure 5-15, demonstrating that the numerical models are capable of predicting the rut depth in ALF and MMLS 3 test.

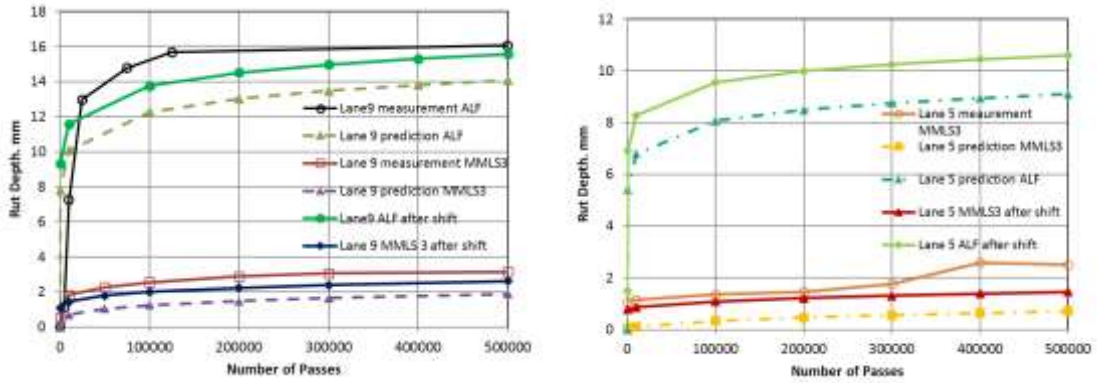

Figure 5-16 Rut depth predictions

5.3 Empirical Rutting prediction in APA

Rutting is one of the critical distresses in pavement, which occurs longitudinally on wheel paths of pavement surface. It is a surface depression together with the upheaval along the sides of rut, caused by the permanent deformation of asphalt material subjected to repeated wheel load. Rutting can result in structural failure and considerably impacts the ride comfort and even drive safety.

There are two mechanisms cause the rutting in asphalt concrete pavement. First, the traffic loads further compact the asphalt mixtures at the early stage of trafficking, in which the air voids of material under wheel path decrease, inducing the densification of the asphalt mixtures. After the initial compaction, the shear flow of asphalt mixtures is the main reason for the rutting development. Figure 5-17 depicts the normal permanent deformation development with the accumulated load cycles, in which the stage 1 or primary stage is mainly induced by the densification of material, stage 2 or secondary stage results from the shear flow and distortion, and stage 3 or tertiary stage is caused by the shear failure.

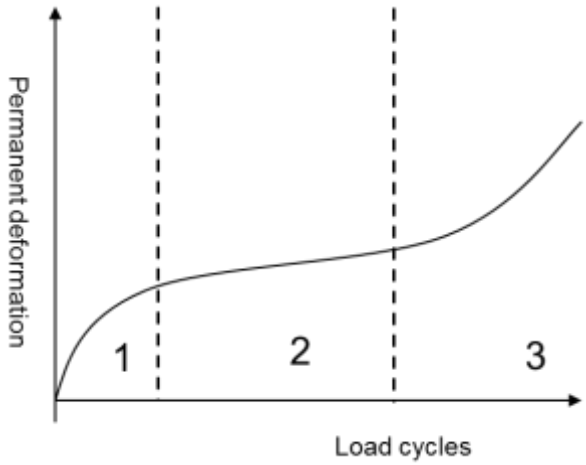

Figure 5-17 Permanent deformation versus load cycles

The permanent deformation development as stage 1 normally takes place at the initial period of traffic loads. In reality, the pavement is maintained and rehabilitated prior to approaching stage 3. Because rut depth reaches agency's threshold or other distresses trigger the maintenance (Carvalho, 2012) before reaching stage 3. Besides, the maintenance or rehabilitation in stage 3 will considerably increase the cost compared to the early-prevented maintenance. Therefore, the rut modeling is usually restricted in secondary stage. As can be seen, in the initial stage, the permanent deformation rate is relatively high, but slows with increasing of load cycles. The rate eliminates to a minimum and becomes nearly constant as the secondary stage begins. The rate in the secondary stage keeps nearly constant, referred to as "steady-state ". In tertiary stage, the permanent deformation exponentially increases with load applications because the material's shape is permanently changed and fracture damage occurs.

APA is widely applied over the world to evaluate the rutting susceptibility of different asphalt mixtures. The rut depth development as the load cycles APA is expected to have the similar pattern as that in Figure 5-18. The rut depth development in APA are pictured in Figure 5-18.

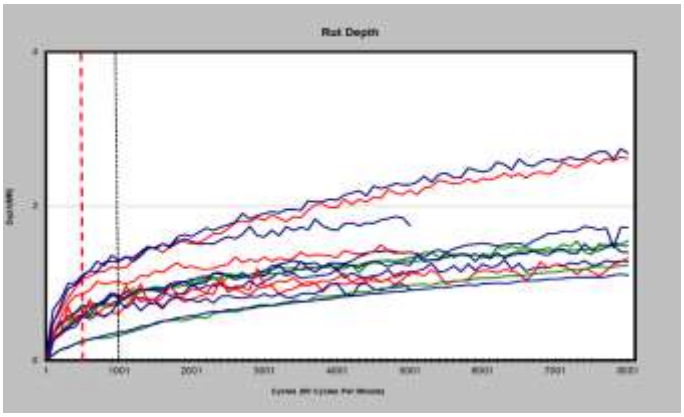

(a) APA

Figure 5-18 Rut depth versus number of load cycles

According to the rut depth development curve in the simulative test, the rut depth curve at secondary stage has a nearly linear correlation with the number of load cycles. In APA test, it is considered that at the first 500 load cycles, the post compaction or densification is the primary cause of the permanent deformation (Skok et al. 2002; Zhang et al. 2002; Bhasin et al 2005). It means the 500 load cycles is regarded as transition load number for primary and secondary stage.

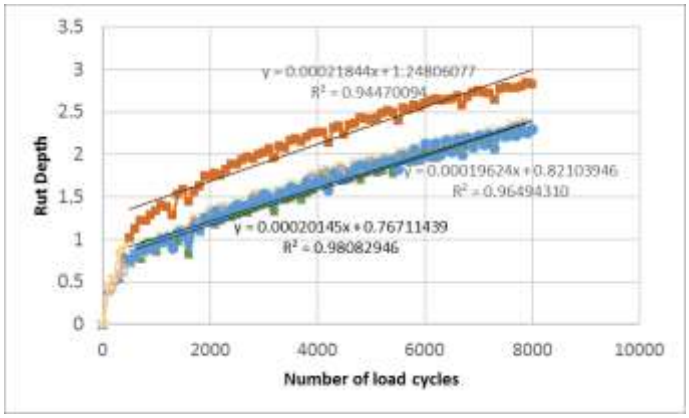

Figure 5-19 APA rut depth versus number of load cycles

The APA rut depth developments of 24 kinds of asphalt mixture including different gradations, virgin and recycled asphalt concrete at various temperatures. Figure 5-19 shows three APA test results, in which the corresponding linear regression between number of load cycles in secondary stage and rut depth is fitted. Table 5-3 lists all the 24-asphalt mixtures linear regression after 500 load cycles as following

$$\text{Rut depth} = A \times N + B \qquad (5\text{-}6)$$

Where,

A, B are the two regression parameters. N is the accumulated number of load cycles.

Table 5-3 linear regression in APA rut depth development

A	B	R-square	rut depth at 500 load applications
0.00020145	0.76710000	0.9783	0.7422745
0.00020272	0.85690000	0.9575	0.718593597
0.00019624	0.832103946	0.966	0.7613548
0.00021844	1.24806000	0.9311	1.012361169
0.00016466	1.06441136	0.9487	0.9667656
0.00021028	0.95764140	0.9572	0.895503998
0.00012484	0.93253597	0.9618	0.8041618
0.00010564	0.81064323	0.9164	0.646202087
0.00006608	0.26378067	0.8892	0.2182297

0.00008077	0.11223156	0.9058	0.1090004
0.00007631	0.66798032	0.9084	0.6018318
0.00013016	0.73905684	0.9725	0.605540454
0.00019682	1.15275997	0.9843	1.055838
0.00020624	1.20583652	0.9638	1.104094744
0.00009651	0.81375446	0.9781	0.6584259
0.00008015	0.72129427	0.9223	0.557691932
0.000094	0.656580	0.9837	0.6667767
0.000078	0.530466	0.9734	0.4898577
0.000108	0.640026	0.9858	0.623473167
0.000096	0.518662	0.9763	0.2512569
0.000069	0.477046	0.9611	0.227441788
0.00012665	0.323025	0.9665	0.2698069
0.000096	0.518562	0.9626	0.4660673
0.000069	0.477046	0.9081	0.481842041

As can be seen in Table 5-3, the linear regression after 500 load cycles has relatively high R-square value. Then correlation between the A, B and the material properties parameters including dynamic modulus (E*), phase angle (φ), E*sin (φ), E/sin (φ) and flow number are verified, while no good correlation is derived. However, it is found that there is a good correlation between A, B and rut depth at 500 load passes, respectively, as Figure 5-20.

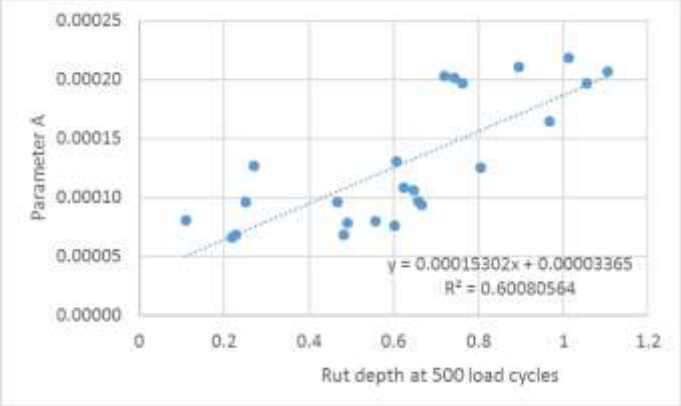

(a)

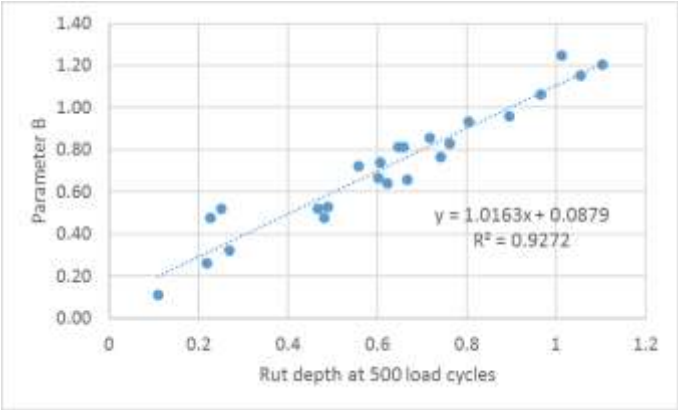

(b)

Figure 5-20 Correlation between parameter A(a), B (b) with rut depth at 500 load cycles

Based on the correlation results, the following equations are derived,

$$A=0.00015302\times R_{500}+0.00003365 \quad (5\text{-}7)$$

$$B= 1.0163\times R_{500}+0.0879 \quad (5\text{-}8)$$

$$Rd= (0.00015302\times R_{500}+0.00003365)*N+1.0163\times R_{500}+0.0879 \quad (5\text{-}9)$$

Where, Rd= APA rut depth at N number of load applications,

R_{500}= rut depth at 500 load cycles

The predicted rut depth at 8000 cycles is plotted against the actual measured rut depth of the 24 asphalt mixtures as Figure 5-21, indicating that Equation 5-9 based on rut depth at 500 load cycles is feasible and validated for the APA rut depth prediction.

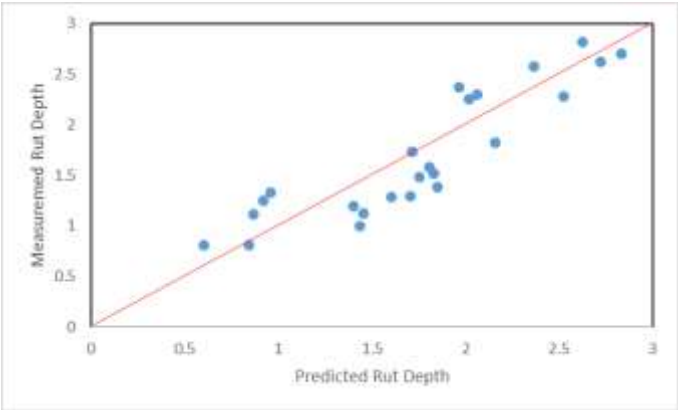

Figure 5-21 Predicted rut depth versus measured rut depth at 8000 load cycles

Aiming to further verifying the empirical rut depth prediction, the rut depth at 1000 cycles in APA test is used to conduct the linear regression as stated above procedures. However, it is found the predicted rut depth at 8000 cycles for the 24 samples has similar correlations as those predicted based on 500 cycles as shown in Figure 5-22. It implies 500 load cycles is sufficient for the prediction of rut depth development in the APA test, which can benefit in time and labor work saving.

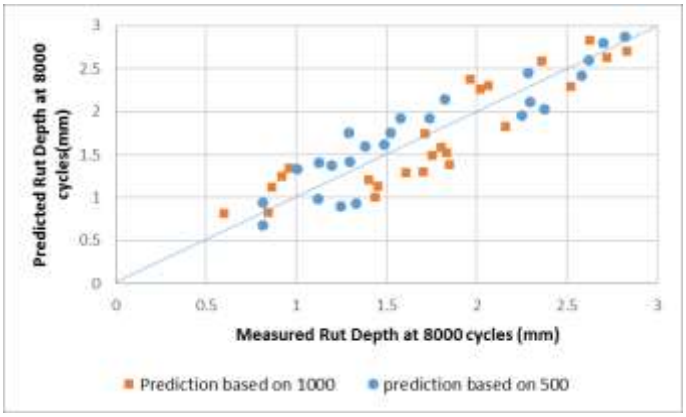

Figure 5-22 Comparisons between predicted and measured rut depth in APA

5.4 Parametric study for the MMLS 3 test

The rut depth development of six slabs in MMLS 3 test is plotted in Figure 5-23. As stated previously, the power law function fits well with rut depth and number of loads before reaching the tertiary stage. Therefore, the rut depth development curve is regressed by a power law function as $Rd = A \times N^{B}$. The power law functions fitting for the six slabs are pictured in Figure 5-24.

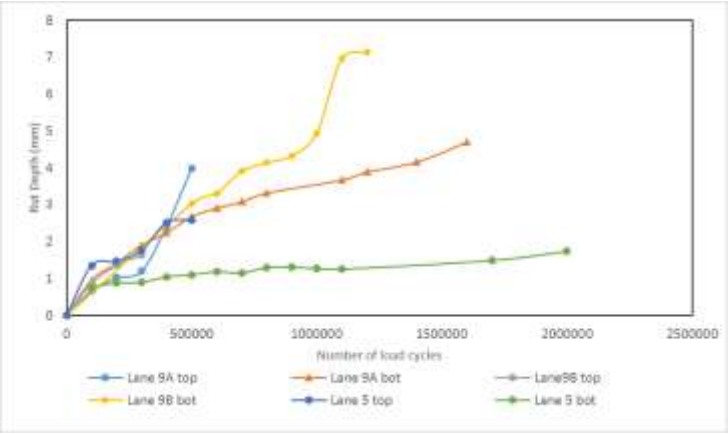

Figure 5-23 Rut depth versus number of load cycles for 6 slabs in MMLS 3 test

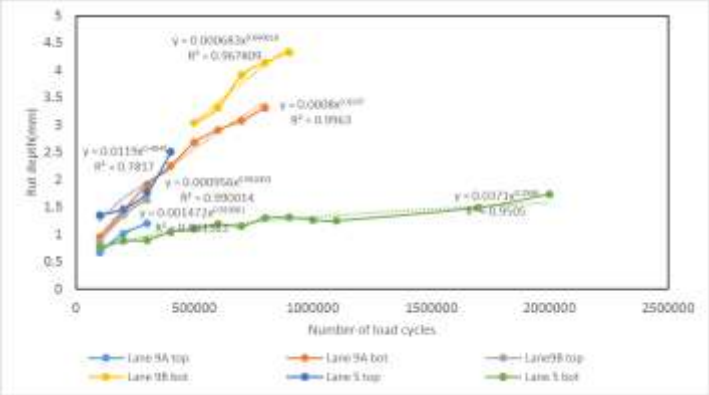

Figure 5-24 Power law function fit for Rut depth versus number of load cycles

For the four lane 9 slabs, the regression curves fitting to the accumulated rut depth –load repetitions phenomenological relationship can be found as follows:

Lane 9A top: $\mathrm{Rd} = 0.00147 \times \mathrm{N}^{0.5331}$

Lane 9A bottom: $\mathrm{Rd} = 0.00086 \times \mathrm{N}^{0.6107}$

Lane 9B top: $\mathrm{Rd} = 0.00096 \times \mathrm{N}^{0.592}$

Lane 9B bottom: $\mathrm{Rd} = 0.00068 \times \mathrm{N}^{0.64002}$

The four lane 9 slabs are composed of same materials and the MMLS 3 tests are performed at same temperatures. The only variable in these four slabs is air void. According to previous studies, air void has an evident effect on permanent deformation. Thus, the correlation between the two parameters in power law functions ($y = A \cdot x + B$) and air void is depicted as Figure 5-25.

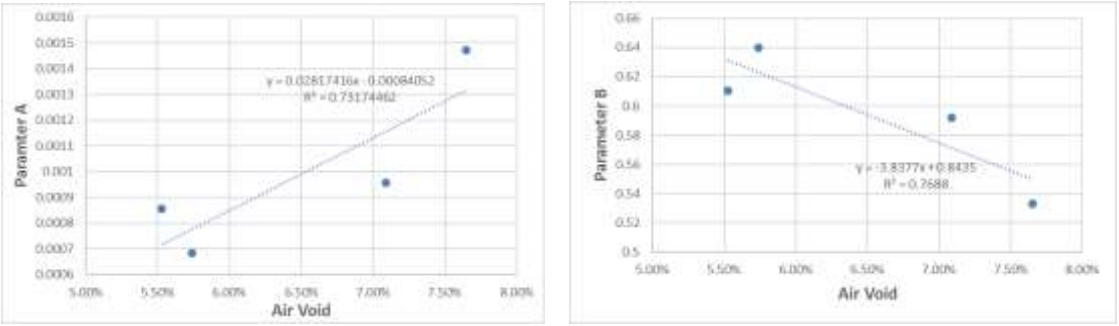

Figure 5-25 Correlation of between parameter A, B and air void for lane 9 material

$$A = 0.02817 \times V_a + 0.00084052 \quad (5\text{-}10)$$

$$B = 3.8377 \times V_a + 0.8534 \quad (5\text{-}11)$$

For Lane 9 material,

$$\mathrm{Rd} = (0.02817 \times V_a + 0.00084052) \times \mathrm{N}^{(3.8377 \times V_a + 0.8534)} \quad (5\text{-}12)$$

Where,

V_a = Air void

Regression analysis confirms that the parameters A and B are affected by the air voids. The parameter A increases as the growth of air void while parameter B decreases with the increase of air void.

5.5 Calibration of MEPDG fatigue model for MMLS 3 Test

Fatigue cracking induced by the repeated traffic loads is also one of the primary distresses in asphalt concrete pavement, which would result in the loss of material integrity, and impact the ride comfort and pavement service life. Huang (2004) pointed out that the allowable load repetitions prior to cause fatigue damage is related to the tensile strain at the top and bottom of surface asphalt layer. The fatigue cracking model in Mechanistic-Empirical Pavement Design Guide (MEPDG) is commonly used to estimate allowable number of load repetitions for fatigue cracking N_f, which is calculated as below,

$$N_f = 0.00432 \times Ck_1'\beta_{f_1}'(1/\varepsilon_t)^{3.9492}(1/E)^{1.281} \quad (5\text{-}13)$$

$$C = 10^M \quad (5\text{-}14)$$

$$M = 4.84\left(\frac{V_b}{V_a+V_b} - 0.69\right) \quad (5\text{-}15)$$

Where: N_f = Number of repetitions to fatigue cracking
β_{f_1}' = Number value
ε_t = Tensile strain at critical location
E = The dynamic modulus of the asphalt mixture at the corresponding stemperature and load frequency
V_a = The air void
V_b = The asphalt content
k_1' = function of asphalt concrete layer thickness

For bottom-up alligator cracking:

$$k_1' = \frac{1}{0.000398+\left(\frac{0.003602}{1+e^{11.02-3.49H_{ac}}}\right)} \quad (5\text{-}16)$$

For top-down longitudinal cracking:

$$k_1' = \frac{1}{0.01+\left(\frac{12}{1+e^{15.676-2.8186H_{ac}}}\right)} \quad (5\text{-}17)$$

Where,

H_{ac} = total thickness of the asphalt concrete layers

The MEPDG fatigue model is used in this study to compare the predicted allowable number of load repetitions with accumulated MMLS 3 load cycles when fatigue cracking manifests, to verify the facility as an effective tool for fatigue performance evaluation.

Table 5-4 Allowable load repetitions in six slabs

MMLS 3	Va (%)	Stiffness (Gpa)	Rut Depth at 500,000 load cycles (mm)	Strain at bottom (με)	Load cycles when half modulus occurred	Allowable load repetitions in MEPDG model	β'_{f_1}
Lane 9 A Top	7.65	9.377	3.97	183	500000	2257245	0.2215
Lane 9 A Bot	5.53	9.55	2.68	171	900000	5293795	0.1700
Lane 9 B Top	7.38	9.28	N/A	187	307500	2308022	0.1332
Lane 9 B Bot	5.74	9.89	3.04	178	800000	5095437	0.1570
Lane 5 Top	7.78	11.16	2.59	165	600000	2601562	0.2306
Lane 5 Bot	7.13	11.67	1.09	152	900000	4273462	0.2106

The allowable load repetitions based on MEPDG fatigue model for the six slabs are calculated as Table 5-4, in which the air voids are measured by cutting the small samples from slabs. The strain values are measured at the beginning of the MMLS 3 trafficking.

It can be noted that the calculated allowable load cycles are much greater than those measured in MMLS 3 tests. Because in the above calculation, the β'_{f_1} is assumed to be the default value as 1, while it needs a local calibration value at different locations and climate regions as stated in MEPDG. The β'_{f_1} for the six slabs are calculated as in Table 5-3, the mean value of β'_{f_1} = 0.1871 is recommended for the case of this study on pavement material at room temperature.

The comparisons between the measured load cycles as fatigue damage occurred and the allowable repetitions obtained from MEPDG model is plotted in Figure 5-26, indicating that β'_{f_1}=0.1871 is the acceptable calibration parameter for the case in MMLS 3 tests. Due to the limitation of funding and test conditions, the quantity of test samples is relatively small, more tests are required to be conducted under MMLS 3 test to verify the calibration parameter.

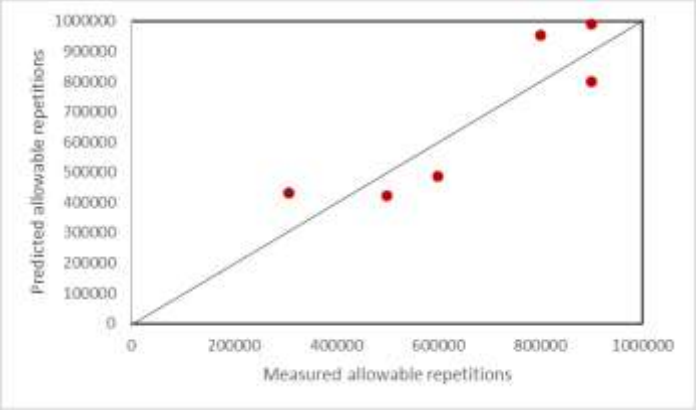

Figure 5-26 Comparison between measured fatigue load cycles and MEPDG model

5.6 Verification of MEPDG Rutting Model for MMLS 3 Test

The empirical MEPDG rutting model is derived from statistical analysis of the correlation between plastic and elastic vertical strain, as following,

$$\frac{\varepsilon_p}{\varepsilon_r} = k_1 \cdot 10^{-3.4488} T^{1.5606} N^{0.479244} \quad (5\text{-}18)$$

$$k_1 = (C_1 + C_2 \cdot depth) \cdot 0.328196^{depth} \quad (5\text{-}19)$$

$$C_1 = -0.1039 \cdot H_{ac}^2 + 2.4868 \cdot H_{ac} - 17.342 \quad (5\text{-}20)$$

$$C_2 = 0.0172 \cdot H_{ac}^2 - 1.7331 \cdot H_{ac} + 27.428 \quad (5\text{-}21)$$

Where, ε_p= accumulated plastic strain at N load applications; ε_r = the resilient strain; T= pavement structure temperature; H_{ac} = the total thickness of asphalt layer; depth= the depth of desired position; k_1, C_1, C_2= depth calibration parameter; N= number of load repetitions.

The vertical resilient strain at any depth of pavement system is defined as:

$$\varepsilon_r = \frac{1}{|E^*|} (\sigma_z - \mu\sigma_x - \mu\sigma_y) \quad (5\text{-}22)$$

Where, $|E^*|$= the dynamic modulus of asphalt mixture at specific temperature and loading rate; μ =Possion ratio; σ_x, σ_y σ_z = stress at X,Y, and Z direction.

σ_x, σ_y, and σ_z can be obtained from the finite element models of Lane 9 and Lane 5 material.

The overall permanent deformation can be computed as the sum of the permanent deformation of each sub-layer.

$$\text{PD} = \sum_1^N \varepsilon_p^i \cdot h_i \quad (5\text{-}23)$$

Where, PD = the pavement permanent deformation; N= the number of sub-layers; ε_p^i= the plastic strain in the ith sub-layer; and h_i= the thickness of the ith sub-layer. In this

study, the thickness of asphalt layer is 5 cm. The rut depth in MMLS 3 test for Lane 9 and Lane 5 material can be calculated using MEPDG rutting model as 1.03 mm and 0.609 mm after 500,000 load repetitions. It can be noted that the predicted rut depth by MEPDG rutting model is smaller than that in measurement, indicating that the MEPDG rutting model is not suitable for rut depth prediction in MMLS 3 test. In other words, more tests need to be performed to calibrate the MEPDG rut depth model for MMLS 3 test.

5.7 Reference:

Bhasin, A., Button, J. W., & Chowdhury, A. (2005). "Evaluation of selected laboratory procedures and development of databases for HMA (No. FHWA/TX-05/0-4203-3)".

Carvalho, R. L. (2012). "Prediction of permanent deformation in asphalt concrete." thesis, presented to University of Maryland, in partial fulfillment of the requirements for the degree of Doctor of Philosophy.

Gibson, N., Qi, X., Shenoy, A., Al-Khateeb, G., Kutay, M.E., Andriescu, A., Stuart, K., Youtcheff, J. and Harman, T. (2012). "Performance testing for Superpave and structural validation (No. FHWA-HRT-11--45)".

Kim, S. M., Hugo, F., & Roesset, J. M. (1998). "Small-scale accelerated pavement testing". *Journal of transportation engineering,* 124(2), 117-122.

Hanche-Olsen, Harald. (2004)."Buckingham's pi-theorem." NTNU: http://www.math.ntnu.no/~ hanche/notes/buckingham/buckingham-a4.pdf.

Huang, Y.H., 2004. *Pavement analysis and design*. 2nd ed. Upper Saddle River, NJ: Prentice Hall.

Van de Ven, M., Smit, A. de F., Jenkins, K. and Hugo, F. (1998) "Scaled down APT considerations for viscoelastic materials", *Journal of the Association of Asphalt Paving Technologists* 67, 602–622.

Skok, E. L., Johnson, E. N., & Turk, A. (2002). "Asphalt pavement analyzer (APA) evaluation."

Zhang, J., Cooley Jr, L., & Kandhal, P. (2002). "Comparison of fundamental and simulative test methods for evaluating permanent deformation of hot-mix asphalt." *Transportation Research Record: Journal of the Transportation Research Board,* (1789), 91-100.

Chapter 6 EFFECT OF TIRE CONFIGURATION, WHEEL LOAD, LOAD VELOCITY AND TEMPERATURE ON PAVEMENT RESPONSE

6.1 Introduction

In reality, the pavement structure is subjected to traffic loads with various combinations of axle loads and configurations, each having a specific effect on pavement response and performance. In pavement design procedure, the mixed axles can be equated to the referenced standard single-axle load, 18 kip. The American Association of State Highway Officials (AASHTO) and Bureau of Public Roads introduced the 18-kip equivalent single axle load since the AASHTO road test is completed in 1961. The 11R22.5 radial tire was identified as one of the most common used truck tires in United States (Kawa et al. 1998).

Tire-axle combinations typically include:

1. Single axle single tire (truck steering axles, etc)
2. Single axle dual tires
3. Tandem axle single tires
4. Tandem axle dual tires

Figure 6-1 Tires assemble configurations (Mahoney, 1984)

The Federal and State transportation agencies establish the maximum allowable gross vehicle and axle weights to limit the pavement damage as well as to ensure the transportation safety. The maximum allowable load of single axle is 71.17 kN (16,000 lbs), and the maximum allowable load for tandem axle is 151.2 kN (34,000 lbs). Therefore, the maximum load of each dual tires in tandem axles is 37.8 kN (8500 lbs).

Different Accelerated Pavement Testing (APT) facilities employ diverse tires with various inflation pressures and tire sizes coupled with differing magnitudes and speeds for trafficking on testing pavements. It is of great importance to investigate the pavement response and performance under different magnitudes and rolling speed of applied wheel

loads, tire inflation pressure and tire sizes, in terms of comprehensive stress and strain analysis in pavement structure.

The APT facility routinely can employ single axle dual tires (275/80R22.5) or super single tire (425 /65R22.5 or new wide-base tires 445/50R22.5 and 455/55R22.5) depending on the needs of the researchers. However, to expedite the damage of pavement. APT facility uses super single tire or wide-base tire with much higher wheel load at lower speed. For instance, HVS in Florida DOT can apply wheel loads between 7 to 45 kips at speed of up to 8 mph. ALF in Federal Highway Administration can apply 9.9 to 16.6 kips at speed of up to 11 mph.

Considerable efforts have been devoted by transportation agencies and researchers, to access the effects of different tire configurations, load speed and other factors. Lourens (1992) found that stress and deflections in the pavement under dynamic loads are significantly different from static loads. He reported that the magnitude of stress in pavement after the load is dependent on the loading speed. Hardy and Cebon (1994) concluded that effect of loading frequency on pavement response was relatively negligible compared with effect of loading speed. Wang (2005) measured tire-pavement contact stress data under different tire load and inflation pressure conditions. He found that increase in tire pressure causes more fatigue cracking and rutting damage to thin pavement compared with thick pavements. At the bottom of AC layer, the transverse strain is more sensitive to tire pressure change than longitudinal strain. The increase of vehicle speed decreases the strain and stress in the pavement structure, and reduces the cracking and rutting distress. Yoo and AL-Qadi (2007) strain responses and residual strains after load passing induced by dynamic transient analysis are greater than that of quasi-static analysis. Wang (2011) reported that the load and tire inflation pressure exhibited different ways to effect the tire-pavement contact stress. The vertical stress at tire edges and longitudinal contact stress increase with the rise of loading magnitude, while the vertical stress at the tire center and transverse contact stress increase as increasing inflation pressure. Sarkar (2015) employed a three-dimensional finite element model to examine the dynamic response of flexible pavement under diverse axles at different speeds. He found that higher speed can also induce less response in pavements than that at lower speed. The trend and rate of strain change with speed change are substantially affected by the pavement thickness.

In comparison to actual truck wheel load, the APT facility is commonly equipped with higher wheel loading, wider tire, but trafficking at much slower speed. Accordingly, the material responses under APT test substantially differentiate from that of actual pavement. The objective of this study is to investigate the effects of load magnitude, tire size and trafficking speed of APT on the performance of flexible pavement, as compared with standard truck wheel load, using Finite Element Method to simulate the APT super single tire and actual truck normal dual tires trafficking on the same pavement structure.

Super single tires have been developed by trucking industry as a substitution of conventional dual tire, which has benefits in improving fuel efficiency, hauling capacity and riding comforts as well as reducing gas emission, noise, manufacture cost, maintenance and recycling cost. (Xue and Weaver, 2015; Ang-Olson and Schroeer, 2002; Janajreh and Pearson, 2000)

Bonaquist (1992) reported that super single 425/65R22.5 induced 4 times greater fatigue damage and 1.0 to 2.4 times deeper rutting than those of dual tires with same wheel load and tire pressure. Al-Qadi et al. (2002) evaluated the effects of wide-based tire on a flexible pavement of the Virginia Smart Road. They pointed out that horizontal tensile strain under the HMA layer induced by wide-base tire is equivalent to that induced from dual tires. These induced tensile strains are lower than those induced from steering axle tires. However, the vertical compressive stresses induced by the wide-base tire are greater on the upper HMA layers. Al-Qadi and Wang (2012) compared the pavement responses under three tire configurations (Dual, 425 /65R22.5 and 455 /65R22.5) with different asphalt pavement structures using accelerated pavement testing (APT) for trafficking. They found that the wide-base 425 tire induces the greatest damage and wide-base 455 tire causes the more bottom-up fatigue cracking and increased the potential for subgrade rutting.

Figure 6-2 Conventional 18-wheeler truck (Bridgemechanics)

In this paper, the dual tire assembly and super single tires of APT are simulated using commercial finite element software ABAQUS, and compared for pavement responses with same axle load and rolling speed. In the ABAQUS simulation implementation, the geometric model of pavement is constructed in three dimensions with an axis of symmetry along the longitudinal direction of tire moving. To promote the computational efficiency, only half of the pavement structure and tire configuration are simulated. The middle of the dual tires and centerline of super single tire is considered as the symmetric axis and the maximum strain/ stress position.

The structure and geometry of the pavement model, the material properties, and the boundary conditions are modeled as that of the ALF test lane model, which are illustrated

in detail above. The tire footprint is estimated using axle load divided by tire pressure, which is assumed uniformly distributed in this model simulation. The moving wheel is simulated by incrementally moving the footprint as stated in Chapter 4. The axle load of the dual tires and super single tire is assumed to be 80 kN and the both tire pressures are 689 kPa. The detailed information of the two types of tires are tabulated as below Table 6-1.

Table 6-1 Dual tire and super single tire comparisons

Tire type	Tire pressure	Size
275/80R22.5	689 kPa	1049 mm & 285 mm
425/65R22.5	689 kPa	1130 mm & 421 mm

The geometry of the half pavement model is shown in Figure 6-3, which includes 23460 nodes and 20672 C3D8R elements. It should be noted that the strain/stress in the half pavement model is regarded as half magnitude of that in the full model.

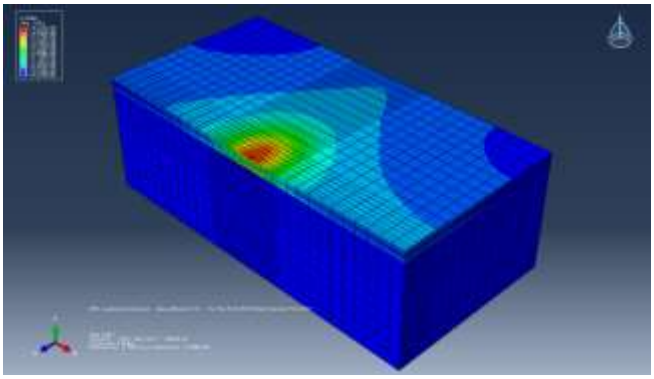

Figure 6-3 Geometry model of the pavement

6.2 Effect of tire configuration on pavement responses

To compare the effects of the tire configuration on pavement responses, the super single tire and dual tire with same axle load is simulated in the numerical simulation at the traveling speed of 18 km/h. The strain at bottom of surface layer, horizontal tensile strain along with depth, compress stress and shear stress along with pavement depth after the same number of load cycles are compared in the ABAQUS simulations for dual tire and super single tire, as shown in Figure 6-4.

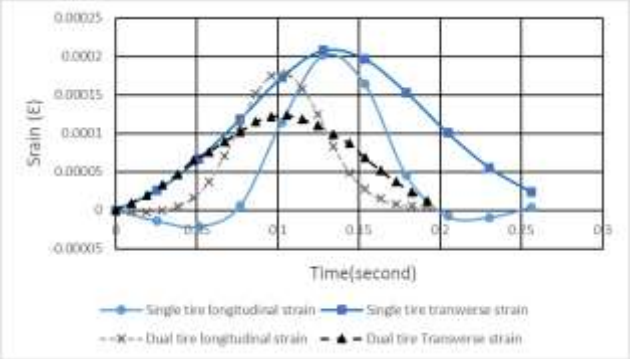

(a) Tensile strain history at bottom of surface layer

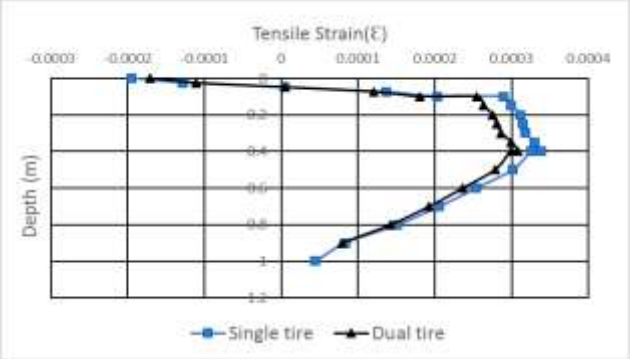

(b) Tensile strain along with pavement depth

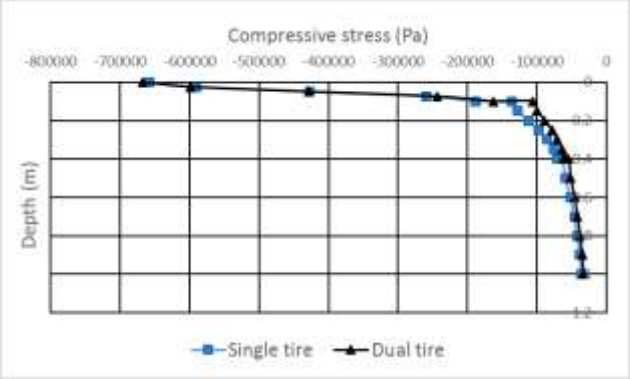

(c) Compressive stress along the depth of pavement

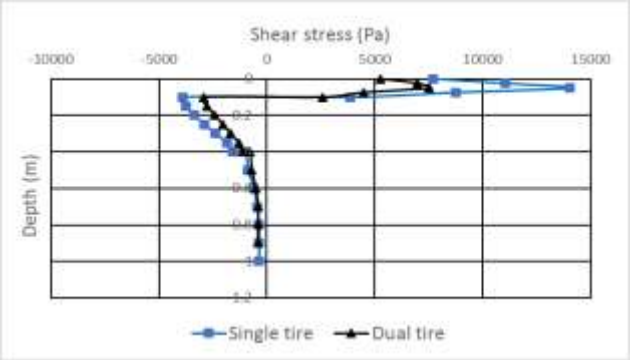

(d) Shear stress along the depth of pavement

Figure 6-4 Comparisons of tensile strain, compressive, shear stress of dual-tire assembly and super single tire

It is noticeable that the super single tire induces greater tensile strain in both longitudinal and transverse direction than dual tire assembly does. It is generally accepted that the fatigue cracking is mainly caused by the repetition of tensile strains at the bottom of HMA. Figure 6-4 (a) and (b) indicate that the super single tire induces more fatigue cracking on the same pavement than dual tire under same wheel load, tire inflation pressure and same load cycles. The compressive stresses distribution along depth under dual tire and super single tire are similar, as shown in Figure 6-4 (c). The compressive stress under surface layer is considered as the primary cause for the permanent deformation of underlying layers. Based on the observation in Figure 6-4 (d), the single tire exhibits greater shear stress than dual tire, especially in top surface layer, implying greater rut depth would be observed under single tire. The difference in pavement response caused by two tire configurations diminishes as the pavement depth increases. It can be concluded that with the same tire pressure and wheel load, single tire induces more damage than dual tire does in both fatigue cracking and rut depth.

6.3 Tire pressure effect

In order to investigate the effect of tire pressure on pavement response, a single tire with axle load of 80 kN inflated with 689 kPa and 800 kPa tire pressure is simulated in the numerical model. The pavement responses under the two tire pressures in numerical models are presented in Figure 6-5.

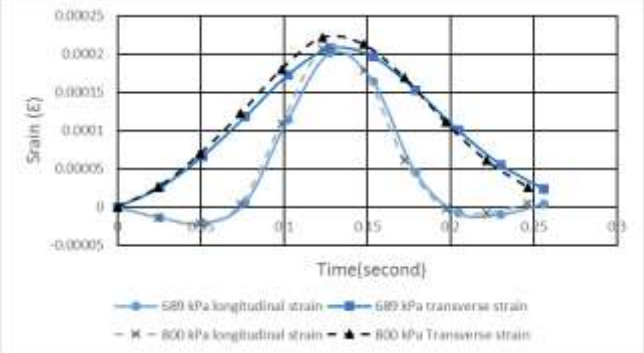

(a) Tensile strain history at bottom of surface layer

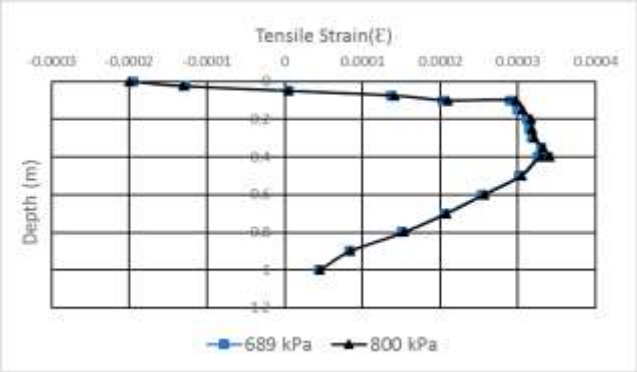

(b) Tensile strain along with pavement depth

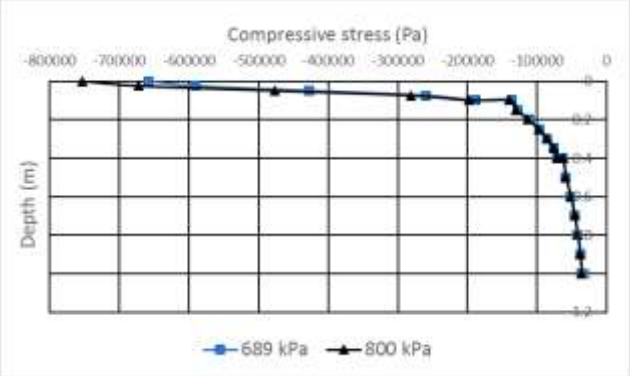

(c) Compressive stress along the depth of pavement

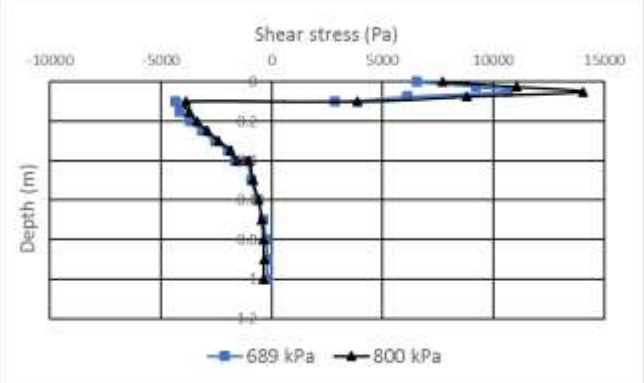

(d) Shear stress along the depth of pavement

Figure 6-5 Comparisons of tensile strain, compressive, shear stress of single tire with 689 kPa and 800 kPa tire pressure

It is noted that with the same wheel load, the difference in tire pressure has slight effects on pavement responses in terms of tensile strain at bottom of asphalt layer, horizontal tensile strain, compressive stress and shear stress along with pavement depth. Higher tire pressure induces slightly greater tensile strain, compressive stress and shear stress within pavement system.

6.4 Axle load effect

Single tire equipped with three axle loads (80 kN, 50 kN and 40 kN) while inflated with the same tire pressure is applied on two pavement structures as shown in Figure 6-6, which have the same underlying courses but varying in thickness of asphalt layer for 10 cm and 20 cm, respectively. The horizontal tensile strain at the bottom of the surface layer, compressive stress on top of subgrade, tensile strain, compressive stress and shear stress along with depth of pavement structure under the combinations magnitude of wheel load and asphalt layer thickness are presented in Figure 6-7. The tires are assumed to travel at constant speed of 18 km/h in the numerical models.

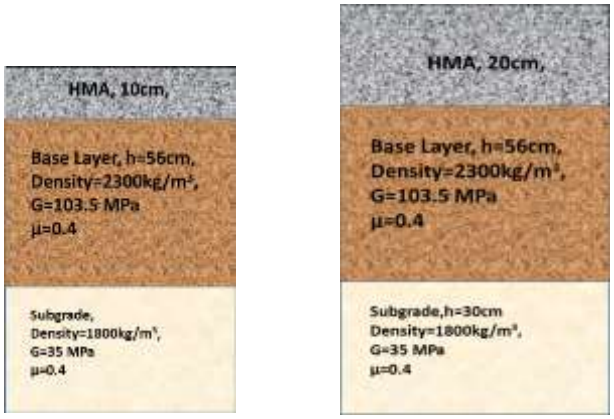

Figure 6-6 Pavement structure with different asphalt layer

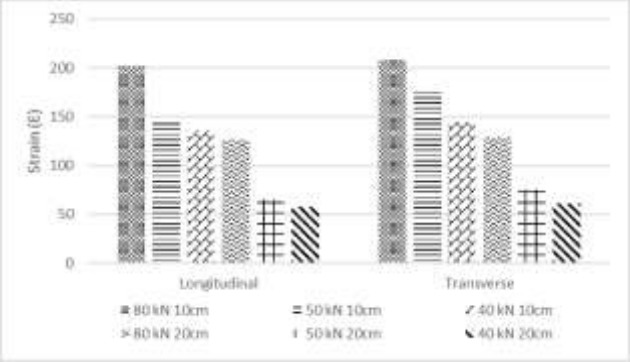

(a) Tensile strain at bottom of asphalt layer

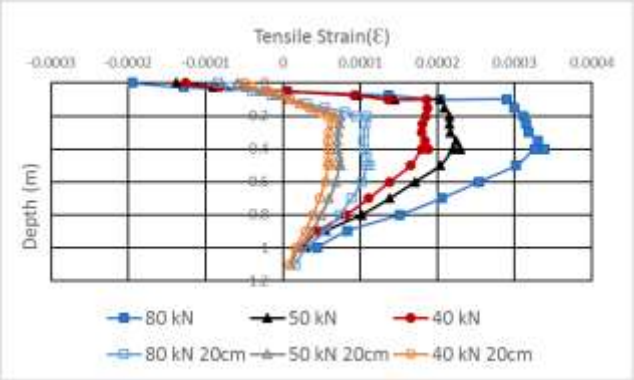

(b) Tensile strain along with depth of pavement

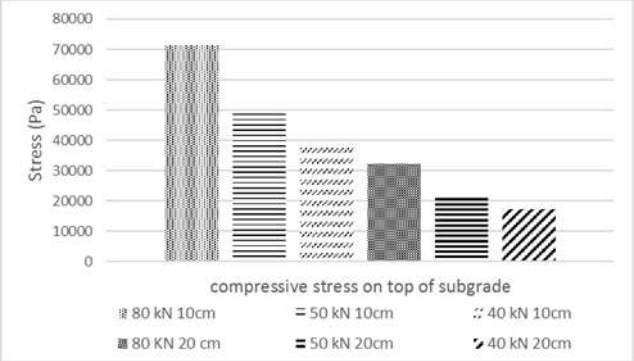

(c) Compressive stress on top of subgrade

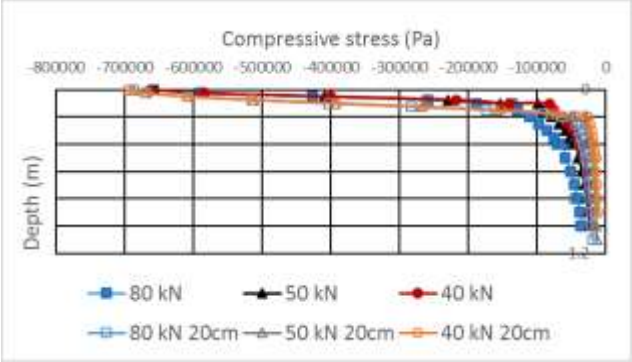

(d) Compressive stress along with depth of pavement

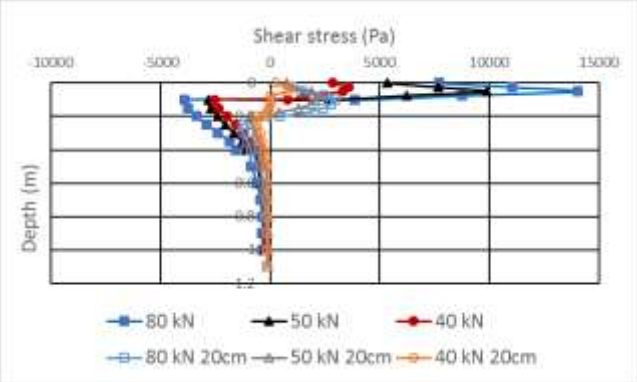

(e) Shear stress along with depth of pavement

Figure 6-7 Comparisons of tensile strain, compressive, shear stress of single tire with different wheel loads and AC thickness

According to Figure 6-7, the amplitude of wheel load has an evident influence on the pavement response. Larger axle load induces greater tensile strain, compressive stress and shear stress along with depth of pavement structure. Compared with the difference in pavement response observed in axle load of 40 kN and 50kN, 80 kN axle load causes a evidently greater horizontal tensile strain and compressive stress within the pavement structure, as compared with 40 kN and 50 kN axle load, in the whole pavement structure. The difference induced by the different axle load diminishes with the increase of the asphalt layer thickness.

Increasing the asphalt layer thickness from 10 cm to 20 cm, considerably decreases the tensile strain at bottom of surface layer and compressive stress on top of subgrade. Significant smaller tensile strain is observed in the whole pavement for the thicker asphalt layer. The profound greater shear stress is observed in the surface layer for the case of thin asphalt layer. This finding demonstrates that the thicker AC surface layer has a better fatigue and rutting performance than the thin layers.

6.5 Speed effect

Five different speeds (18km/h, 36 km/h, 54 km/h, 72 km/h and 108 km/h) are adopted in the model simulation to investigate the speed effect on pavement response and performance. The pavement responses under different wheel load speeds are plotted as following Figure 6-8.

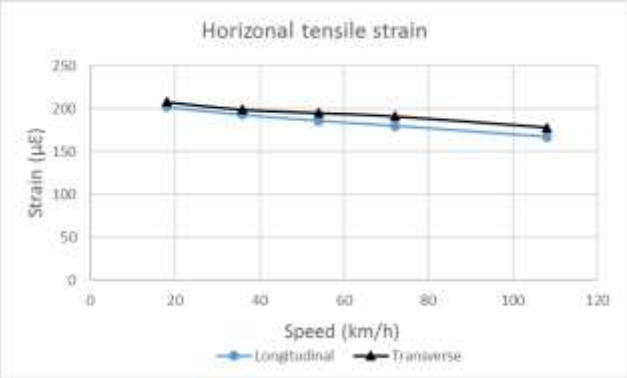

(a) Tensile strain at bottom of asphalt layer

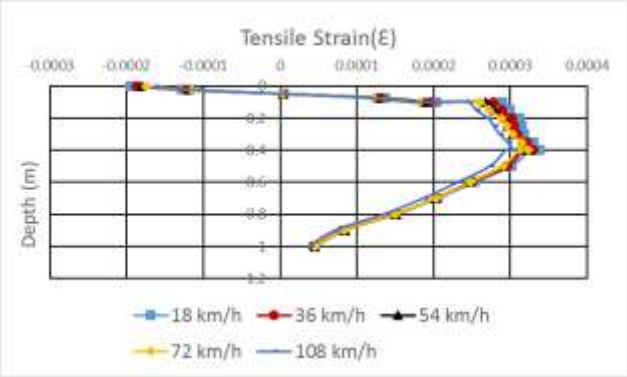

(b) Tensile strain along with depth of pavement

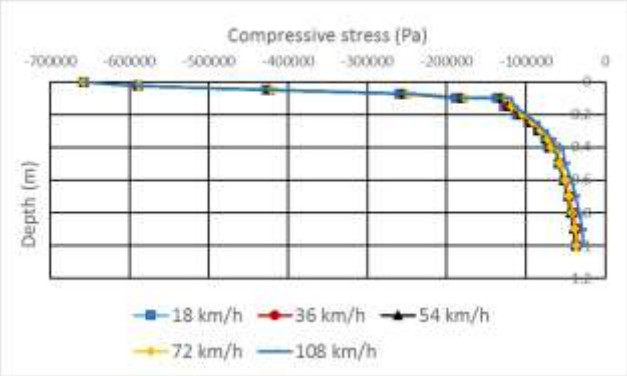

(c) Compressive stress along the depth of pavement

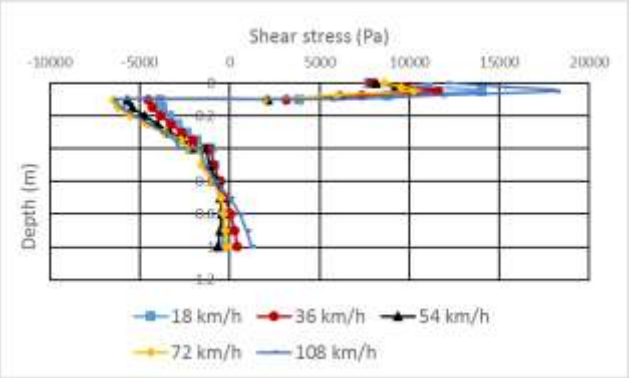

(d) Shear stress along the depth of pavement

Figure 6-8 Comparisons of tensile strain, compressive, shear stress of single tire at different speeds

It is clear that increasing the speed decreases the horizontal tensile strain and compressive strain within pavement structure, which is consistent with the previous studies on actual filed measurement (Al-Qadi & Wang; 2009; Greene et al. 2010). It should be pointed out that the effect of speed on pavement response is not evident. In addition, it is found that higher speed induces greater shear stress within pavement structure, even if the smaller tensile strain and compressive stress is observed under higher wheel load speed.

6.6 Temperature effect

It is well known that asphalt mixture is temperature-dependent, which exhibits a wide variety of properties at different temperatures. To this end, the effect of temperature on pavement response cannot be neglected. The numerical simulation is conducted at different temperatures to investigate the influences. The maximum tensile strain at asphalt layer bottom, compressive stress on top of subgrade, horizontal tensile strain, compressive stress and shear stress along the depth of pavement structure are plotted at temperature of 20 ℃, 30 ℃, 40 ℃ and 60 ℃, as in Figure 6-9. One can note that temperature has a profound effect on pavement response. The temperature effect from 20 ℃ to 30 ℃ is slighter than that of temperature greater than 30 ℃. Higher temperature induces greater tensile strain, compressive stress and shear stress in the pavement structure. The difference in pavement response caused by different temperatures eliminates with the increase of pavement depth.

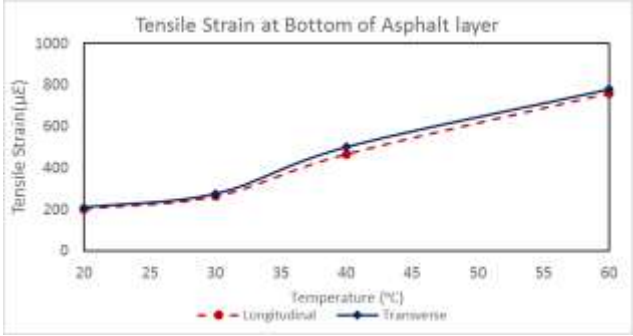

(a) Tensile strain at bottom of asphalt layer

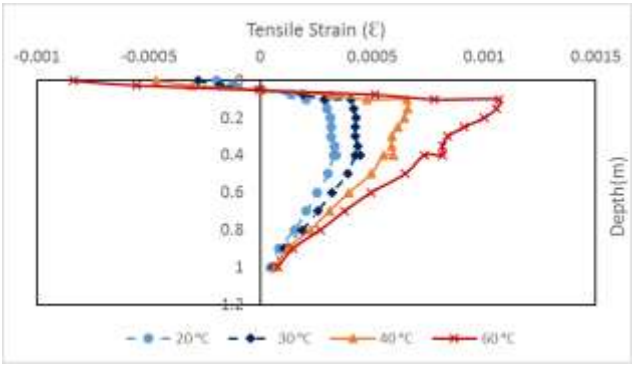

(b) Tensile strain along with depth of pavement

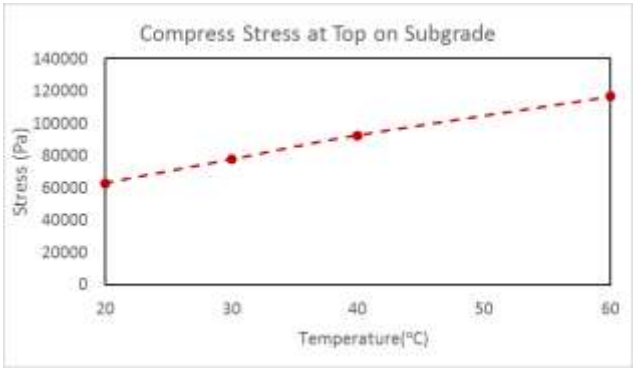

(c) Compressive stress on top of subgrade

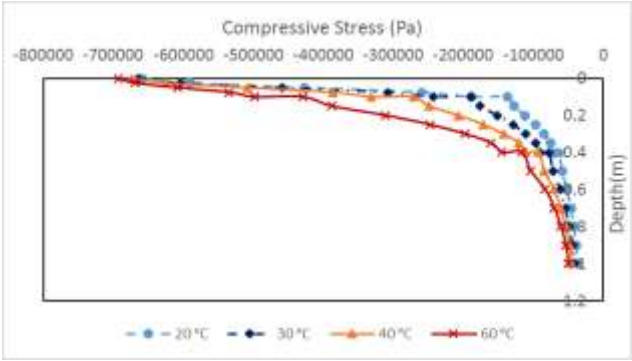

(d) Compressive stress along with depth of pavement

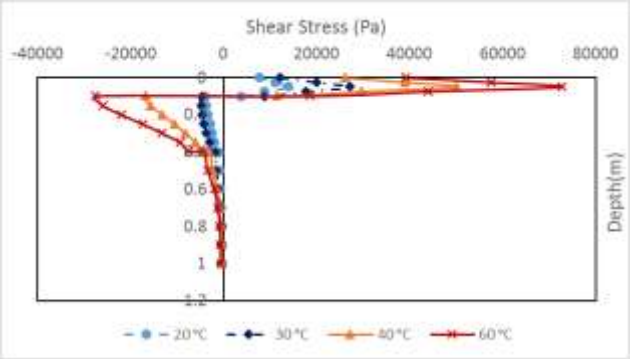

(e) Shear stress along with depth of pavement

Figure 6-9 Comparisons of tensile strain, compressive, shear stress at different temperatures

6.7 Reference:

Al-Qadi, I., Loulizi, A., Janajreh, I. and Freeman, T., (2002). "Pavement response to dual tires and new wide-base tires at same tire pressure". Transportation Research Record: Journal of the Transportation Research Board, (1806), pp.38-47.

Al-Qadi, I. and Wang, H., (2012). "Impact of Wide-Base Tires on Pavements: Results from Instrumentation Measurements and Modeling Analysis". Transportation Research Record: Journal of the Transportation Research Board, (2304), pp.169-176.

Al-Qadi, I. L., & Wang, H. (2009). "Full-depth pavement responses under various tire configurations: accelerated pavement testing and finite element modeling." *Journal of the Association of Asphalt Paving Technologists*, 78, 721-760.

Ang-Olson, J. and Schroeer, W. (2002). "Energy efficiency strategies for freight trucking – potential impact on fuel use and greenhouse gas emissions". Transportation Research Record: Journal of the Transportation Research Board, 1815,11–18.

"Bridgemechanics". < http://www.dot.state.mn.us/bridge/pdf/insp/birm/birmchapt5-bridgemechanics.pdf > (Jan, 2017)

Hardy, M.S.A., and Cebon, D. (1993) "Response of Continuous Pavements to Moving Dynamic Loads," *Journal of Engineering Mechanics*, Vol. 119, No. 9, ASCE, pp. 1762-1780.

Greene, J., Toros, U., Kim, S., Byron, T., & Choubane, B. (2010). "Impact of wide-base single tires on pavement damage." *Transportation Research Record: Journal of the Transportation Research Board*, (2155), 82-90.

Janajreh, I. and Pearson, A. (2000). "On vehicle testing of Michelin new wide base tire". Warrendale, PA: Society of Automotive Engineers.

Kawa, I., Zhang, Z., & Hudson, W. R. (1998). "Evaluation of the AASHTO 18-kip load equivalency concept (No. FHWA/TX-05/0-1713-1)". *Center for Transportation Research, Bureau of Engineering Research*, University of Texas at Austin.

Lourens, J.P. (1992). “Nonlinear Dynamic Analysis and Design of Road Pavements”. RR 90/030, Department of Transport, Pretoria, South Africa.

Mahoney, J. P. (1984). “A Research Summary Report Evaluation of Present Legislation and Regulations on Tire Sizes, Configurations and Load Limits.” *Research Report 59.2, Washington State Department of Transportation*, Olympia, WA.

Dowling, N. E. (2012). Mechanical behavior of materials. Pearson.

Sarkar, A. (2015). “Numerical comparison of flexible pavement dynamic response under different axles”. *International Journal of Pavement Engineering*, pp.1-11.

Wang, F. (2005). “Mechanistic-Empirical Study of Effects of Truck Tire Pressure on Asphalt Pavement Performance”. PhD. Dissertation. University of Texas at Austin.

Wang, H. (2011). "Analysis of tire-pavement interaction and pavement responses using a decoupled modeling approach." PhD diss., University of Illinois at Urbana-Champaign.

Xue, W. and Weaver, E. (2015). “Influence of tire configuration on pavement response and predicted distress”. *International Journal of Pavement Engineering*, *16*(6), pp.538-548.

Yoo, P.J. and Al-Qadi, I.L. (2007). “Effect of transient dynamic loading on flexible pavements”. *Transportation Research Record*, 1990, 129–140.

Chapter 7 CONCLUSION AND RECOMMENDATION

7.1 Overview

In first chapter, this dissertation introduces the simulative test as an effective and efficient method to evaluate properties and performances of various materials in a compressed time. The relative APT researches are reviewed, in which the full-scale APT facilities all over the world and the laboratory wheel tracking devices that are commonly used in pavement engineering community are tabulated and summarized. On the other hand, it describes the background of this comparative study. Chapter 2 documents the test preparation, implementation procedures and results of the ALF, MMLS and APA experiments. Chapter 3 describes the traditional instrumentations implemented in Full scale APTs and proposes a wireless sensor network based on Internet of things technology for MMLS 3 and APA test instrumentations, which can be successfully used to monitor axle load information and pavement performance at early stage. Chapter 4 details the finite element models of the different simulative test systems, including the material models, corresponding parameters determination, applied load methods, and boundary conditions. The dimensional analysis is discussed in Chapter 5 to prompt the insights in the comparisons in model and prototype. The test and simulation results among ALF, MMLS 3 and APA are analyzed and discussed in Chapter 5 as well. Chapter 6 investigates the effects of tire configuration, tire pressure, axle load magnitude, wheel load speed, and temperature on the pavement response.

7.2 Conclusion

Based on the findings of experimental and numerical simulation results of ALF, MMLS 3 and APA, it can be concluded that 1) MMLS 3 is a feasible apparatus to evaluate fatigue performance of asphalt mixture as ALF pertaining to relative structures due to similar tensile strain distribution within the slabs, while APA test is not capable of subjecting the samples to close-to-field tensile strain/stress condition, indicating APA test is not a good option to assess fatigue performance of asphalt mixture. 2) The slab under MMLS 3 trafficking undergoes the similar compressive stress as that in ALF test, while the sample in APA test is subjected to much smaller compressive stress. 3)The findings from one third scale MMLS3 test and full scale ALF test on pavement fatigue and rutting performance are comparable in terms of rutting depth, strain response and seismic stiffness. This validated the MMLS 3 to be an effective, economic and reliable trafficking tool to characterize rutting and fatigue performance of pavement materials with due regard to the relative structures. The MMLS3 is much more efficient in trafficking and takes much less time to reach the failure inertia as compared to the Full-Scale ALF. 4) Due to the high load frequency and lower initial and operational cost, MMLS 3 can be used to enhance economic pavement designs with unproven composite materials, which can also be performed as the screen testing for establishing full-scale testing protocols as desired or required. 5) A power law function fits well for the accumulated rut depth versus number of load repetitions before the material reaches tertiary stage in MMLS 3 test. For the same material in MMLS 3 test, the two parameters of fitted power law function have a satisfying regression with air voids; 6) The rut depth development of APA tests exhibits a close-to-liner regression with number of load cycles after the initial

500 load repetitions. The slope and intercept of linear regression are found to be correlated well with the rut depth at 500 cycles. 7) The MEPDG fatigue model is used to estimate the allowable load repetitions for the MMLS 3 test on the 6 slabs. The β'_{f_1}=0.1871 is recommended as a calibration parameter in MEPDG model for the case of 6 slabs under MMLS 3 trafficking at 20 ℃, which provides the comparable estimation on the allowable repetitions with the actual measurement. 8) The finite element models adopted in this study can accurately predict the longitudinal tensile strain at bottom of asphalt mixture layer, while underestimates the transverse tensile train. The model can reveal the rut depth development as the number of load cycles, but not capable of reflecting the volumetric change as that occurred in realistic tests, and underestimates the rut depth compared with the measurement. 9) With the same tire pressure and axle load, single tire induces larger tensile strain, compressive stress and shear stress than dual tire does. Tire pressure and wheel load speed have little effects on pavement response. The higher speed causes smaller pavement response in terms of tensile strain and compressive stress along the depth of pavement system, while higher speed induces greater shear stress within pavement structure. Increasing the axle load amplitude and decreasing the pavement thickness significantly amplify pavement response. The temperature has a profound effect on asphalt properties resulting in significant influence on stress/strain conditions in pavement system. 10) The wireless sensor network based on Internet of things technology is implemented in laboratory for the MMLS 3 test, which provides a convenient solution for researchers on long-term observation and monitoring without being physically presented. It can be used to monitor the wheel load information and reflect the modulus change an early stage. 11) The latter finding is considered important for the planning and execution of tests that could be affected in a similar manner.

7.3 Recommendation for the further study

There are eleven composite asphalt pavement lanes consisting of different content percentage of Recycled Asphalt Pavement (RAP) and Reclaimed Asphalt Shingle (RAS) mixtures employing diverse warm mix asphalt technologies and binder grades, were constructed at Turner-Fairbank Highway Research Center (T-F). But only Lane 9 and lane 5 material are conducted for the comprisable study in the different simulative tests. It is recommended that extra slabs should be drilled from other test lanes to further support the findings in this study. In addition, as a result of the limitations for the test conditions and amount of the mixtures and the complexity of the collaborative project, no tests for characterizing the plasticity of asphalt mixtures were conducted to attain the corresponding parameters which are adopted in the numerical simulation. The parameters inverse method is adopted in this dissertation for parameters input in the numerical simulation, which might be questioned for the feasibility. It is recommended that, in future, the systematic laboratory tests for acquisition of asphalt mixture properties including the dynamic modulus tests, creep or relaxation test should be performed. In this thesis, the generalized Maxwell model and two-layer viscoplasticity Model are used to characterize the viscoelasticity and viscoplasticity of asphalt mixture layer, respectively. For future numerical implementations, some other advanced constitutive

models accounting for non-linear viscoelasticity and visoplasticity with damage effects should be adopted to characterize the asphalt mixtures, and the anisotropic non-homogenous properties of pavement materials should be considered. The asphalt mixture is the composite material, which is supposed to be modelled with air void, asphalt mastic and aggregate in three phases and the model should account for the volumetric variables. Besides, the moving wheel load is simulated as a shift of footprint, which can not accurately reveal the dynamic interaction between tire and pavement surface. It is recommended to model moving tires on pavement with consideration of surface texture, which would reflect the contact stress and dynamic effect more accurately.